Hungarian Academy of Sciences
Research Centre for Natural Sciences

# Yearbook

2013

## Institute of Technical Physics and Materials Science

http://www.ttk.mta.hu/
http://www.mfa.kfki.hu/

Hungarian Academy of Sciences

Research Centre for Natural Sciences

**Institute of Technical Physics and Materials Science**

*Director:* Prof. István Bársony, corr. member of HAS

*Address:* Konkoly-Thege Miklós út 29-33,
H-1121 Budapest, Hungary
*Postal:* P.O.Box 49, H-1525 Budapest, Hungary
*Phone:* +36-1-392 2225
*Fax:* +36-1-392 2226
*E-mail:* info@mfa.kfki.hu, info@ttk.mta.hu
*URL:* http://www.ttk.mta.hu/
http://www.mfa.kfki.hu/

MTA TTK MFA Yearbook 2013

*Editors:* Miklós Menyhárd and Csaba S. Daróczi
*Published by:* MTA TTK MFA, Budapest, Hungary, 2014

# CONTENT

# DIRECTOR'S FOREWORD

Further tightening the belt… In 2013 this is the most appropriate summary of the operation of the Institute of Technical Physics and Materials Science (MFA) as part of the Research Centre for Natural Sciences of HAS.

By the end of the year all other institutes of the Centre moved into the 31M€ new building, which was inaugurated November 15, 2013 as a XXIst century research facility. MFA, however, continues to operate in its old, albeit renovated premises at the Csillebérc KFKI campus, ca. 9 km from the administrative centre. In order to abide by the well proven strategy in pursuing materials science, i.e. to conduct exploratory research on nanoscale functional materials and creatively exploit the obtained results in integrated micro- and nanosystems, we had to rationalize our operation. This meant a considerable reduction of the floorspace occupied down to 5000 $m^2$, ca. 20% less area than a year ago, to decrease the related utility costs, and a cutback of expenditures in general. We completed the movements in connection with the realisation of the CERN@Wigner datacentre project involving the reshuffling and reconstruction of the laboratories. As a final step the renovation of the conference room and the directorate was accomplished, too.

The internal organisation structure of the institute was changed in 2013. The *Department for Ceramics and Nanocomposites* was dissolved, its tasks and coworkers were integrated into the *Department of Thin Film Physics* and the *Department of Microtechnology*. The *Nanobio-sensorics Lendület Group* was established as an independent research group.

In 2013 at the Institute 75 projects were running parallel, constituting a severe load for the centralised TTK administration: 5 of them were KMR industrial development projects, 10 EU FP7, 2 ENIAC, 26 OTKA and several bilateral collaboration projects.

The scientific qualification of our staff was further improved. *Prof. László Péter Biró* was elected by the General Assembly of the Hungarian Academy of Sciences as new corresponding member of HAS.

Four new Ph.D. degrees (*Péter Nemes-Incze*, *László Kótis*, *Zoltán Fekete* and *Zsófia Baji*), and 4 new MTA Dr. titles (*Ákos Nemcsics*, *Zsolt Czigány*, *Tivadar Lohner*, and *Béla Szentpáli*) were conferred, and 32 Ph.D. research projects were supervised in the institute. The number of student projects: TDK (16), B.Sc. (30), M.Sc. (21) conducted at MFA is extraordinarily high, which is a proof of the continuing attractivity of the institute - despite the geographic distance from the universities. Eight postdoctors of the staff were temporarily working in leading research institutes and universities abroad.

Also a number of distinctions and prizes were obtained by our colleagues. Just to name a few: *Péter B. Barna*, professor emeritus obtained the Officer's Cross of the Order of Merit of the Republic of Hungary; the 80. year jubilee founder director of MFA, *József Gyulai*, ordinary member of HAS received the Antal Máriás Memorial

Prize; *Béla Pécz* was awarded the Arnold Ipolyi Prize for Science development by OTKA; *János Lábár* became Honorary Member of the European Microbeam Analysis Society; *Levente Tapasztó* and *András Deák* received the Young Researcher Prize of HAS; *Zoltán Fekete* won a Postdoctoral Fellowship; and *Orsolya Tapasztó*, and *András Deák* wond Bolyai Fellowships of HAS.
In 2013 the Institute granted the MFA Researcher Prize to *Péter Fürjes* and the MFA Junior Prize to *Dániel Patkó*. Three of our colleagues, *Károly Bodnár*, *Norbert Nagy* and *Krisztina Szakolczai* received the MFA Prize for Excellent Research Support for their contribution to the completion of renovation of the central facilities.
We are proud that our colleague, *Zoltan Juhász* for his excellent accomplishments in Hungarian folk music was elected as member of the Hungarian Academy of Arts. Despite the extreme difficulties in financing and administration, the collective spirit characteristic for MFA could be maintained, which led to formidable scientific records and advancement. This keeps alive the hope for materials science deserving to be recognised as a discipline by having a dedicated centre within the research network of the Academy in the near future.

Budapest, March 2014

István Bársony
director, corr. member of HAS

# GENERAL INFORMATION

## Organisation of RCNS (TTK)

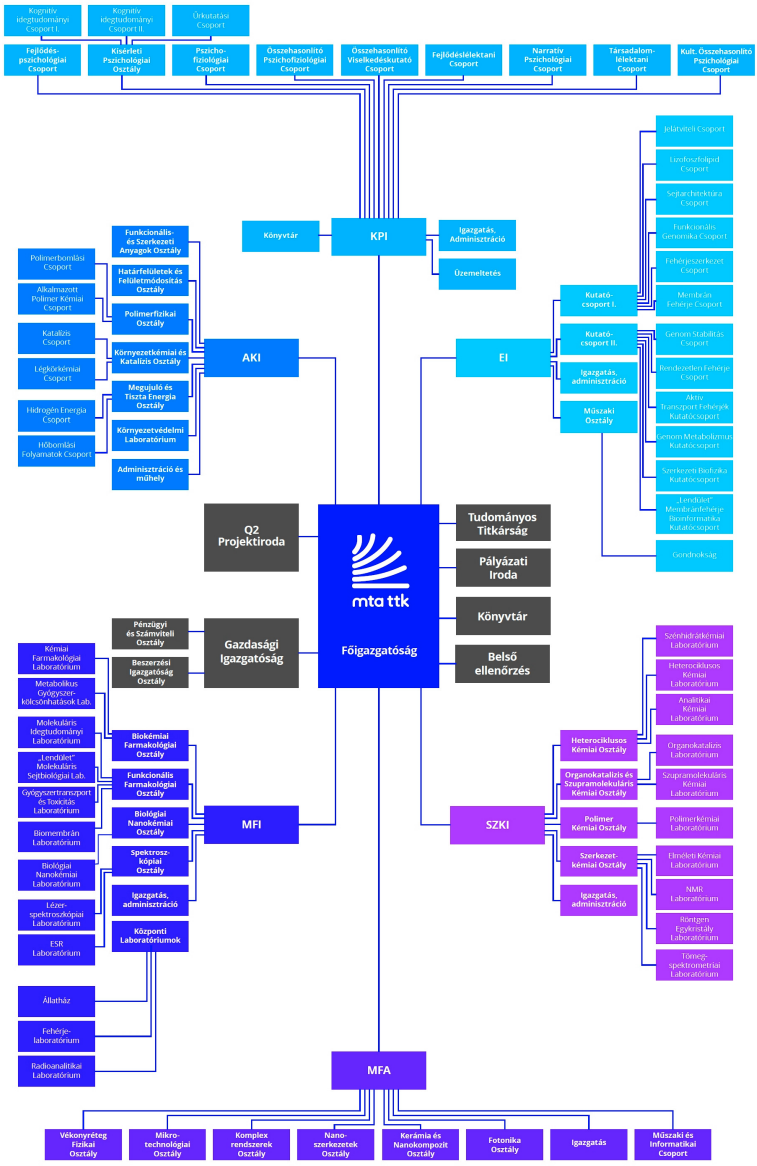


Source: http://www.ttk.mta.hu/rolunk/szervezeti-felepites/

# Organisation of MFA

**Director** - *István BÁRSONY*

| Scientific Departments / Groups | | Support | |
|---|---|---|---|
| **Thin Film Physics** | *János LÁBÁR (until 30.06.2013)* | **Head of Scientific Council** | *Miklós MENYHÁRD* |
| | *Béla PÉCZ (from 1.07.2013)* | | |
| **Nanostructures** | *László Péter BIRÓ* | **Scientific Secretary** | *Krisztina SZAKOLCZAI* |
| **Photonics** | *Miklós FRIED* | | |
| **Ceramics&Nanocomp** (Department dissolved by June 2013) | *Csaba BALÁZSI (until 1.06.2013)* | **IT Support** | *Gergely TAMÁS* |
| **Nanobiosensorics "Lendület"** | *Róbert HORVÁTH* | **Technology Transfer (IPR)** | *Antal GASPARICS* |
| **Complex Systems** | *György SZABÓ* | **Quality Assurance** | *Andrea Cs. BOLGÁR* |
| **Microtechnology** | *Gábor BATTISTIG* | **Financial Administration** | *Anita Sz. RITTER* |
| | | **Technical Support** | *Károly BODNÁR* |

# *Key Financial Figures of MFA*

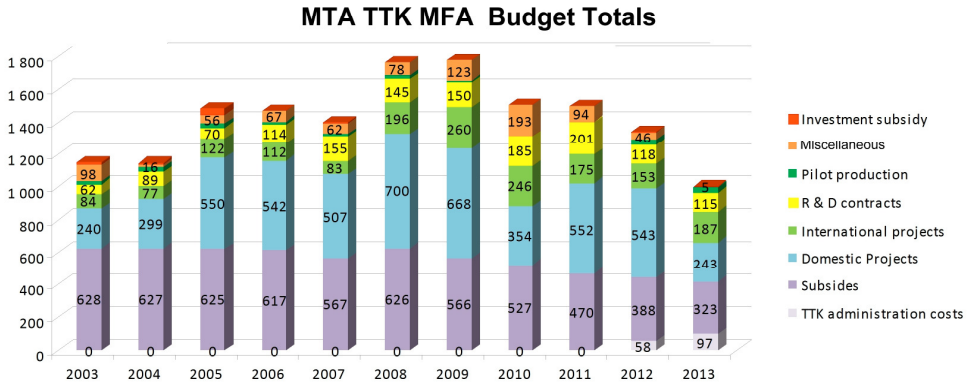


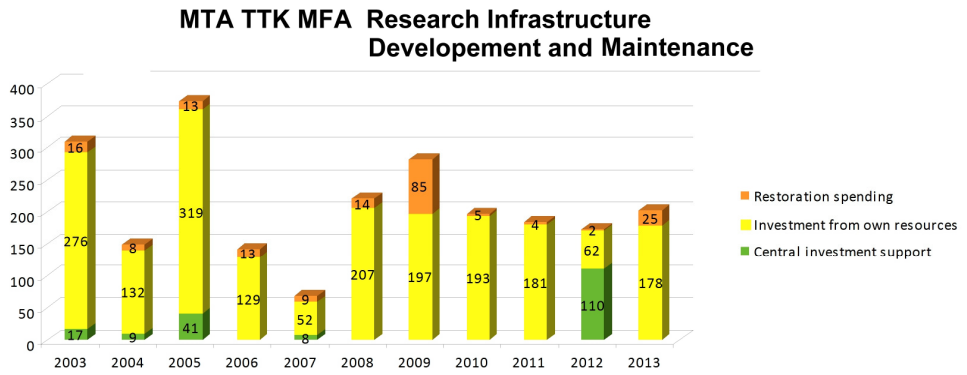

# Publications & Citations of MFA

According to the Thomson-Reuters ISI "Web of Knowledge", and MTMT databases, the Institute has an average publication activity of ca. 100 scientific papers in IF journals a year.

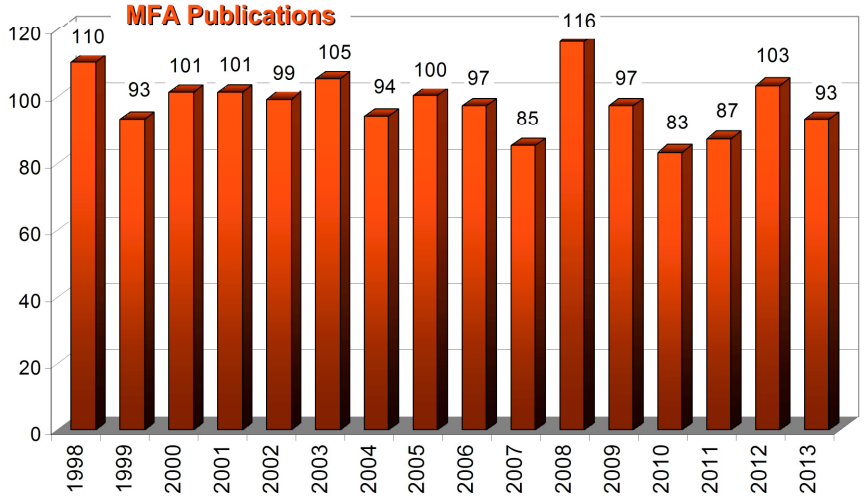


The complete 2013 publication list of MFA – with considerably more titles than listed by the ISI Web of Science and MTMT – is included at the end of this yearbook.
A good measure of recognition of MFA's scientific activity is the **h-index of 67**, and the steady growth of the number of independent citations.

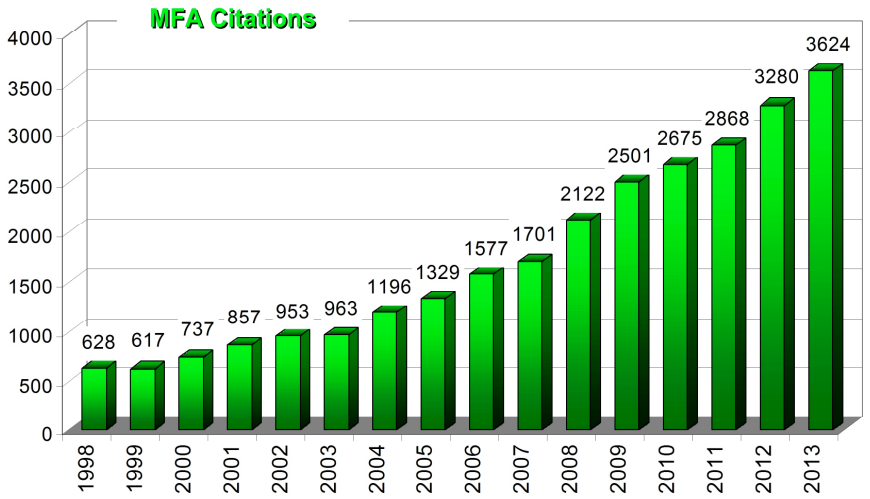

# Prizes, distinctions

| | | |
|---|---|---|
|  | **BARNA, B. Péter** | Officers Cross of the Hungarian Order of Merit |
|  | **GYULAI, József** | Antal Máriás Memorial Prize and Honoris causa Jedlik Ányos Prize |
|  | **PÉCZ, Béla** | Arnold Ipolyi Prize for Science Development by OTKA |
|  | **LÁBÁR, János** | Honorary member of the European Microbeam Analysis Society |
|  | **TAPASZTÓ, Levente** | Young Researcher Prize of the Hungarian Academy of Sciences |
|  | **DEÁK, András** | Young Researcher Prize of the Hungarian Academy of Sciences |
|  | **FÜRJES, Péter** | MFA Prize (Researcher) |
|  | **PATKÓ, Dániel** | MFA Prize (Ph.D. student) |
|  | **BODNÁR, Károly** | MFA Prize for Excellent Research Support |
|  | **NAGY, Norbert** | MFA Prize for Excellent Research Support |
|  | **SZAKOLCZAI, Krisztina** | MFA Prize for Excellent Research Support |

# Renovation and modernisation

*The external renovation and heat-isolation of the MFA central building is completed.*

*Farewell to our colleagues A. Süveges, L. Gosztonyi after decades of service, and to the MFA conference room…*

*Last glimpse at the old conference room of MFA, inherited from the predecessor, the KFKI Microelectronics Research Institute.*

*The so called "György-terem" was built by the former director György Zimmer over 25 years ago.*

*As a final act in the central building, the reconstruction of the facilities of the secretariat, and directorate starts.*

*The new conference room slowly taking shape.*

# Most advanced LED lighting installations in GE cooperation

*The conference room and the renovated offices of the management equipped with intelligent, economical room lighting installations of GE Lighting, Budapest (http://www.gelighting.com/eu/tungsram/products_en.html )*

*Solar cell plant installed on the roof of the technology building providing power back-up for the intelligent street lighting system. (In the background the buildings of Cern@Wigner data center.)*

*Weather-station for collection of the information (insolation, temperature, humidity, wind sensor) used in intelligent control of power management and operation.*

*LED street-lighting in standby operation (no traffic on the street).*

*Intelligent LED lighting activated by motion sensors (a car was passing by).*

## Industrial Interest

*The 2nd Hungarian & Korean Technology Day opened in the new Conference Room by President J. Pálinkás and Ambassador Nam Gwan-Pyo.*

*The director of the Korean Trade-Investment Promotion Agency in Budapest, Mr. Kim is testing the 3D TV display of the Budapest University of Technology.*

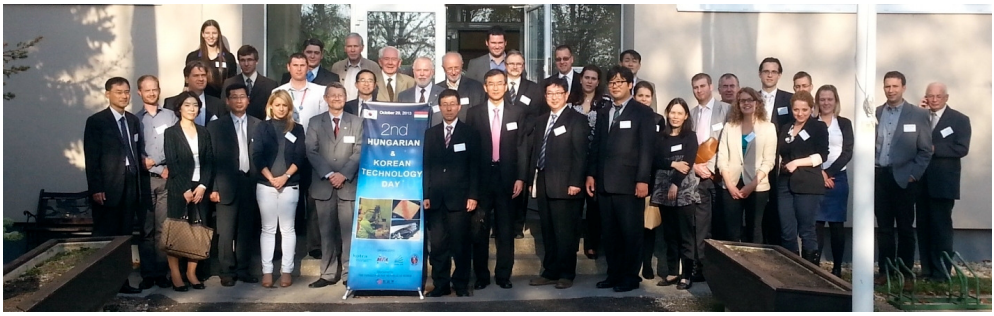


*Participants of the brokerage event in front of the main building of MFA.*

## Public outreach

In the framework of the MFA Summer School we welcome Hungarian speaking secondary school students for a week of real scientific work at our laboratories (this year between November 24-28).
The Open Day at MFA is a yearly organised PR event (this year in November 22), which is always well visited by high-school classes and interested civilians. The purpose is to increase the public awareness for the scientific research financed by the tax-payers.

*What do we see on a Scanning Electron Microscope image?*

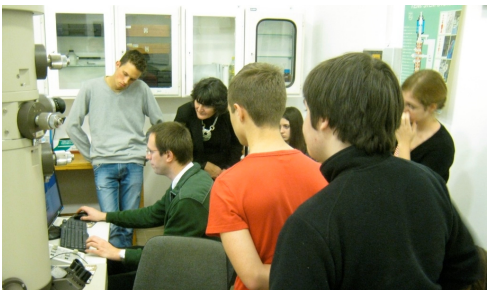

*Practical demonstration of the use of Transmission Electron Microscopy.*

*Students at work in the laboratories during the 6th MFA Summer School for High School students (June 26, 2013).*

*Evaluation of ellipsometry spectra.*

*Night spectacle – visit at the observatory of the Research Institute for Astronomy.*

Glimpses from the traditional MFA Day organised at the KFKI sport fields. This informal event offers a chance for leisure activities and get together with families and alumni at the white table.

*It is a sport's day, after all...*

*Fire extinguishing must be practiced as well!*

*It is a sport's day, after all...*

*Highlight of the day, the lunch is being served!*

*The first "Girl's Day" organised at MFA - an all female event coordinated by K. Balázsi.*

## Visit of the Engineering Chapter of HAS



*The Engineering Chapter of the Hungarian Academy of Sciences visiting MFA in November, 2013.*

*Celebration of the 80th birthday of the founder- past director and former chair of the Chapter, J. Gyulai by his successors G. Stépán and I. Bársony.*

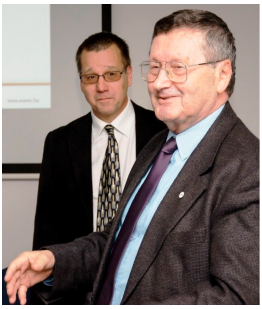

*L. P. Biró, head of the Nanostructures Department (left) and G. Battistig, head of the Microtechnology Department (right) greeting their peer.*

*T. Czvikovszky reading his sonett to the jubilee.*

*Gy. Gergely congratulates to the young birthday kid.*

*The jubilee receiving congratulations.*

# RESEARCH HIGHLIGHTS

## Sputtered biocompatible TiC/a:C nanocomposite thin films

***(OTKA PD10453, OTKA K109021, EU FP7 HypOrth 602398)***

N. Oláh, O. Tapasztó, M. Menyhárd, Zs. Fogarassy, A. Sulyok, V. Viktor, L. Illés, and K. Balázsi

There are more than 400 000 artificial hip joint operations made every year in the world and there are some 25 000 000 people who have either a partial or a total hip replacement. The human body is at the same time both a very hostile and sensitive environment for foreign objects, the life span of a hip implant is limited. With time, the wear and risk of the implant loosening increases so that after 10 years 10-20% of the implants have to be renewed.

Biomaterials used for implant in different parts of the human body as artificial valves in the heart, stents in blood vessels, dental implants (Fig. 1), replacement implant in shoulders, knees, hips (Fig. 2) and orodental structures should possess some important properties in order to long-term usage in the body without rejection. The materials used for orthopaedic implants should possess excellent biocompatibility, superior corrosion resistance in body environment, excellent combination of high strength and low modulus, high ductility and be without toxicity.

316L stainless steel, cobalt-chromium alloys and pure titanium or its alloys are the materials currently used for implants. One negative property of Ti is a low abrasion resistance and minute Ti abrasion powders may cause inflammatory reactions (Fig. 1). From this point of view, TiC is a very stable phase in comparison to pure Ti or Ti alloys. Titanium carbide (TiC) is a useful material for biomedical instruments because it possesses a range of desirable properties. The combination of very high hardness, high melting temperature, and excellent thermal and chemical stabilities makes TiC suited to a number of commercial applications, mainly biomedical.

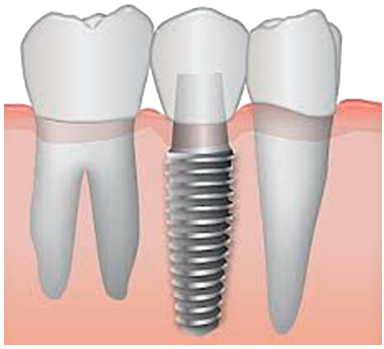

***Figure 1.*** *Schematic view of titanium dental implant.*

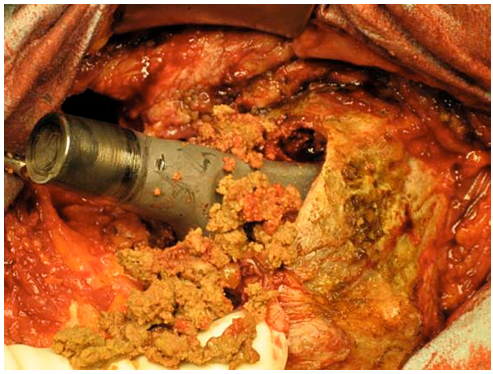

***Figure 2.*** *Real implant in the body with reaction.*

In MTA TTK MFA Thin Film Physics Department, the deposition of TiC based nanocomposites was carried out using a DC magnetron sputtering system in argon atmosphere at the pressure of 0.25 Pa, with one Ti target and one C target facing each other. The TiC based nanocomposite films were deposited onto 300 nm thick oxidized Si(001) wafers at room temperature. The input power of the C target was kept at a constant value of 150 W while the input power of the Ti target varied between 15 and 50 W. The film thickness was controlled by the deposition time in such a way that all deposited layers had the same thickness of 450 nm.
We studied the correlation of structure, mechanical, chemical and biological properties of nanocomposite thin films. Measurements confirmed improvement of mechanical properties with increasing of TiC content in the film. The film with best mechanical properties (nanohardness ~66 GPa, elastic modulus ~405 GPa) was deposited at 50 W. In all cases, structural investigations showed the nanosized TiC crystallites embedded in thin amorphous carbon matrix. The Ti content of films was increasing with growing Ti magnetron power.

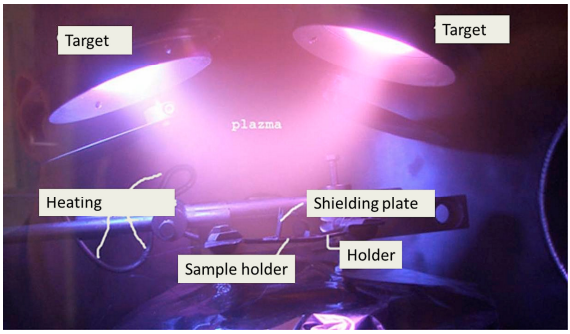


***Figure 3.*** *Preparation of films by DC magnetron sputtering in argon atmosphere.*

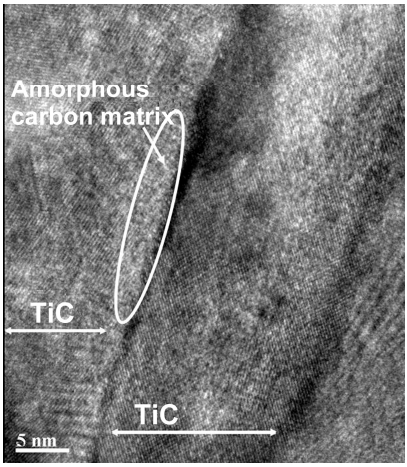


***Figure 4.*** *TEM image of TiC/a:C thin films.*

The bulk composition of TiC layers determined by X-ray Photoelectron spectrometry (XPS) demonstrated the transformation of carbon into amorphous phase and into carbide according to their binding energy: 284.0 eV (amorphous matrix) and 281.8 eV (carbide; TiC). The lowest Ti content (16 at%) is produced by the lowest Ti power (15 W). Then, the Ti content increases with the power to the last specimen reaching 40 at%. The carbon in carbide state increases parallel with the Ti content. The remaining part of carbon is in amorphous state that changes oppositely with Ti deposition rate: from ~70 at% to ~ 8 at%. It is reasonable to assume that all the Ti atoms reaching the target surface are bound to TiC during the deposition process. The excess carbon remains in amorphous state.
MG63 osteoblast cells were applied for biological measurements of TiC/a:C thin films. The cell–matrix adhesion involved cell adhesion with many integrin or other adhesion receptors of an appropriate type, associated with cell differentiation, and

also the formation of a large number of mature cell-matrix adhesion sites (Figs. 6 and 7). The 7-day lasting tests showed a higher value of cells on TiC/a:C nanocomposite surface. Biological aspects showed that the sputtered TiC nanocomposite thin film is biocompatible.

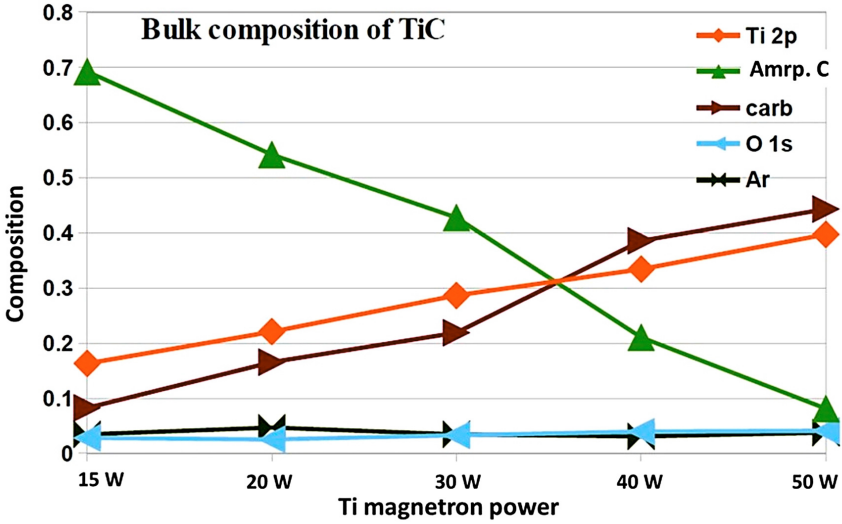


***Figure 5.*** *Bulk composition of TiC/a:C thin films deposited at various Ti target power.*

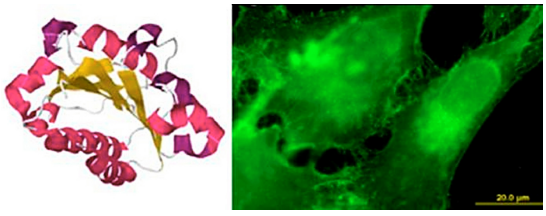

***Figure 6.*** *The β1-integrin adhesion receptors have been localized predominantly in the central region of the cells.*

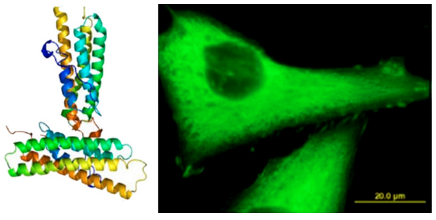

***Figure 7.*** *Vinculin, which formed dot-like structures, has been located on the whole surface of cells in case of TiC/a:C.*

## Conclusion

The combination process of Ti and C is relatively easy and inexpensive, and at the same time TiC possesses good mechanical properties. It can be expected that the formation of TiC based surface coating has a passivation effect to titanium implants. This passivation effect means that TiC layers act as a barrier and Ti ions which are thus kept in the bulk implant having been introduced in the living organism.

# Scenes from a marriage
# 25 year relationship of WPD and STM

*(KHJLN 2010K000980, OTKA NKTH 101599)*

G. I. Márk, P. Vancsó, Ph. Lambin (UNamur, Belgium), Ch. Hwang (KRISS, Korea), and L. P. Biró

Towards the end of the last millennium, around 1986, I had held a "Computer simulation in physics laboratory" at the Budapest University of Technology, together with Prof. Pál Pacher. Computer simulation provides a solution to a major problem: how to teach modern physics in limited hours and without using advanced math. To this end, we searched the literature for conceptionally simple and easy to implement methods and thus we found wave packet dynamics (WPD). Erwin Schrödinger introduced the concept of wave packets (WPs) in 1926 to bridge the gap between classical and quantum mechanics. The WPD method is a scattering experiment inside the computer: an incoming WP is "shot" into the localized potential representing the physical system and the time development of the WP is calculated by solving the time dependent Schrödinger equation. The computers of the 1980's allowed us to calculate only in one spatial dimension (1D), but already at that level I was astounded to see the wealth of phenomena a WP can describe: transport properties, quasi-bound states, ordinary- and resonant tunneling, quantum revival – just to name a few, see Fig. 1a.

***Figure 1a.*** *1D resonant tunneling. Probability density is shown by a thick line. The quasi localized state in the double barrier region is decaying in distinct impulses.*

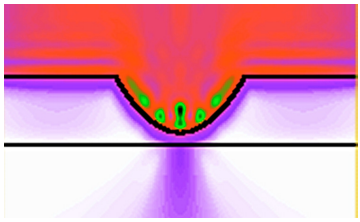

***Figure 1b.*** *2D calculation of tunneling from an STM tip of radius 0.5 nm into the sample surface. Note the narrow tunneling channel – this explains the high spatial resolution of STM.*

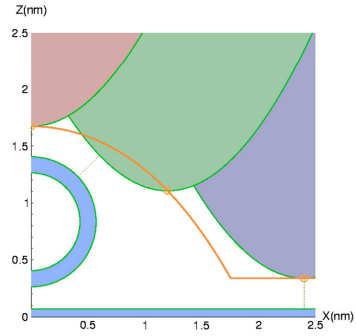


***Figure 1c.*** *Tip convolution pheno-menon by STM scanning a carbon nanotube. Orange line is the geometric line cut drawn by the apex of the tip. Several, typical tip positions are shown, with different colors. Nearest tip and sample points are joined by thin dashed lines.*

This period, the 1980's, saw the "childhood" of Scanning Tunneling Microscopy (STM) and at that time I, still at the Technical University, was an informal member of the small STM group of Prof. E. Balázs. She made possible for me to spend half a year at Prof. H. J. Güntherodt's STM group at University of Basel, in 1990-91. That institution was a kind of background laboratory for IBM Rüschlikon (Zürich), where the STM was born in 1982. They tried to get me involved into their highly advanced experimental work, but I was more interested in their workstation computers, because those machines provided me a possibility to extend the WP simulation for 2D systems and thus construct a simple quantum mechanical model of the STM tip – sample tunneling phenomenon. This was timely, because at those early years the STM theory had to face the basic questions such as why does STM has atomic resolution (see Fig. 1b) and what exactly are the hills and dips on an STM image.
Next scene of the story came in 1997, when Profs. J. Gyulai and L. P. Biró had their first STM images of carbon nanotubes (CNTs). These measurements showed a puzzling phenomenon: images of small diameter CNTs seemed very much broadened and it was proven not to be because of a mechanical flattening. The broadening was intuitively explained by the so called "tip convolution phenomenon", which is because the STM tip has a small, but finite radius of curvature and this distorts the images of small objects.

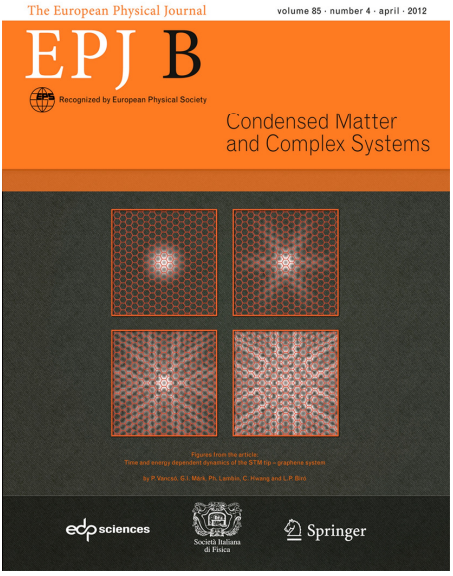


***Figure 2a.*** *Spreading of a wave packet on the graphene surface, featured on cover page of EPJ B in 2012. The WP is inserted from an STM tip (not shown) at the middle. Note the anisotropic spreading due to the anisotropic dispersion relation of graphene.*

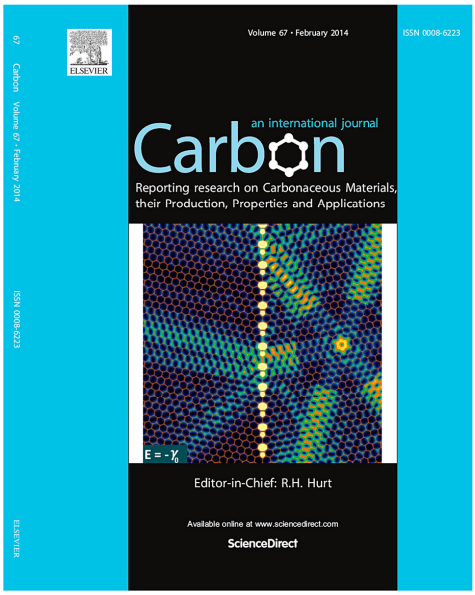


***Figure 2b.*** *Wave packet probability density on the graphene sheet with an 5–7 grain boundary, featured on cover page of Carbon in 2013. The grain boundary works as a beam-splitter for the electrons.*

Indeed, when we move the STM tip *forwards* along a line above the sample and above a small hill at the surface, the tunneling point moves *backwards*, because the tunneling always occurs between the closest points, see Fig. 1c. WPD calculations justified this expectation, but also showed the importance of the electronic structure of the CNT and the presence of the second tunneling gap (that between the CNT and the support surface).

To cut the long story short, I would like to show some recent results on graphene (Fig. 2), when we investigated the WP spreading through regular- and irregular grain boundaries on graphene surface. This is important, because grain boundaries can substantially deteriorate the excellent electrical and mechanical properties of graphene. Our simulations showed that this occurs on amorphous grain boundaries, predominant in CVP produced samples. This is, already, of course a full 3D simulation, and we plan to extend the program to 4D in the future, in order to investigate electron-electron interaction effects.

To conclude this brief report, I return to my starting point: physics education. Recent development of computer technology made us possible to prepare an interactive, "cloud" version of our WPD simulation, which is accessible even from a smartphone, see Fig. 3. This brings "spectacular quantum mechanics" out of the "computer simulation laboratory" and makes it available to any college- and high school student.

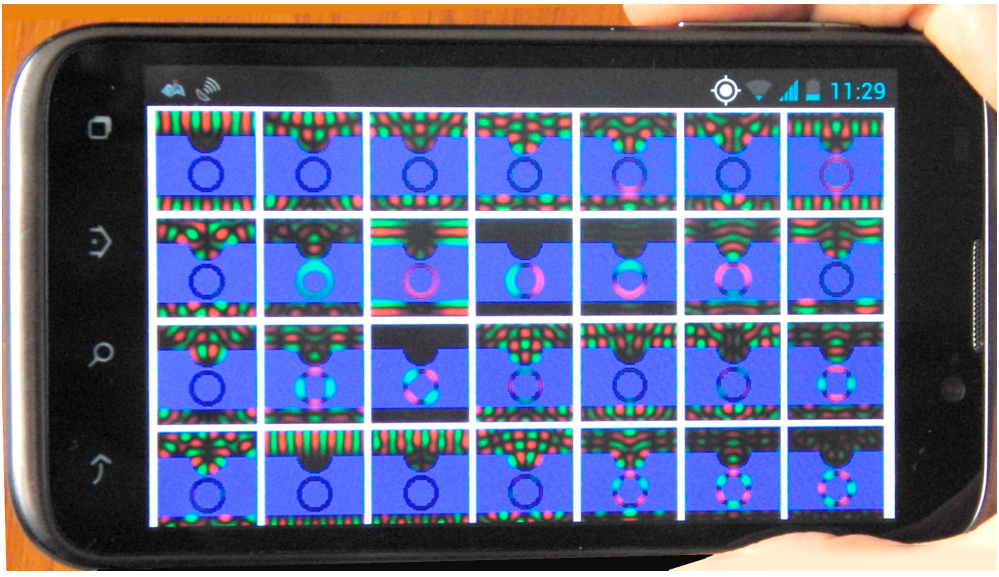


***Figure 3.*** *Wave functions of the STM tip – nanotube – support model on a screen of an Android smartphone, calculated by the software Web-Schrödinger:* *http://www.nanotechnology.hu/online/web-schroedinger/index.html*

# SCIENTIFIC REPORTS

## *Thin Film Physics Department*

**Head: János László LÁBÁR, D.Sc., scientific advisor**
from September**: Béla PÉCZ, D.Sc., scientific advisor**

**Research Staff**

- Katalin BALÁZSI, Ph.D. (from September)
- György SÁFRÁN, C.Sc.
- Zsolt CZIGÁNY, D.Sc.
- László DOBOS, Ph.D.
- András KOVÁCS, Ph.D., (on leave: Ernst-Ruska Centr, Jülich)
- Viktória KOVÁCSNÉ-KIS, Ph.D. (on maternity leave)
- Miklós MENYHÁRD, D.Sc.
- Fanni MISJÁK, Ph.D.
- György RADNÓCZI, D.Sc.
- György Zoltán RADNÓCZI, Ph.D.
- Attila SULYOK, Ph.D.
- Péter SÜLE, Ph.D.
- Lajos TÓTH, C.Sc.
- Csaba BALÁZSI, Ph.D. (till June)
- Gréta GERGELY, Ph.D.
- Reza Allazadeh Mohammad, Ph.D.
- Orsolya TAPASZTÓ, Ph.D.
- Árpád BARNA, D.Sc., emeritus inst.
- Péter B. BARNA, D.Sc., emeritus inst.
- György GERGELY, D.Sc., emeritus inst.

**Ph.D. students / Diploma workers**

- Zsolt FOGARASSY, Ph.D. student
- Ákos Koppány KISS, Ph.D. student
- László KÓTIS, Ph.D. student (defended)
- János SZÍVÓS, Ph.D. student
- Klára NAGY, Ph.D. student (from September)
- Nikolett OLÁH, Ph.D. student (from September)

**Technical Staff**

- Noémi SZÁSZ
- Sándor GURBÁN
- Andor KOVÁCS
- István KOVÁCS
- Katalin PUSKÁS (from September)
- Attila PETRIK
- Viktor VARGA
- Ferenc WÉBER

Thin Film Physics Department worked on some related subjects. Their traditional field is the study of **structure evolution in polycrystalline layers**. They constructed models, which are planned to use in the field of materials with low friction, hard coatings and magnetic layers. Moreover **semiconductor layers**, heterostructures and contacts to semiconductors are among their important research areas. Their third working field is the ion-solid interaction, ion mixing in layers and at interfaces. One

of their modern research field is the **ceramics** and the development of **biocompatible implants**.
In July 2013 Csaba Balázsi accepted a new position (director of BAYATI) and from his former department the ceramics group joined the Thin Film Physics Department. Even before this there were many connections between them in the field of tribology and microscopy. The research subject of ceramics fits very well to the research of modern functional materials, layers and interfaces on which the Thin Film Physics Department is working back for more than 50 years.

As a continuation of the successful tradition, both preparation and characterization of 3D and 2D structures continued. They explained the formation of <111> texture in TiN layers instead of the common <001> texture and correlated that with the high oxygen content (> 15 at%). of the layers. Developing self-organised diffusion barrier layers of Cu-Mn they could get a barrier layer on the substrate in amorphous layers with 40-70 at% Mn content. They prepared titan-carbon thin layers for bioinert implants with a few nm large, cubic TiC crystallites embedded in amorphous carbon matrix. They could increase the stability of quasicrystalline ribbons. Sintered Al-$Al_2O_3$ nanocomposites were prepared and using pure Al additives they could get very compact sintered probes. Aluminium-oxide layers were prepared and then nanostructured by pulse excimer laser via Langmuir-Blodgett nanospheres which focused the laser light to the target. They prepared Ag-Au bimetal catalyst on $SiO_2$ substrate. They developed a new tool for the preparation of combinatorical thin films, which is planned to be patented. Optimization of deposition parameters resulted in graphene on nickel in which large area (~20 µm in diameter) contained only a single layer of graphene as shown by HRTEM investigations. They made atomistic level computer simulation corrugation and Moire in graphene. Their in situ annealing experiments showed, that nickel-silicide is formed already at 250 °C at the interface of amorphous Si/Nickel.

The research group published 30 papers in refereed journals in 2013 with cumulative impact factor of 63 and additional 23 papers in conference publications with no impact factor. The members of the group presented 2 invited lectures, 15 oral talks and 23 posters at international conferences. The group received **1376 independent citations** in the examined last two years.
Two members of the group lectured special subjects for full semesters at ELTE and 4 members hold laboratory practices for full semesters (ELTE, BME). Additionally 12 weeks of summer practice and special labs were also conducted. In addition to the 6 Ph.D. students, 3 diploma workers were also supervised.
Social activity of the group is landmarked by awards (Officers Cross of the Order of Merit of the Republic Hungary; EMAS Honorary Membership; OTKA Ipolyi Arnold Prize) 15 memberships in different committees of the Academy and OTKA and boards of societies, and giving 2 elected representatives to the General Assembly of the Academy.

# Texture change of TiN films due to anisotropic incorporation of oxygen on the various crystal faces

*(Sapientia Univ., Tg-Mures, Romania; Eötvös Univ., Budapest, Hungary; Bay Zoltán Nonprofit Ltd, Miskolc, Hungary)*

D. Biro (Sapientia), M. F. Hasaneen, L. Székely, M. Menyhárd, S. Gurbán, I. Dódony (ELTE), P. Pekker (Bay Zoltán Ltd), and P. B. Barna

A comprehensive structural analysis of a series of TiN thin films prepared on Si single crystal substrates at 400 °C by unbalanced magnetron sputtering in dedicated experiments revealed possible mechanisms responsible for changing the texture from <111> to <001> when the level of oxygen doping increased from 11 at% to 20 at% (Fig. 1). It has been shown that the development of the <001> texture takes place also by competitive growth of TiN crystals like the <111> texture in non-doped or oxygen doped (4 and 11 at%) films (Figs. 2 and 3). It has been shown that the change of growth competition is due to the anisotropic incorporation of oxygen into the crystal lattice and to the different growth mode of the segregating $TiO_2$ phase. According to the XPS results oxygen segregated completely on the {111} crystal faces while on {001} faces only 35 at.% (Fig. 4). Segregated oxygen formed rutile $TiO_2$ which was growing in the form of a 2D surface layer on {111} crystal faces, while on {001} faces in 3D aggregates. This 2D $TiO_2$ surface layer limits the growth of <111> oriented crystals, however the 3D aggregates can disturb the crystal growth only locally. Consequently, the <001> oriented crystals win the growth competition leading to a film structure constituted of V-shaped columns and <001> texture. The segregation of oxygen species can take place on the {111} crystal faces by kinetic processes, while on the {001} faces both surface kinetic segregation and surface spinodal decomposition in the subsurface layer might operate. These results indicate that this phenomenon discovered at first by Barna and Adamik in case of aluminium-oxygen system [Thin Solid Films, 317 (1998) 27–33] has more general importance.

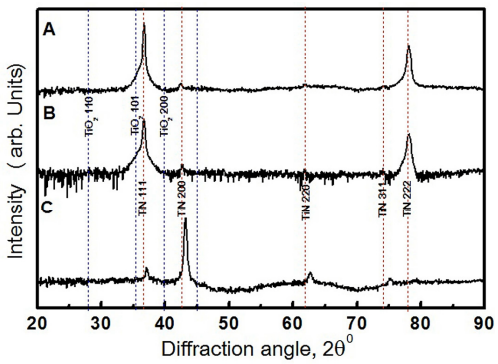


***Figure 1.*** *XRD spectra of TiN films doped with (a): 4, (b): 11, and (c): 20 at% oxygen.*

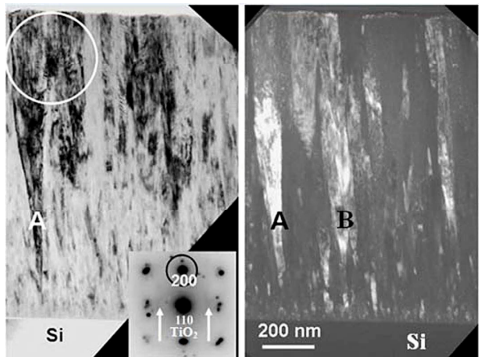


***Figure 2.*** *Cross-sectional bright field (BF) and dark field (DF) TEM images of TiN film doped with 20 at% oxygen. DF image is taken by TiN 200 reflexion.*

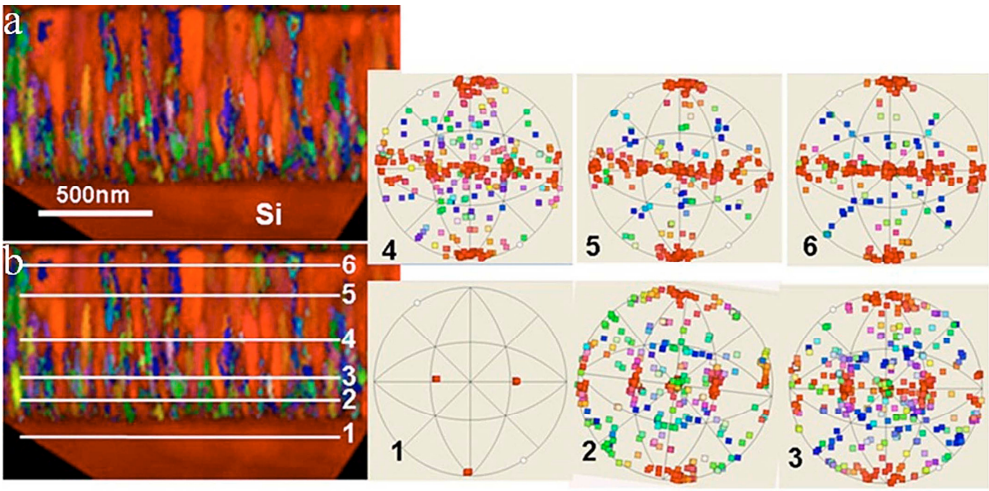


***Figure 3.*** *Colored image of the TiN film doped with 20 at% oxygen taken by the precession electron diffraction (PED) and ASTAR techniques. Crystals with <001> crystal axes nearly parallel with the substrate surface normal are shown in red. Insets 1–6 are the pole figures, taken on the sections marked in the lower TEM image, illustrate the evolution of the <001> texture with thickness.*

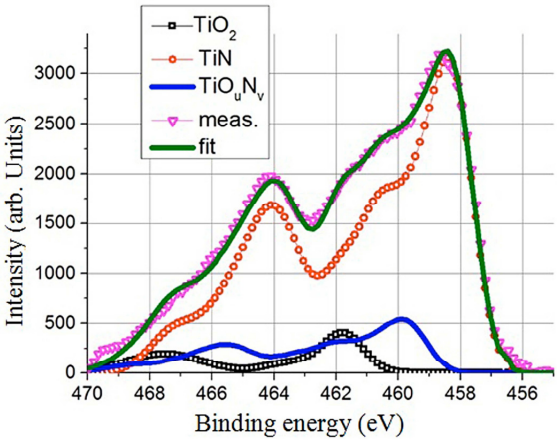


***Figure 4.*** *XPS spectrum measured at the Ti 2p peak. The experimental spectrum (dashed line) and the summarized spectrum of the fitting procedure (thick line). The three components are: TiN (79 at%), $TiO_uN_v$ (u>v, solid solution 13 at%) and $TiO_2$ (8 at%).*

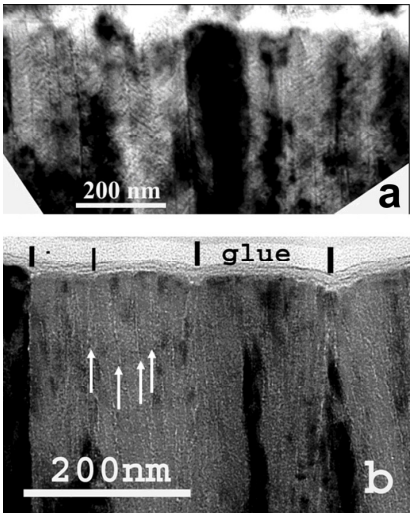


***Figure 5.*** *Phase contrast X-TEM images of TiN films showing the morphology and distribution of $TiO_2$ phase, level of oxygen doping (a): 11 at%, (b): 20 at%.*

# Formation and Properties of self-organizing barrier layer films

***(OTKA K81808 )***

F. Misják, K. Nagy, Zs. Czigány, and Gy. Radnóczi

The fast development of the electronic industry raises the need of development faster and smaller devices. Consequently, the elements of the integrated devices become smaller and smaller. This, however, puts stringent demands on the contacts and interconnects. Around the presently used copper contacts a barrier layer must be manufactured which prevents the interdiffusion of copper into the dielectric materials. Utilization of self-organized barrier layers can provide a new solution to this problem. Cu-Mn alloy films as barrier layers appear a promising material for future technologies. The aim of the project is to build a comprehensive view of the phases, structures and morphologies occurring in the Cu-Mn thin film system as well as their physical properties providing the basic knowledge of their consequent functional utilization.

Our earlier results showed that the phases and concentration boundaries of their occurrence were different from that expected on the basis of the equilibrium phase diagram. The most apparent difference was the formation of an amorphous phase. The difficulties in detection of an amorphous phase, present in small amounts and the strong affinity of the system to oxide formation caused uncertainties in determination of the exact concentration boundaries between phases. However, measurement of physical properties could possibly refine the results based on structural observations.

Eleven films of 1 μm thickness were grown by DC magnetron sputtering covering the whole concentration region in the system. Then the electrical resistivity (in cooperation with P. Lobotka, Electrotechnical Inst. SAV, Bratislava) was measured as the function of composition. The results were interpreted in conjunction with structural investigation of the same films on cross sectional samples by TEM.

The electrical resistivity of the films varied between 1.7 and 205 μΩcm and except of two concentration regions it showed linear dependence on Mn concentration. Utilizing these results the whole alloy region was divided into five parts. Three single phase regions were identified. Below 20 at% Mn content an fcc solid solution of Mn in Cu exists, in the 40-70 at% Mn region the structure is a amorphous alloy of Cu and Mn, and finally above 80 at% Mn an α-Mn based solid solution forms. Two-phase regions exist in the concentration regions between the single-phase ones: at Mn concentrations between 20 and 40 at% the fcc solid solution and the amorphous phases are present, while in the 70-80 at% Mn region the amorphous phase and the α-Mn based solid solution keep balance with each other.

The resistivity measurements and the structural information obtained by TEM were used for modelling the conduction mechanisms in the films. By combining the Matthiesen's rule and the Mayadas-Shatzkes model the scattering contribution of solute atoms and grain boundaries was calculated. As a result, we could conclude, that in the fcc solid solution region and in the amorphous structures the resistivity is composed from thermal and solution (Nordheim) scattering. In the two-phase regions

and in the Mn based solid solution region, in addition to the above scattering mechanisms, grain boundary scattering is giving a significant contribution (Fig. 1). In the concentration regions, where the contribution of solute scattering is important Moiij correlation (high resistivity and small negative TCR) was also observed.
The best interfacial layer between the film and substrate ($SiO_2$) was observed in the amorphous films of 40-70 at% Mn content by TEM. EELS measurements revealed the barrier layer character of the formed interfacial layers of a few nm thickness (the presentation of this result won "Best Poster Award" at the Electron Microscopy Conference in Regensburg). It was also investigated how these samples behave when exposed to higher temperatures. In situ heat treatment of the amorphous films in the TEM showed that the crystallization temperature depends on composition and falls between 200 and 300 °C. The process of crystallization is fast and the forming crystalline phase has very small grain size. The forming phases differ for different film compositions, fcc γ-Mn or α-Mn phases are forming.

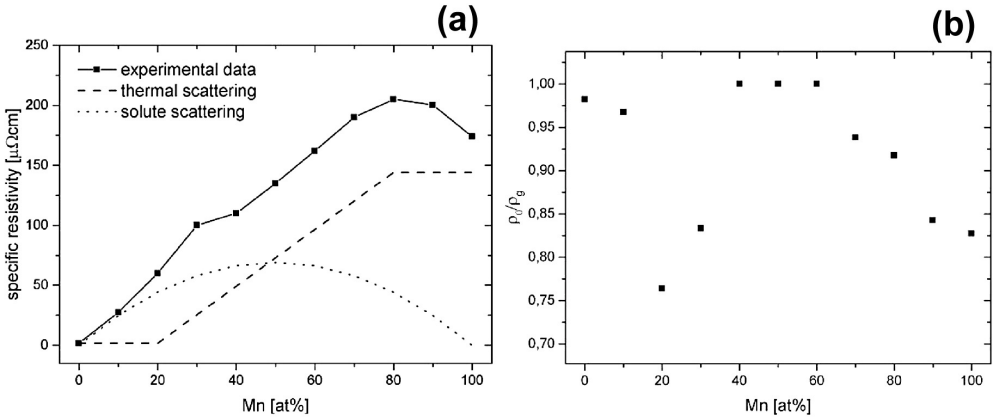


***Figure 1***. *Experimental, thermal and solute scattering (a), and the ratio of solute and thermal ( $\rho_0$ ) to measured film resistivity ( $\rho_g$ ) (b), as the function of Mn content. Grain boundary scattering is measurably contributing where $\rho_0/\rho_g$ is below 1.*

For precise investigation of the existing crystalline phases in the system diffraction studies were carried out. A novel observation has been achieved, namely, at high temperatures (~450 °C) the two-phase alloys are composed from the fcc γ-Mn phase and from a Mn-rich monoclinic phase of elongated unit cell (with participation of Tamás Kolonits, this work was awarded with 1st prize at the National Student Competition (OTDK), Budapest).
Also in the frame of this project the investigation of growth and phase separation processes, important for enabling the growth of reproducible structures was continued. The phase separation in Cu-Ag nanoparticles was investigated in detail. The parameters of the Monte Carlo simulations were refined (Zoltán Erdélyi, Debrecen University) and the simulation results were compared to HREM images of nanoparticles. We have shown that the extent of the phase separation and its mechanism depends on particle size and composition (Fig. 2). Phase separation was

observed at low Ag concentrations in particles larger than 5 nm (with participation of Eszter Bokányi, second prize at the National Student Competition (OTDK), Budapest).

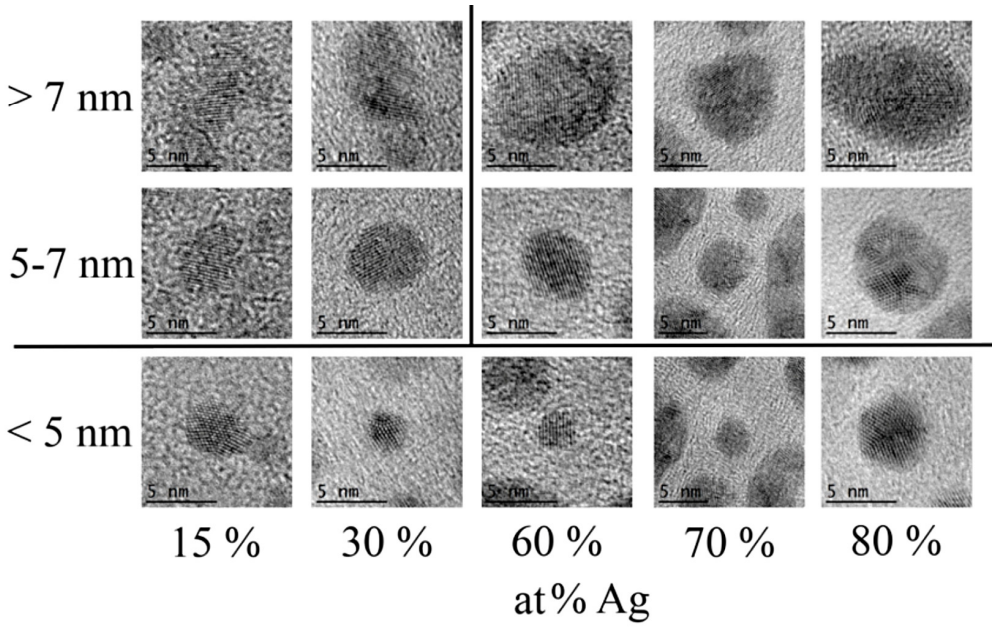


***Figure 2.*** *Morphology of Cu-Ag alloy particles as the function of their size and composition.*

## The influence of sintering process on the dispersion of carbon nanotubes in ceramic matrix composites

O. Tapasztó, H. Lemmel (Institut Laue Langevin), K. Balázsi, Cs. Balázsi, and L. Tapasztó

Optimizing the dispersion of carbon nanostructures in ceramic matrix composites is a fundamental technological challenge. So far efforts have only been focused on improving the dispersion of nanostructures during the powder phase processing, due to the lack of information and control on their possible redistribution during the sintering. Here, we compare multi-walled carbon nanotubes reinforced $Si_3N_4$ samples prepared from the same starting powder dispersion but subjected to different sintering processes. We employ ultra-small angle neutron scattering measurements to gain reliable information on the dispersion of nanostructures allowing a direct comparison of their redistribution during the sintering.

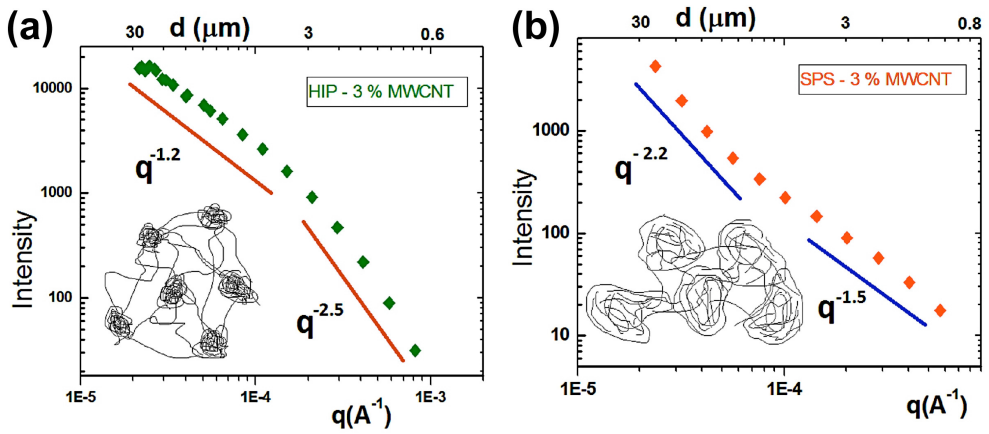


***Figure 1.*** *Ultra small angle neutron scattering intensities as a function of scattering wavenumber for $Si_3N_4$/carbon nanotube composites prepared by (a): Hot Isostatic Pressing, HIP, and (b): Spark Plasma Sintering. Insets show the structural models of nanotube aggregates constructed based on the USANS data.*

Based on USANS (Ultra Small Angle Neutron Scattering) data, we can draw the conclusion that the sintering process has a substantial influence on the dispersion of the nanostructures within the ceramic matrix.

Starting from the same powder phase dispersion during the HIP sintering nanotubes form smaller but denser micron-scale aggregates interconnected by several microns long individual nanotubes or ropes; while during the SPS sintering, larger aggregates of several microns diameter form, that consist of a looser net of individual nanotubes.

The mechanical properties of the resulting composites also revealed striking differences as shown in [Chem. Phys. Lett. 511, pp.340-343 (2011)]. HIP samples were found to be tougher, while the ones prepared by SPS were stiffer and harder.

Understanding the influence of the sintering process on the distribution patterns of the carbon nanotubes is expected to open up new routes towards optimizing the dispersion of nanostructures in ceramic hosts and therefore to fully exploit the potential of nanoscale fillers in engineering the properties of ceramics composites.

# Bioactive, low cost and environmentaly friendly biogenic hydroxyapatite

***(OTKA K105355, EU FP7 HypOrth 602398)***

K. Balázsi, O. Tapasztó, G. Gergely, A. Petrik, V. Varga, F. Wéber, and Cs. Balázsi

The incidence of bone fractures worldwide is constantly increasing, due to increasing traffic accidents and natural disasters. Filling of bone defect is a significant question in every day clinical work. Hydroxyapatite (HAp) is one of the most used biomaterial. The natural-biological origin HAp has several important advantages: worldwide availability in almost unlimited supply, very low cost of raw materials, utilization of very simple and inexpensive apparatuses, rapid and very efficient transformation from raw materials into HAp.

Nanostructured HAp from eggshells or seashell was prepared in different forms like powder or polymer/HAp composite fiber. High-efficient attritor milling was used for HAp production.

Biological behavior of different HAp samples prepared from eggshell (Fig. 1), seashell (Fig. 2) or synthetic commercial HAp. were compared in a joint project with Gangneung-Wonju National University, Korea.

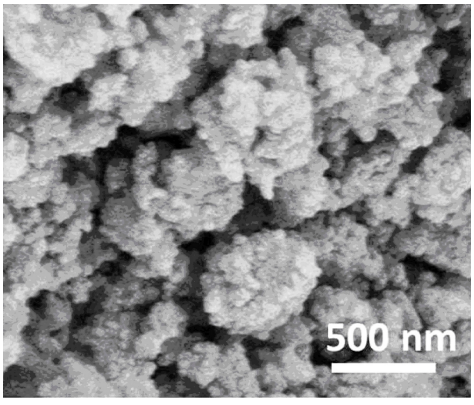


***Figure 1.*** *SEM images of nanosized HAp prepared from eggshells.*

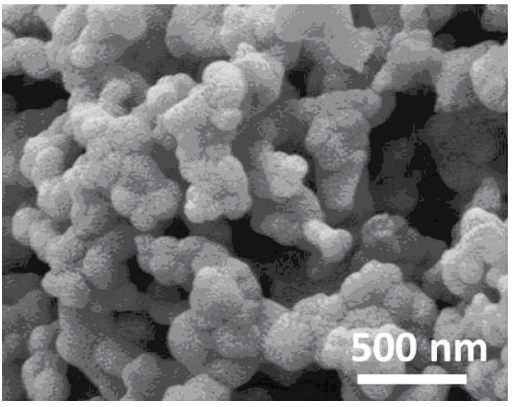


***Figure 2.*** *SEM images of nanosized HAp prepared from seashells.*

Our study showed that the recycled HAp form eggshell and seashell showed larger regenerated bone volume than the synthetic HAp. This biogenic HAp can be considered as candidate for bone graft material.

# Structure and activity of Au-Ag/$SiO_2$ bimetallic catalysts

***(OTKA NN107170, OTKA K101854, OTKA K101897, and cooperation of MFA and the Centre for Energy Research HAS)***

T. Benkó, A. Beck, K. Frey, D. F. Srankó, B. Maróti, Z. Schay, O. Geszti, G. Sáfrán

$SiO_2$ supported Ag-Au bimetallic catalysts were prepared by sol adsorption method with 10/90, 20/80, 33/67, and 50/50 Ag/Au molar ratios. Reduction of $HAuCl_4$ in Ag sol resulted in alloyed Ag-Au colloid particles and that structure remained after calcination and reduction treatment. The alloy structure of the catalysts was confirmed by UV-visible spectroscopy and High Resolution Transmission Electron Microscopy (HRTEM) (Fig. 1). The Au-Ag bimetallic effect and its dependence on the Ag/Au molar ratio was studied in glucose oxidation where synergistic activity increase was observed compared to the Au/$SiO_2$ reference sample in case of the bimetallic samples with less than Ag/Au=50/50 molar ratio (Fig. 2). The Ag/$SiO_2$ was inactive at the same conditions. The Ag/Au surface atomic ratios – calculated by X-ray photoelectron spectroscopy (XPS) – were slightly higher than in the bulk – determined by prompt gamma activation analysis (PGAA). The increased activity of the bimetallic samples is suggested to be caused by the improved $O_2$ activating ability provided by Ag sites. Further increase of Ag loading above the optimum concentration may dilute the Au to such an extent that the population of extended active sites of gold necessary for glucose activation decreases that deteriorates the activity.

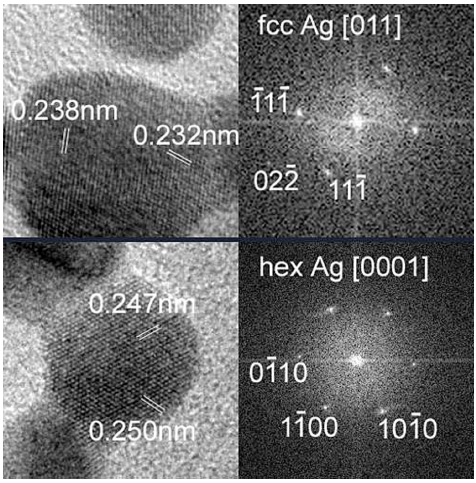


***Figure 1****. HRTEM revealed, besides the usual fcc Ag structure (above), unique 4H hexagonal one (below) in the parent Ag sol. The bimetallic Ag(Au) samples, however, showed exclusively fcc structure!*

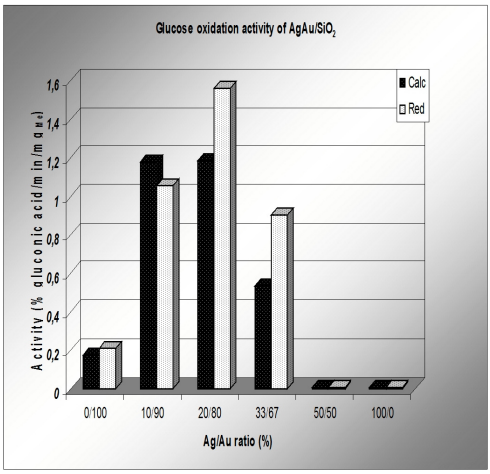


***Figure 2.*** *Activity of AgAu/$SiO_2$ bimetallic catalysts in glucose oxidation as a function of the Ag-Au composition. T=35 °C, pH 9.5, $c_{glucose}$ =0.1M.*

# Al-matrix composites reinforced with $Al_2O_3$ particles

***(TET_09_IN_DST (ALNANO09), REG-KM-09-1-2009-0005)***

J. L. Lábár, K. Balázsi, A. L. Tóth, F. Wéber, Z. Károly*, H. Hargitai**, and A Dhar***

*Research Institute for Natural Sciences of the HAS, Institute of Materials and Environmental Chemistry.,Hungary
**Material Testing Laboratory, Széchenyi István University, Hungary
***National Physical Laboratory, New Delhi, 110070 Delhi, India

Aluminium matrix composites are favourable materials for applications like brakes. Materials properties can be tuned by a combination of the properties of the matrix and the reinforcing material. An application specific good compromise can be reached in hardness, fracture toughness, tribological and other physical parameters. An improvement in properties is expected by reducing the grain size and particle size to the submicron level for the nanocomposites produced by powder metallurgy (PM).

Al-$Al_2O_3$ nanocomposites were produced by both milling at room temperature in Ethanol and by cryogenic milling in liquid nitrogen and subsequent sintering. Cryogenic milling proved to be more efficient in producing nano-sized mixed powders. Next, spark plasma sintering (SPS) was used to prevent grain growth during sintering. A solution was also needed to overcome the problem of high melting point alumina (both native oxide on the surfaces of grains and the alumina nanoparticles in the mixture) surrounding the low melting point Al and so hindering the sintering process.

Both density and hardness were measured on the sintered nanocomposites, furthermore, tribology was used to measure friction coefficient and wear rate. The structure was measured by electron microscopy and related analytical techniques (SEM, TEM and EDS). Effect of additional elements (mainly Si, Ni and Fe that were mixed to the Al-powder) was also studied. Optimization of the sintering parameters improved density and mechanical properties.

Both pure Al and alloyed Al were mixed with 30% $Al_2O_3$. Best densification (97%) and lowest wear rate ($4.1*10^{-4}$ $mm^3/m$) was achieved with pure Al, sintered at 600 °C, while the hardest composite was obtained with an Al-27%Si-7%Ni alloy. The same hardness (2.75 GPa) was reached with two preparation conditions for the 70% (Al-27%Si-7%Ni alloy) +30% $Al_2O_3$ samples. First, 600 °C sintering temperature was needed for powders milled in Ethanol at room temperature. Second, the same powder mixture milled in liquid nitrogen sintered to the same hardness at 560 °C. Dry sliding properties were studied with pin-on-disc geometry at low speed (0.3 m/s) at low load (1 N). The wear mechanism involved is dominated by adhesion.

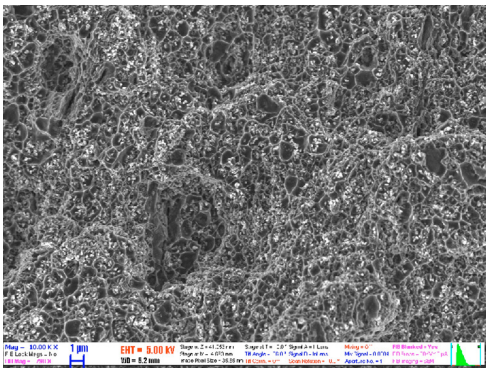

***Figure 1.*** *SEM secondary electron image of broken surface of a 70%Al+30%$Al_2O_3$ sample. Milled in Ethanol at room temperature for 1 h at 600 rpm with $ZrO_2$ balls. Spark Plasma Sintered at 647 °C for 5 minutes. Uniform distribution of the $Al_2O_3$ particles is seen.*

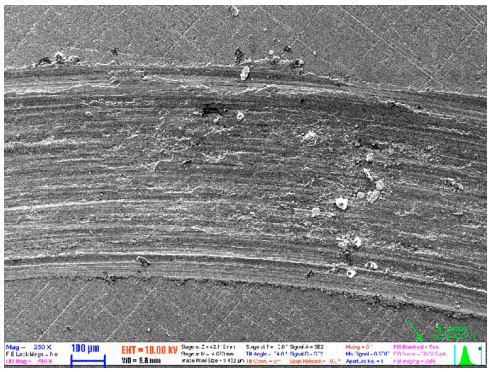

***Figure 2.*** *SEM secondary electron image from the surface of a 70%Al+30%$Al_2O_3$ sample after tribology measurement. Milled in Ethanol at room temperature for 1 h at 600 rpm with $ZrO_2$ balls. Spark Plasma Sintered at 640 °C for 5 minutes. Traces of adhesion are seen.*

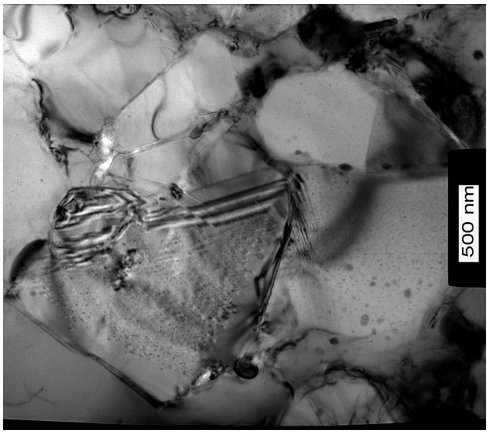


***Figure 3.*** *TEM bright field image from a 70%(Al-27%Si-7%Ni alloy) +30%$Al_2O_3$ sample. Milled in Ethanol at room temperature for 1 h at 600 rpm with steel balls. Spark Plasma Sintered at 600 °C for 5 minutes. Traces of porosity are seen together with $Al_2O_3$ particles. EDS proved that Al and Si remained separated even after sintering.*

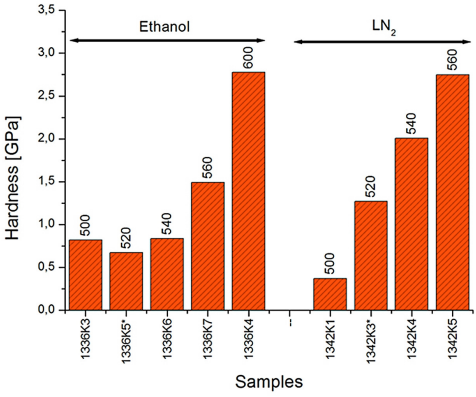


***Figure 4.*** *Hardness values measured for samples prepared from alloyed Al but milled under different conditions. Mass fraction of $Al_2O_3$ is 30% in each case. Sintering (SPS) temperatures are indicated as labels above the columns.*

# Chemical vapour deposition (CVD) of Graphene on nickel (111)

Zs. Fogarassy, J. L. Lábár, G. Dobrik, L. P. Biró, M. H. Rümmeli (IBS Center, Korea), S. Gorantla (Leibniz Institute, Germany), A. Bachmatiuk (Leibniz Institute, Germany), K. Kamarás (Wigner RC, Hungary), and K. Havancsák (ELET, Hungary)

In the present work, graphene was grown on a Ni(111) single crystal layer, used as a substrate. The Ni layer itself was grown on a single crystal sapphire (0001). Carbon was deposited by chemical vapor deposition using a mixture of methane precursor with argon and hydrogen at atmospheric pressure implementing a constant gas flow. Varied were in the different experiments both the gas composition, deposition temperature and cooling rate Layers were examined under optical microscope, Raman spectroscopy, AFM, STM, SEM, EBSD, TEM and Cs-corrected HRTEM.

Formation of continuously grown epitaxial single layer graphene was observed over Ni(111) thin film substrate. Epitaxial growth was proven through STM measurements. The graphene atomic lattice is visible in the higher magnification STM images, in the smaller magnification images from the same place, nickel atomic steps are identified that mark traces of the nickel (111) planes at the surface. The atomic resolution STM images precisely match the orientation of the Ni steps. The nickel (111) planes are parallel to zigzag edges of the graphene according to our observation in several areas. Electron diffraction studies, also confirmed by STM, demonstrated that only one dominant orientation exists in the graphene by sampling several areas far (10μm–1mm away) from each other, both giving evidence of the epitaxial growth over an at least 1mm wide area.

On top of the continuously grown single layer graphene additional graphene and/or graphite flakes were observed with sizes varying between 10nm and 10μm. Most of the top flakes are turbostratically related to the epitaxial graphene. When the $H_2$ gas flow was increased during the deposition smaller flakes disappeared (Fig. 1). The remaining large flakes are located above the 30° grain boundaries or incoherent twin boundaries in the nickel substrate, as identified by SEM and EBSD investigations. Large areas (≈20-40 μm in diameter) of single layer, single crystal graphene, free of additional deposits and flakes were obtained for the best set of growth parameters.

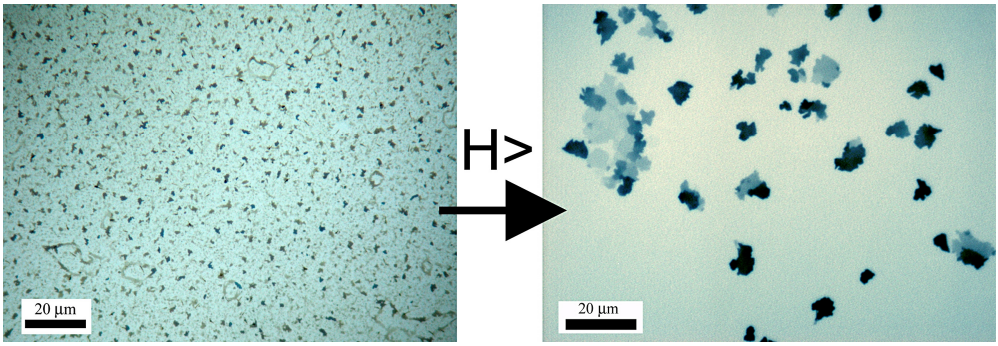


***Figure 1.*** *Optical images (left): low hydrogen flow rate, (right): the smaller flakes did not appear due to the larger hydrogen flow during the deposition.*

# Macroscopic characterization of graphene sheet grown on SiC surface by means of Auger Electron Spectroscopy depth profiling

L. Kotis, S. Gurbán, B. Pécz, A. Sulyok, and M. Menyhárd

Graphene because of its exceptional features is one of the most investigated material nowadays; practically all adaptable measurement methods have been applied to characterize its properties. As industrial scale production of graphene is mainly based on chemical vapour deposition, CVD, this fact has prompted new efforts to develop methods, e.g., for the determination of the thickness and homogeneity of the macroscopic graphene layers. If the graphene layer is on Ni and or SiC substrate, Raman spectroscopy, an otherwise versatile and accurate method, cannot be applied, thus, Auger Electron Spectroscopy, AES, was proposed to solve the task. Besides ease of use, AES has an additional advantage as it is applicable to study reasonably large surfaces with good lateral resolution. Furthermore, in this brief summary it will be shown that using AES depth profiling instead of single AES measurements the accuracy of the method is strongly improved. Macroscopic graphene sheets grown on SiC by CVD were depth profiled. To determine graphene thickness, AES depth profiles were simulated and then combined with "trial and error" method. Here, assumed initial structure of the sample (i.e., thickness of the graphene, that of the interface layer, and composition of the latter) was varied until simulated and measured depth profiles agreed. A typical result is shown in the Figure. It shows the measured and simulated depth profiles of $Si_{LVV}$ and $Si_{KLL}$ Auger peaks. Agreement between measured and simulated $Si_{LVV}$ depth profiles is reasonably good with R squared value of 0.98. The simulation resulted in the following parameters: graphene and interface layer thicknesses are 0.53±0.1 nm and 0.3±0.12 nm, respectively, while the Si concentration in the interface layer is 0.2 at%.

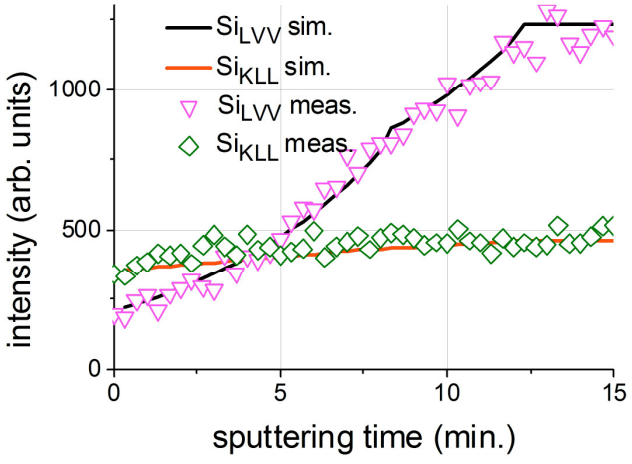


***Figure 1.*** *Intensity vs. sputtering time.*

# In situ investigation of Ni induced crystallization in amorphous Si thin films

***(TÉT-10-1-2011-0570, HUN92)***

Gy. Z. Radnóczi, E. Dodony, G. Battistig, B. Pécz, I. Stoimenos*, N. Frangis*, and N. Vouroutzis* (*Aristotle University, Thessaloniki, Greece)

The MILC (Metal Induced Lateral Crystallization) process was investigated in-situ in transmission electron microscope with a heatable sample holder. Model structures were grown onto thermal oxide coated Si substrates consisting of a CVD grown amorphous silicon (a-Si) layer, a silicon oxide ($SiO_x$) mask layer and a thin nickel layer as shown in Fig. 1. Prior to Ni deposition, windows (10x10 $\mu m^2$ and 100x10 $\mu m^2$) were opened in the $SiO_x$ mask layer to bring Ni in contact to the a-Si layer. Ni and a-Si thicknesses were selected such that all Ni could be accommodated in the underlying Si during nickel-silicide ($NiSi_2$) formation.

Cross sectional TEM specimens of the relevant sample areas near the window edge were prepared with FIB (Focussed Ion Beam), and heat treated in the microscope.

Gradual nickel-silicide formation starting from the interface was observed in-situ at temperatures as low as 250 °C as shown in Fig. 2. Further increasing the temperature caused the whole Ni amount in the window area to diffuse into the a-Si layer and start of lateral crystallization originating from newly formed $NiSi_2$ seeds. At higher temperatures up to 650 °C the lateral crystallization process was observed and investigated with analytical tools to prove the migration of $NiSi_2$ phase.

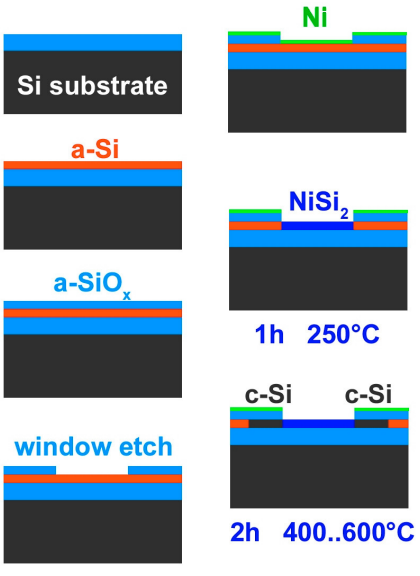


***Figure 1.*** *The construction of the model structure and in situ heating experiment.*

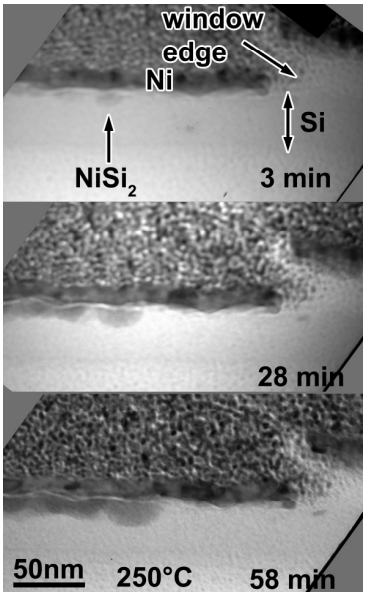


***Figure 2.*** *Nickel-silicide phase formation at the Si/Ni interface.*

# Solid phase epitaxy induced in Si by laser diode crystallization

J. L. Lábár, T. Schmidt*, and F. Falk*
*Leibniz Institute for Photonic Technology, Jena, Germany

Solid phase epitaxy (SPE) is a commonly applied technique in both transistor fabrication and production of solar cells. Beside other techniques, like aluminium-induced crystallization or furnace-based solid state epitaxy, laser-induced crystallization plays a crucial role in producing such c(rystalline)-Si layers. One of the most important factors during this process is the competition of SPE with random nucleation and growth in the volume of the starting a(morphous)-Si layer. Effect of the speed of temperature rise is examined in the present communication.

Pieces (1"*1"size) of n-type Si wafer with <111> orientation was used as a substrate. Amporhous Si of 550nm thickness was deposited on the cleaned wafer by electron beam evaporation at 250 °C. Crystallization of that a-Si is induced by a diode laser (λ=808nm). Time resolved reflectivity (TRR) was used to monitor the crystallization during the recrystallization process with a helium neon laser (λ=633 nm). Complete crystallization of the layer was reached. Finally, TEM lamellae were prepared from the cross-sections of the samples by mechanical cutting, followed by Ar-ion milling at 7keV. The lamellae were investigated in a JEOL 3010 HRTEM with the camera in the GATAN GIF Tridiem imaging filter.

The impacts of two laser powers were compared. The first caused the recrystallization temperature (≈1000 °C) be reached in 80ms, while for the other the same temperature rise took 2500ms.

The TEM bright field (BF) images show that for the slow temperature rise sample (Fig. 2) a much wider belt closer to the substrate has the same contrast as the substrate than in the sample with slower temperature rise (Fig. 1). This is an indication of the same orientation that was also proved by selected area electron diffraction patterns (SAED). Figs. 3 and 4 demonstrate that the epitaxial layer close to the substrate is full of stacking faults and twins. Twinning is seen both as the straight lines in Fig. 3 and in the appearance of the extra spots at 1/3 and 2/3 distances between the regular diffraction spots in the {111} type reciprocal directions. As enhanced twinning is frequently caused by small amount of contamination, we take it as an indirect evidence for the presence of contamination, which was below the detection limit of our instrumentation. SAED patterns recorded in areas like the bright regions in Fig. 1 show that those regions are misoriented from the substrate and that they are polycrystalline. Consequently, those regions are crystallized by random nucleation and growth.

Comparison of the two samples resulted in the conclusion that the speed of temperature rise plays a crucial role in moving the margin between epitaxial growth and random nucleation growth. Our final conclusion is that the nucleation rate rises faster with the temperature than the growth velocity does.

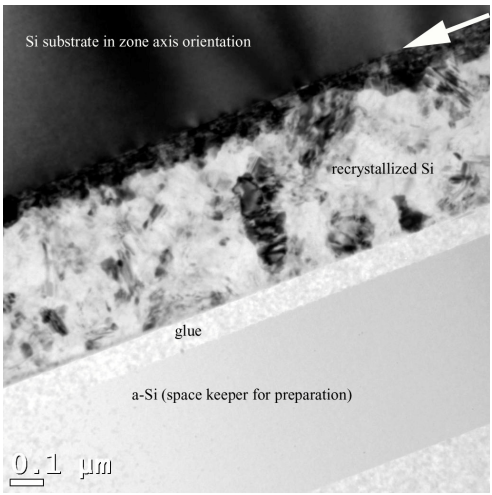


***Figure 1.*** *TEM BF image from the cross section of the sample with fast temperature rise (80 ms). Only a thin belt close to the substrate has the same contrast (and same orientation as proved by diffraction) as the substrate.*

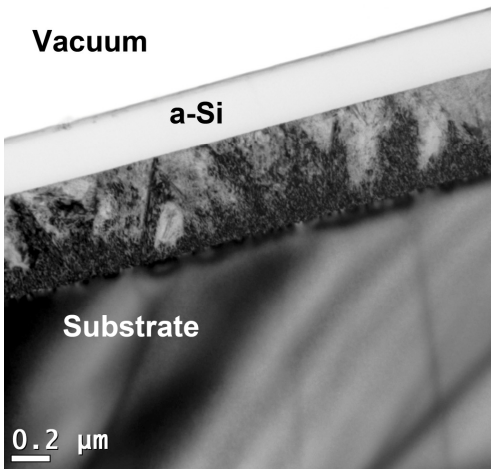


***Figure 2.*** *TEM BF image from the cross section of the sample with the slow temperature rise (2500 ms). Much larger fraction of the layer has the same contrast (and same orientation as proved by diffraction) as the substrate.*

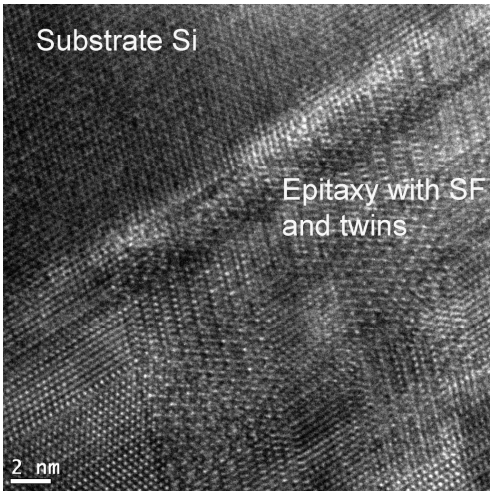


***Figure 3.*** *HRTEM image from the cross section of the sample with fast temperature rise (80 ms). Enhanced twinning is seen.*

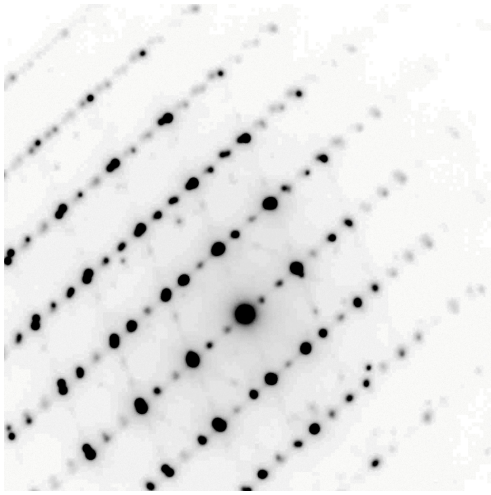

***Figure 4.*** *Selected area electron diffraction from the region shown in Fig. 3. Extra spots are caused by twinning.*

# Nickel metallization to p-InGaAs

J. L. Lábár, M. Menyhárd, S. Gurbán, K. Hoummada (IM2NP, UMR CNRS, Marseille, France), E. Ghegin (CEA, LETI, Grenoble, STMicroelectronics, Crolles, France), F. Nemouchi (CEA, LETI, Grenoble, France)

In a recent publication formation of a single $Ni_4InGaAs_2$ phase with hexagonal structure was described and epitaxial growth to the InGaAs substrate at 250 °C was claimed [J. Vac. Sci. Technol. B 31(1) 012202 (2013)]. Although formation of the hexagonal structure is confirmed in our studies, formation of a polycrystalline $Ni_6InGaAs_2$ reaction layer is observed at 350 °C.

A 300 nm thick lattice matched p-$(In_{0.53}Ga_{0.47})As$ layer was grown epitaxially on InP substrate. 20 nm Ni was deposited on it and covered with 7 nm TiN protecting film. The samples were RTP annealed for 60 s at 350 °C in nitrogen atmosphere to induce the solid state reaction between Ni and the InGaAs layer. The reaction product was studied by Auger depth profiling, cross sectional TEM and Atom Probe Tomography (APT). The AES analysis used 5 keV primary electron energy, 20 nA beam current with a diameter of 40 µm. For the depth profiling $Ar^+$ ions of 1 keV energy were applied and the angle of incidence with respect to the surface normal was 80°. All specimens were rotated during sputtering. The Ar pressure was $2.5*10^{-7}$ torr. The TEM lamellae were prepared by Ar-ion milling (10 keV, 2 mA) till perforation, followed by 2 keV ion milling to remove damaged layer. Both BF and HRTEM images and selected area electron diffraction patterns were recorded in a JEOL 3010, operated at 300 keV. The GATAN camera in the GIF Tridiem was used for imaging and a GATAN Orius camera in the JEOL 3010 recorded the diffraction patterns. Fast Fourier transforms (FFT) of the HRTEM images were also analyzed identically to diffraction patterns.

The reaction layer is about 55-60 nm thick polycrystalline film (Fig 1). Its composition is close to $Ni_6InGaAs_2$, as measured by AES. The same composition was also determined by APT. Examining both the individual grains one-by-one in the HRTEM image and of the FFTs from different grains in that HRTEM, we see that the growth is not epitaxial in general, since all grains have different orientations. As an example, a HRTEM image and the FFT for the reaction product grain indexed with the ProcessDiffraction program [Ultramicroscopy 103(3) 237-249. (2005)] are shown in Figs. 3, and 4, respectively. For the indexing we used the hexagonal structure published in [J. Vac. Sci. Technol. B 31(1) 012202 (2013)] but allowed for a small tolerance in the measured d-values. It is consistent with our observations in XRD measurements that the measured diffraction lines were slightly shifted from the values reported in the literature. The small change in the lattice parameters may be connected to the different composition.

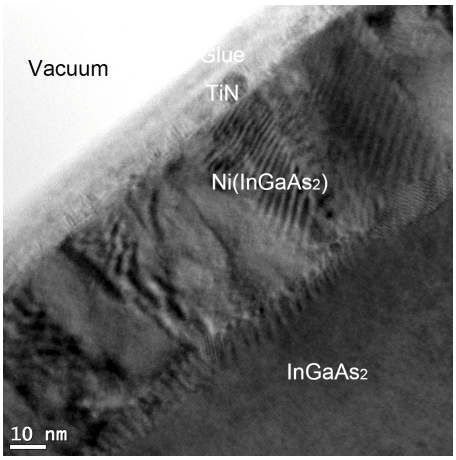


***Figure 1.*** *Polycrystalline reaction layer. The interface to the InGaAs is close to planar at large scale however, non-perfect planarity is obvious from the undulations following grains at the bottom interface.*

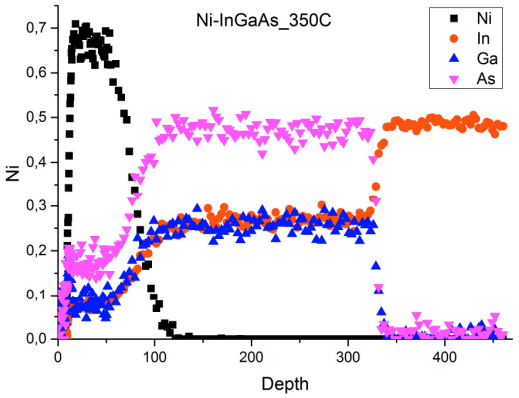


***Figure 2.*** *Auger depth profile of the distribution of elements in the reaction layer. It is seen that the composition is almost constant along the depth of the layer and it is close to $Ni_6InGaAs_2$, a value also measured with APT.*

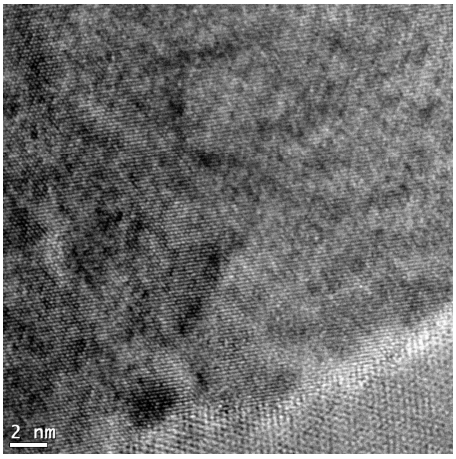


***Figure 3.*** *HRTEM image with a grain of the reaction product.*

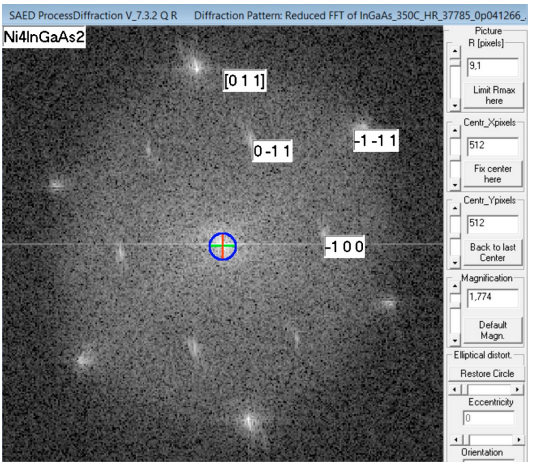


***Figure 4.*** *Central part of the FFT from the grain in Fig. 3, indexed as $Ni_4InGaAs_2$ allowing for a small tolerance in the d-values.*

# Novel improvement of a software for HRTEM investigation of grain boundaries

Á. K. Kiss, J. L. Lábár, E. F. Rauch (SIMaP, INP/CNRS, France),
and S. Nicolopoulos (NanoMEGAS Sprl, Belgium)

The new method helps to find neighbouring grains in polycrystalline materials, which can be oriented within the range of the TEM-goniometer into beneficial orientation for applying high resolution techniques on both of the grains. This experiment needs orientation mapping by transmission electron microscope and also calibration of the instrument. The orientation mapping is attained by the ASTAR precession/scanning tool [Materials Science Forum, Vol. 644 (2010) pp.1-7] installed on JEOL 3010 HRTEM. For calibration purposes, not only the rotation between diffraction and image mode but also the direction of the tilt axes of the sample holder compared to the image has to be measured. The tool used to obtain orientation maps serves orientation data of crystalline in a large area therefore in a short time a big amount of data is ready for the evaluation process looking for proper details. This is a real advantage compared to the manual, CBED-based orientation determining methods we used before.

In the next step we look for beneficial conditions for HRTEM imaging realized simultaneously in neighbouring grains: in the best scenario we are able to set low index zones parallel with the electron beam resulting in simultaneous lattice resolution, while the grain boundary lies also parallel with that. Of course this kind of optimum scenario has a low chance in the case of random orientation. Additionally, any of required orientations can only be tilted to the beam when it lies within the tilting range of the sample holder. Thus, investigations of grain boundaries are sometimes carried out with some compromise: we get compromised high resolution results also by orienting only one of the neighbouring grains to zone axis orientation, while only a single plane is resolved for its neighbour.

The evaluation process can be applied on both cubic and non-cubic crystal systems and even phase boundaries could be examined in principle, since the calculation of orientations and sample tilts are based on general, metric matrix formalism, using the same formalism to all crystal systems. Since the microscope has been calibrated, further investigations are available also on other instruments without the need of newly measured orientation maps.

In the present communication the method is illustrated on a cubic TiN polycrystalline thin film grown on a Si substrate. This is an example of compromised orientation, when only one of the grains is in true zone axis orientation and only one plane is resolved for the other. The dashed line on the HRTEM image helps the eye to follow the grain boundary.

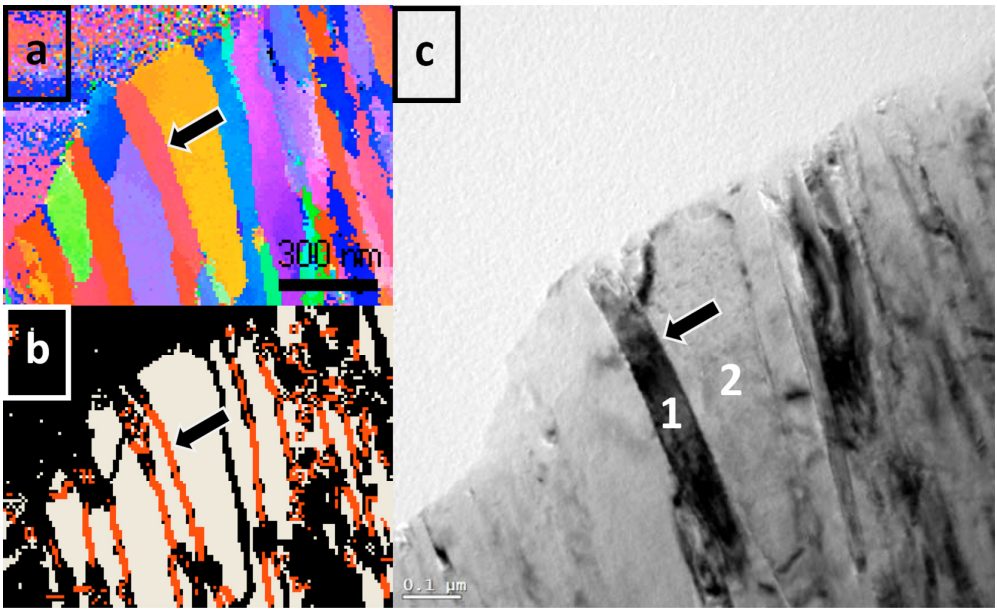


***Figure 1***. *Image of the scanned area in fcc-TiN: the chosen GB are marked by arrow, the neighboring grains are referred by "1" and "2". The orientation map of the scanned area, made by Astar – the different colors represent different orientations (a), GB-map with highlighted boundaries, which are appropriate to get simultaneous lattice resolution (b), BF image of the scanned area –grain "1", lying in zone axis orientation exhibits dark contrast (c).*

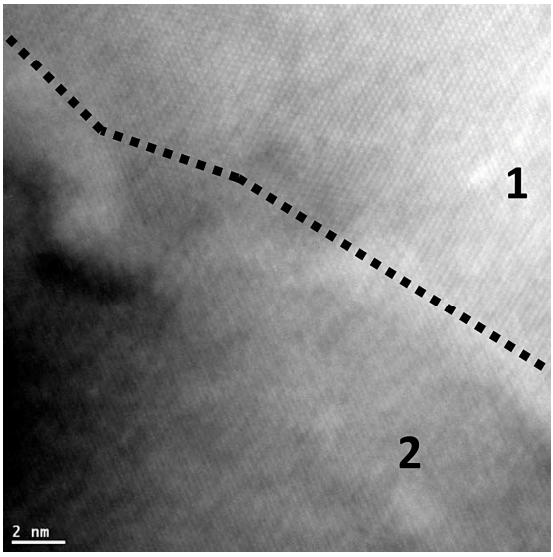


***Figure 2.*** *HR image taken on the chosen GB. Grain "1" shows lattice resolution in the [110] zone direction, while the (200) planes are only resolved for grain "2".*

# *Nanostructures Department*

**Head: Prof. László Péter BIRÓ, Corresp. Member of the HAS, Res. Prof.**

**Research Staff**

- Zsolt Endre HORVÁTH, Ph.D.
- Prof. József GYULAI, Member of the HAS (Professor Emeritus)
- Antal Adolf KOÓS, Ph.D. (on leave till September 2013)
- Géza István MÁRK, Ph.D.
- Zoltán OSVÁTH, Ph.D.
- Levente TAPASZTÓ, Ph.D.
- Krisztián KERTÉSZ, Ph.D
- Péter NEMES-INCZE, Ph.D.
- Enikő HORVÁTH, Ph.D (on leave)
- Zofia VÉRTESY, Ph.D.

**Ph.D. students / Diploma workers**

- Gergely DOBRIK, Ph.D. student
- Gábor MAGDA, Ph.D. student
- Péter Lajos NEUMANN, Ph.D. student (on leave)
- Bernadeth PATAKI, Ph.D. student
- Gábor PISZTER, Ph.D. student (from September 2013)
- István TAMÁSKA, Ph.D. student (until June 2013)
- Péter VANCSÓ, Ph.D. student
- Vince OBRECZÁN, diploma worker

**Technical Staff**

- Zoltánné SÁRKÁNY, technician

The Nanostructures Department has an almost two decades expertise in the production and characterization of various nanostructures. In recent years in the focus of work were various carbon nanostructures (CNTs, graphene and few layer graphite) their nanoarchitectures, bioinspired photonic nanoarchitectures and applications of these nano-objects in various fields in nanotechnology, nanoelectronics, sensorics and environmental protection. The most relevant results in 2013 are detailed below:

- We implemented our atomic resolution STL method developed on the surface of HOPG for cutting GNRs to work on CVD grown graphene
- We developed an AFM based method to write strain supperlattices in graphene/$SiO_2$/Si
- We developed an edge selective chemical etching method to produce armchair edges in HOPG and transferred the nanopatterns on $SiO_2$/Si
- By detailed computer modeling of the grain boundaries we explained the deterioration of electronic transport in CVD graphene
- We started the STM work on novel 2D materials, on $MoS_2$ we obtained good atomic resolution and spectroscopic data in agreement with the literature
- We showed that the photonic nanoarchitectures in the scales of butterflies can be conformally modified by ALD and this has effect on the sensor behavior.

For more details, please feel free to visit the web page of the Nanostructures Department: ( http://www.nanotechnology.hu/ )

# Preparing graphene nanoribbons with zigzag and armchair edges on gold substrates

*(KHJLN 2010K000980, OTKA PD84244, OTKA K101599)*

P. Nemes–Incze, L. Tapasztó, G. Zs. Magda, Z. Osváth, G. Dobrik, X. Jin (KRISS, Korea), C. Hwang (KRISS, Korea), and L. P. Biró

The application of graphene in nanoelectronic devices, particularly as active elements in digital – logic circuits needs a lot of innovation on multiple fronts. The most challenging aspects of this research are twofold. Firstly, we need to be able to prepare graphene on a large scale, with good control over the quality of the graphene crystal and having low defect concentration and overall homogeneous properties. Secondly, the properties of the graphene layer need to be modified, most importantly to open a band gap, while keeping the good charge transport properties of the material. Tuning the properties of graphene and inducing a band gap can be achieved by confining the charge carriers along one direction in the graphene plane by cutting graphene into ribbons of a few nanometers in width. The properties of graphene nanoribbons are dependent on both the nanoribbon width and the crystallographic orientation of the edges. Our group has developed the scanning tunneling microscope lithography (STL) based method which is able to create graphene nanoribbons with well-defined edge orientation, having a width of a few nanometers [Tapasztó L., et al.: Nat. Nanotechnol. 3, 397–401 (2008)]. However, it has only been demonstrated on the top layer of graphite. In order to allow practical applications of this powerful lithography technique, it needs to be implemented on single layer graphene. We demonstrated the preparation of graphene nanoribbons with well-defined crystallographic orientation on top of gold substrates [Nemes-Incze P. et al.: Appl. Surf. Sci. 291 (2014) 48–52].

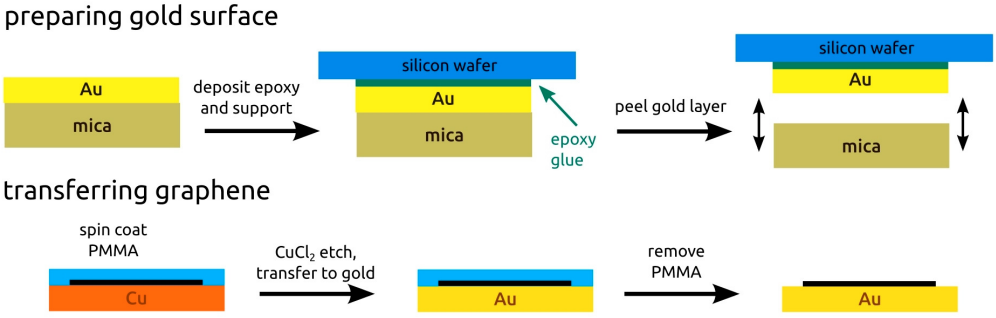


***Figure 1.*** *Preparing the gold surface and transfer of CVD graphene onto the gold. In the first step, gold is thermally evaporated onto freshly cleaved mica. A piece of silicon wafer is glued to the top of the gold by epoxy. After the epoxy has cured, the gold can be peeled off the mica surface. The gold surface which was in contact with the mica can then be used as an atomically flat substrate to transfer graphene. The CVD graphene transfer to the gold was done by the standard transfer technique using PMMA.*

So called “stripped gold” substrates have and atomically smooth surface and are an ideal support for graphene and STL. The sample preparation procedure is outlined in Fig. 1. The atomically flat terraces of the gold surface can be used to cut the graphene layer by STL. After revealing the armchair and zigzag directions of the graphene surface by atomic resolution imaging, the STM tip is moved across the surface in the given direction, with a speed of 1 nm/s and a bias voltage of 2-2.6 V. The magnitude of the required bias voltage is dependent on the ambient humidity and it is carefully raised until the etching of the graphene under the tip is observed this insures a smooth cut. Nanoribbons with both armchair and zigzag edges have been prepared, as can be seen in Fig. 2.

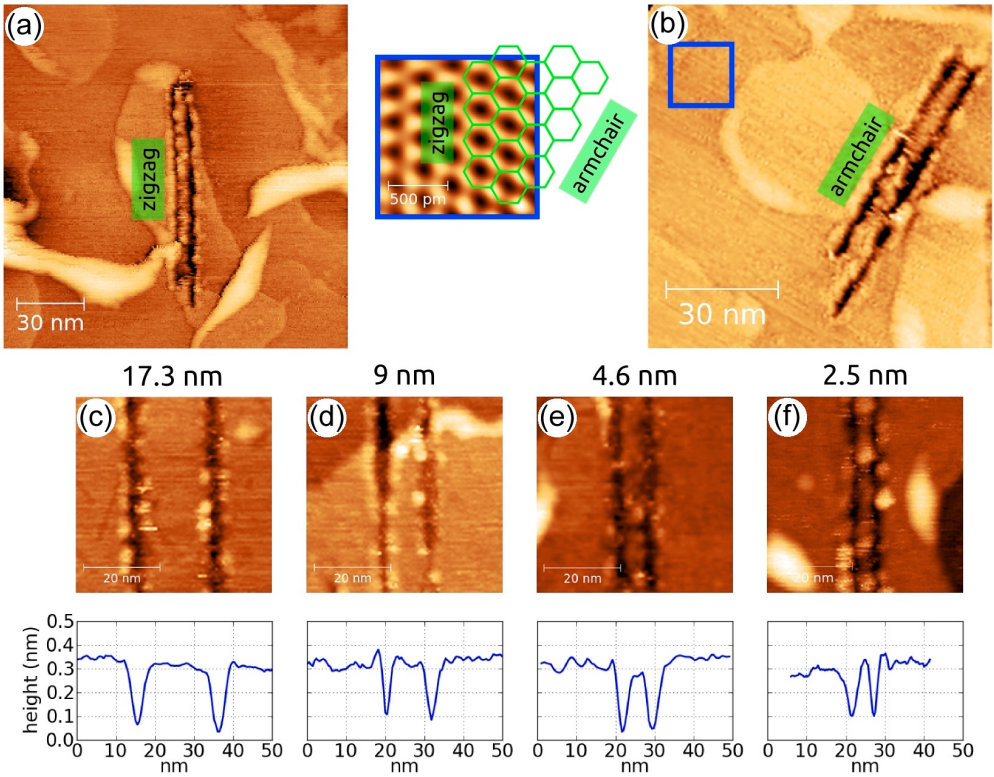


***Figure 2.*** *Various nanoribbons cut into the CVD graphene layer on the gold surface. (a) Zigzag edged nanoribbon and (b) armchair edged nanoribbon cut by STL. Inset: atomic resolution image of the graphene surface, showing the zigzag and armchair directions. (c-f) Nanoribbons cut in the zigzag direction, with various widths. Height profiles can be seen beneath the STM topography images.*

Because of the high resolution of STL, we have been able to prepare GNRs with a lateral size down to 2.5 nm, which corresponds to roughly 10 benzene rings across. The narrow width of these nanoribbons and their well oriented edges paves the way for the exploration of the band structure and edge specific physical properties of these nanostructures.

# Tailoring strain superlattices in graphene

*(KHJLN 2010K000980, OTKA PD84244, OTKA K101599)*

P. Nemes–Incze, C. Hwang (KRISS, Korea), and L. P. Biró

Graphene is a two dimensional material with very promising properties, mainly due to the Dirac fermion-like behaviour of its charge carriers. Also due to the 2D nature of graphene its properties can be readily tailored using scanning probe techniques. Our group has demonstrated this by using scanning tunneling microscope lithography to cut extremely narrow ribbons from graphene, having semiconducting or metallic properties. The physical properties of graphene can also be tailored by inducing superlattices in graphene. Such superlattices can typically be created by moire patters in van der Waals heterostructures, periodic doping etc. These artificial lattices create new quasi-particles in graphene, which allow us to explore new realms of physical phenomena, not previously accessible in condensed matter systems [Hunt B, et al.: Science 340, 1427–1430 (2013)]. However, the lattice parameters of the superlattices prepared thus far are not easily tuneable.

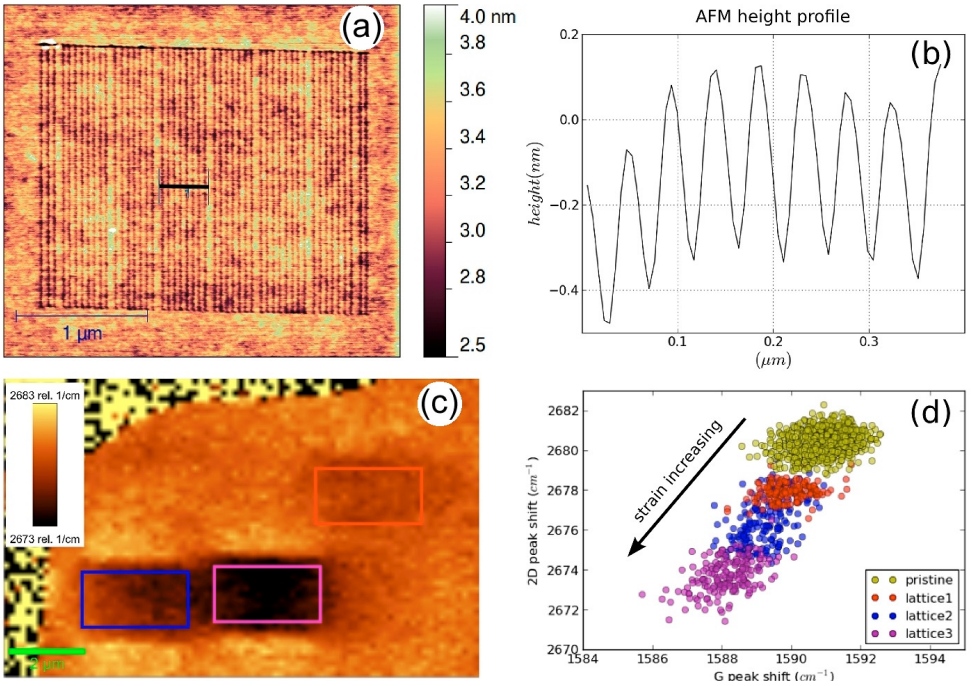


***Figure 1.*** *(a) AFM image of a 1D strain lattice in graphene. (b) Height profile along the black line in (a). (c) Raman map of the 2D peak shift on a graphene layer having three periodic line patterns with differing indentation depth, shown by colored rectangles. The lower the downshift of the 2D mode wavenumber, the higher the tensile strain in the graphene layer. (d) Correlation graph of the G and 2D Raman peaks of the three indentation line patterns and of pristine graphene. The lower the redshift, the higher the tensile strain.*

We have developed an atomic microscopy (AFM) lithography based technique to create superlattices in graphene with tunable lattice parameters. The tip of an AFM can be used to indent the graphene sample supported on $SiO_2$. This way the support suffers plastic deformation and the graphene layer on top adheres to the deformed substrate. The place where the graphene has been pushed into the substrate mechanical strain is induced in the graphene. Due to the versatility of the AFM, this kind of indentation can be done in a periodically patterned fashion. Fig. 1 shows one such periodic lattice of indentation lines in graphene. This one dimensional lattice increases the strain in the graphene layer, giving rise to significant changes in the Raman spectra of the graphene. In graphene subjected to tensile strain, as is the case here, the most intense peaks in the Raman spectra of graphene suffer a redshift in their wavenumber. Thus, by scanning the laser spot of a confocal Raman microscope along the graphene sample, the strain induced by the superlattice can be mapped.

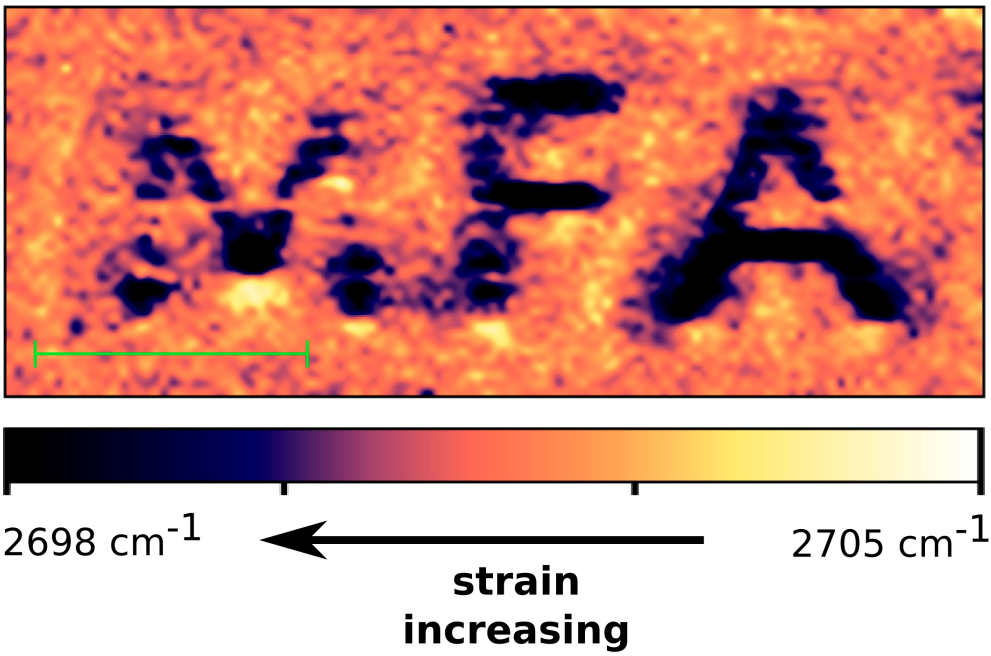


***Figure 2.*** *Demonstrating the versatility of the strain patterning. The abbreviated name of our institute has been written into a graphene layer supported on $SiO_2$. The strain can be visualized by measuring the change in the wavenumber of the Raman 2D peak of graphene. The scalebar is 4 microns long.*

To demonstrate the highly versatile patterning possibilities we have “written” the initials of our institute into a flake of graphene by strain (see Fig. 2). Our AFM based superlattice preparation technique may open new possibilities for tailoring the properties of graphene by strain engineering.

# Selective etching of armchair edges in graphite

*(OTKA PD 84244, OTKA K101599)*

G. Dobrik, L. Tapasztó, and L. P. Biró

Due to its high electron mobility and long coherence length, graphene attracts an increasing interest as a promising new material for next-generation electronic devices. However, a major drawback for mainstream logic applications is that graphene remains metallic even at the charge neutrality point. The production of graphene nanoribbons (GNRs) with well controlled crystallographic orientation and atomically precise edges is considered to be the most straightforward way to open a gap in the electronic structure of graphene. Theoretical studies predicted that this gap strongly depends on both the width and crystallographic orientation of GNRs. The largest band gap can be achieved for narrow armchair-edged ribbons. A deviation of a few degrees from the armchair crystallographic orientation can drastically decrease the size of the band gap. Therefore, if nanoelectronic applications are envisaged, experimental methods producing graphene nanostructures with precisely armchair orientations are of particular importance.

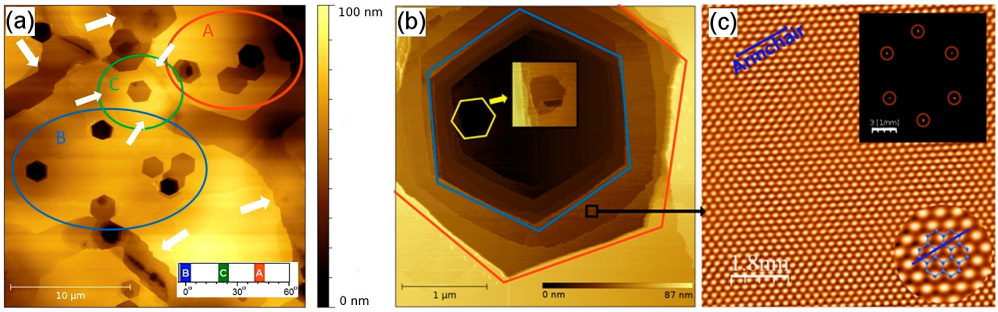


***Figure 1.*** *(a) AFM image of the etched HOPG surface. The surface exhibits two types of characteristic features: wide trenches (marked by white arrows) and hexagonal holes (marked by colored ovals). (b) STM image of an etched hexagonal hole revealing several graphite grains of different orientation (c) Atomic resolution STM image near the red hexagonal edge (marked by a black square).*

Recently we proposed [29] a simple method for producing highly regular hexagonal holes with precisely armchair oriented edges in graphite, then exfoliate them into patterned graphene and few layer graphite flakes (FLG). Our method is based on the crystallographically selective oxidation of graphitic layers in controlled, oxygen containing atmosphere. When HOPG samples are heated up in oxygen containing atmosphere the etching of their surface occurs (Fig. 1 (a)). The surface exhibits two types of characteristic topographic features: i) randomly curved and branching trenches, and ii) hexagonal holes of very regular shape. The first type features originate from etched grain boundaries while the second type features most probably originate from point-like native defects. The STM image of a nested hexagonal hole-

system can be seen in Fig. 1 (b). The atomic resolution image in Fig. 1 (c) was acquired close to the hole-edge in the third layer (marked by a black square). In the atomic resolution STM image in Fig. 1 (c) the blue line is parallel with the edge of the etched hexagon at the same level (third layer from top). It is apparent that the type of edge is exactly of armchair orientation as also shown in the inset in the lower right corner.

We found that the size of the etched hexagons strongly depends on three particular parameters; namely, the etching temperature, the duration of the oxidation and the oxygen concentration of the reaction atmosphere. The average diameter of the resulting hexagons exponentially depends on temperature, and is linearly dependent on both the heat treatment time and the oxygen concentration of the gas mixture. Therefore, if these parameters are precisely regulated, then not only the edge orientation but also the size of the as produced nanoarchitectures can be controlled.

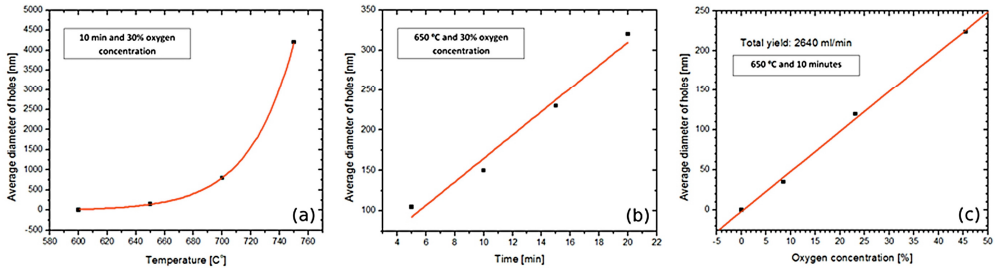


***Figure 2.*** *Average diameter of the hexagonal holes as a function of the etching temperature (a.), duration (b.), and oxygen concentration (c).*

The above described method provides bulk HOPG crystals with nanopatterned top layers containing hexagons of precisely armchair oriented edges. By exfoliation of these samples it is possible to produce graphene and FLG samples with hexagonal holes of armchair edges. Fig. 3 (a) shows a FLG flake with a hexagonal structure exfoliated and transferred onto $Si/SiO_2$ substrate. Fig. 3 (b) shows a single layer graphene flake with a 80 nm diameter armchair-edged hexagonal hole on $Si/SiO_2$ substrate [29].

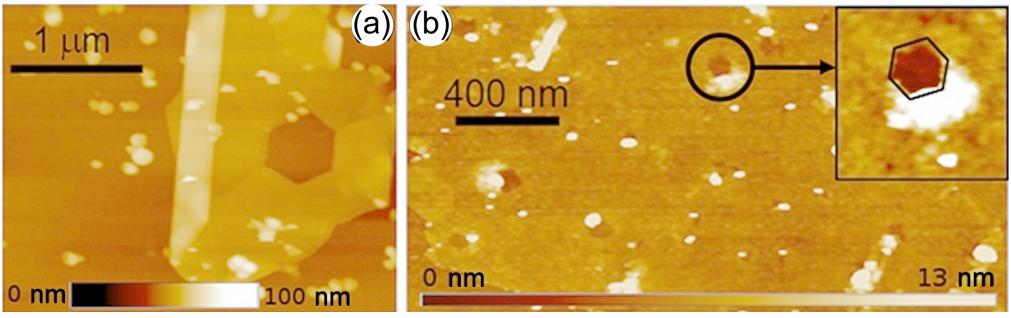


***Figure 3.*** *Nanopatterned FLG (a), and graphene (b) flakes transferred onto $SiO_2$ surface.*

# Effect of the disorder on the electronic and transport properties in graphene grain boundaries

*(OTKA NKTH 101599, KHJLN 2010K000980, EU FP7 FAEMCAR 318617)*

P. Vancsó, G. I. Márk, Ph. Lambin (FUNDP, Belgium), A. Mayer (FUNDP, Belgium)
C. Hwang (KRISS, Korea), and L. P. Biró

Chemical vapour deposition (CVD) on Cu foil is one of the most promising methods to produce graphene samples despite of introducing numerous grain boundaries (GBs) into the perfect graphene lattice. By using wave-packet dynamical (WPD) simulations and tight-binding (TB) calculations we investigated the effect of the structure of GBs on the transport and electronic properties. In the WPD simulations the electrons are injected from a simulated scanning tunnelling microscope (STM) tip, which is situated above one of the grains, far from the GB line, and then their time evolution is followed while crossing through the GB.

Three model GBs with increasing disorder were created in the computer (Fig. 1): a periodic 5-7 GB, a "serpentine" GB, and a disordered GB containing 4 to 8 membered rings and vacancies. In the first and the second geometry, the C atoms preserve their sp2 symmetry, but the disordered geometry has two-coordinated C atoms as well.

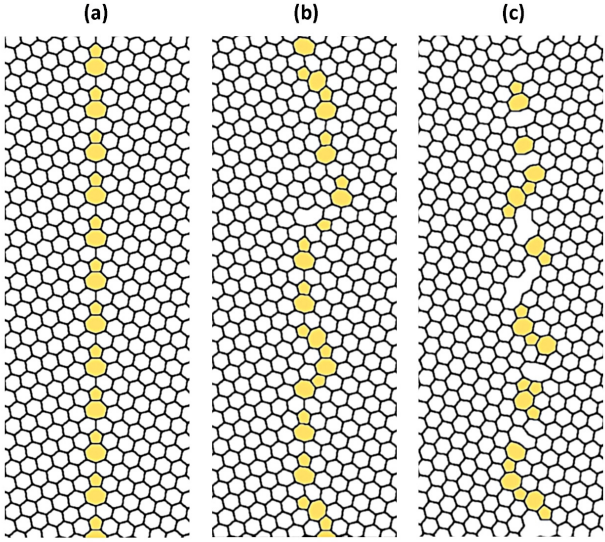


***Figure 1.*** *Structures of the GBs, pentagons and heptagons are highlighted. (a) Periodical pentagon-heptagon GB (b) Serpentine GB without periodicity (c) Disordered GB containing several defects and non-hexagonal carbon rings. Structure (b), and (c) generated by a Monte-Carlo like procedure.*

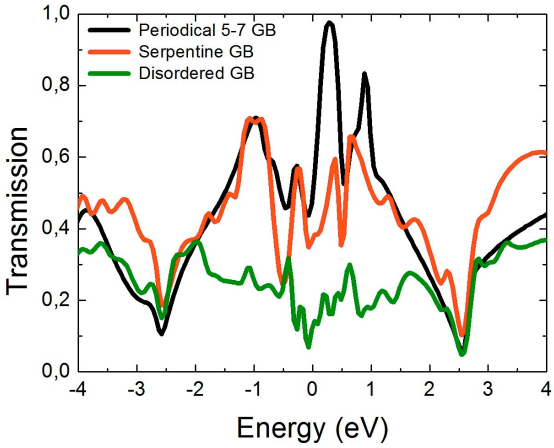


***Figure 2.*** *Transmission functions of the GBs calculated by WPD method. Reduced transmission values appear for the low energy charge carriers in the case of the disordered GB (green line).*

Transmission functions of three modelled GBs are shown in Fig. 2. Due to the preserving sp2 symmetry and the high ratio of pentagons and heptagons, the periodical and "serpentine" GB has similar transmission values. In contrast to the previous geometries, we observed suppressed transmission values around the Fermi energy in the case of the disordered GB. In order to identify the main scattering centres of the disordered GB we performed TB electronic structure calculations. The results have shown that vacancies and "extreme" (4 or 8 membered) polygons has significant density of states (DOS) values at the Fermi energy (Fig. 3). We identified these defects as the main scattering centres inside the disordered boundaries, which considerably diminish the electron transmission of the disordered grain boundaries.

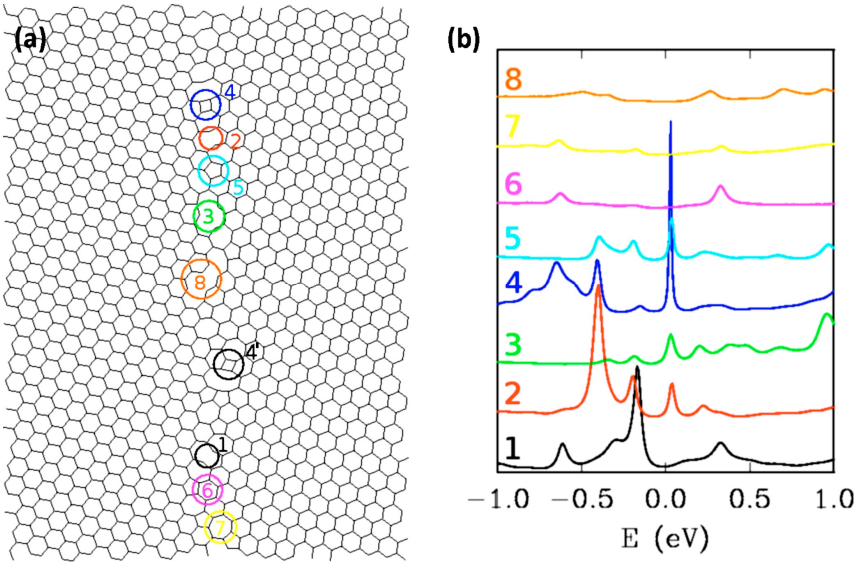


***Figure 3.*** *Tight-binding electronic structure calculations for the disordered GB: (a) Different defects are numbered and marked by circles, (b) LDOS functions of the atoms within the circles.*

# Novel 2D materials beyond graphene: $MoS_2$

***(OTKA K108753)***

G. Magda, G. Dobrik, L. P. Biró, and L. Tapasztó

The discovery of graphene in 2004 has drawn the attention of researchers towards a whole new family of layered (Van der Waals) materials that can in principle be exfoliated into single layers. One particularly interesting material of this new class is molybdenum disulphide ($MoS_2$).

From many aspects $MoS_2$ is similar to graphene, but it also has its very distinctive properties. Just like graphite, $MoS_2$ is a layered crystal, but when exfoliated into single layers, it does not truly consist of one atom thick layer, but three layers: two sheets of sulphur atoms sandwiching a single molybdenum layer between them. On the other hand, in contrast to graphene, $MoS_2$ is a semiconductor. This could be a big advantage for electronic applications; however, a limiting factor is that $MoS_2$ sheets cannot match the outstanding mobility offered by graphene.

We have prepared multilayer $MoS_2$ samples by mechanical exfoliation and performed Scanning Tunneling Microscopy investigations. The STM image in Fig. 1a reveals that $MoS_2$ has indeed a layered structure consisting of atomically flat sheets. We were able to achieve atomic resolution images revealing a hexagonal lattice with a lattice constant of about 0.32 nm (Fig. 1b). This can be interpreted by imaging only the top hexagonal lattice of sulphur atoms. The corresponding structural model for our STM findings is shown in Fig 1c.

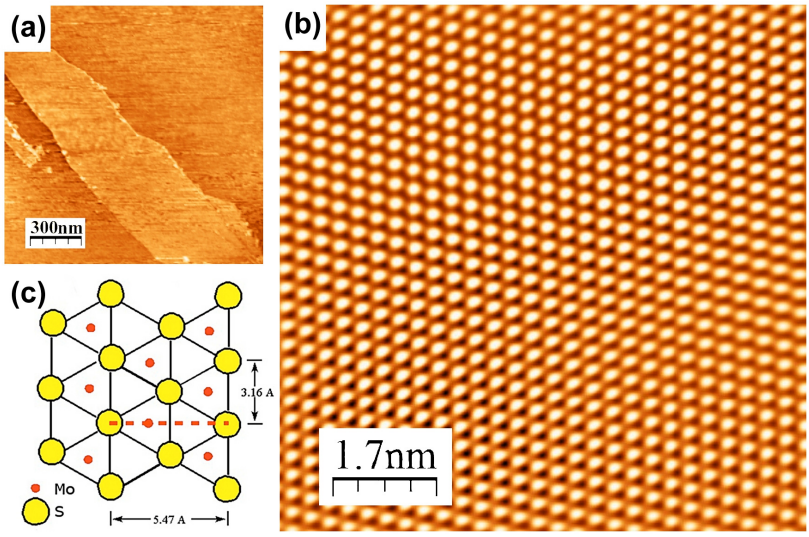


***Figure 1.*** *(a): STM image of the surface of exfoliated multilayer $MoS_2$ flake, (b): Atomic resolution STM image of $MoS_2$ revealing a hexagonal lattice of sulphur atoms, (c): Schematic atomic structure of $MoS_2$ surface, corresponding to our STM observations.*

In order to investigate the electronic properties of $MoS_2$ sheets we have performed tunneling spectroscopy measurements. Our spectroscopy data shown in Fig. 2 reveal the opening of a band gap of about 1.2 eV. This is in striking contrast to the case of graphene where no band gap was found in similar measurements. Our measured band gap is in good agreement with the expected band structure of bulk $MoS_2$ samples having an indirect band gap of 1.29 eV. The good agreement with the gap bulk value is due to the fact that the measured flake is a multilayer. Once the $MoS_2$ is exfoliated into single layers, the indirect band gap of 1.2 eV is expected to transform into a direct band gap of about 1.9 eV.

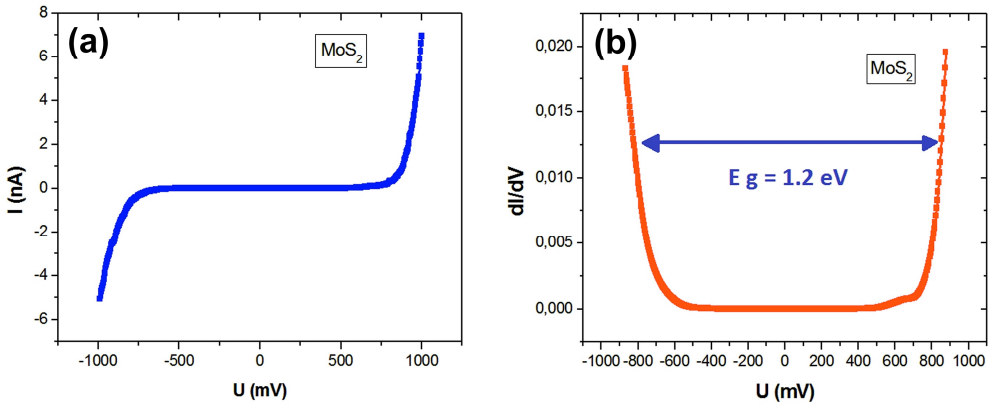


***Figure 2.*** *(a): Scanning tunneling spectroscopy measurements on multilayer $MoS_2$ revealing the semiconductor nature of the material, (b): with a band gap of 1.2 eV.*

While graphene has to be engineered with almost atomic precision in order to open a band gap and enable its use in digital electronic devices, the above demonstrated semiconducting nature of $MoS_2$ single layers makes them directly suitable for electronic applications. One drawback, compared to graphene, is the much more reduced mobility of charge carriers in these samples, which does not make it suitable to replace graphene for future high speed electronic applications.

Similar to graphene, if we are able to fabricate nanostructures from $MoS_2$ sheets new physics and applications possibilities will open up. It has been predicted theoretically, that removing a top sulfur atom creates a new electronic state within the gap, near the Fermi energy. This implies that removing a whole line of sulfur atoms in principle gives rise to a metallic wire within the semiconducting $MoS_2$ layer.

Also particular edges of well-defined crystallographic orientations in $MoS_2$ nanoribbons are expected to give rise to intriguing magnetic edge states, which could be exploited in future spintronic applications. We are working on adapting our STM lithographic method, which is the most precise nanofabrication technique of graphene, in order to pattern $MoS_2$ sheets with nanometer precision and predefined crystallographic edge orientation. This is expected to give us access to the so far unexplored physic of $MoS_2$ nanostructures.

# Vapour sensing on bare and modified Blue butterfly wing scales

***(OTKA PD83483)***

K. Kertész, G. Piszter, Zs. Baji, E. Jakab (CNS, Hungary),
Zs. Bálint (HNHM, Hungary), Z. Vértesy, and L. P. Biró

In the case of butterflies possessing structural colour, the wing scales contain a photonic nanocomposite material constituted from chitin (high refractive index) and air (low refractive index). The reflected colour is defined by the periodicity and refractive index contrast of the structure. Measurable structural color change occurs when its low refractive index component is replaced by an (air + vapour) mixture, resulting in a concentration and vapour species dependent optical reflectivity variation. It was shown that the reflectivity of the nanoarchitecture, its surface chemistry and characteristic pore size can be modified with a high degree of precision by Atomic Layer Deposition (ALD) of $Al_2O_3$ onto the scales. If the thickness of the deposited layer is controlled with nanometer precision, the spectral position of the reflectance maximum can be finely tuned. The response signal of pristine and ALD modified butterfly wings is compared in vapour sensing experiments.

In our experiments we used Polyommatus icarus butterfly species, well characterized earlier both structurally and spectrally. For a complete surface modification all the pores in the scales have to be covered uniformly along the full depth of the layered nanostructure. It was shown that with proper precursor management even in very high aspect ratio structures the complete coverage can be achieved with ALD.

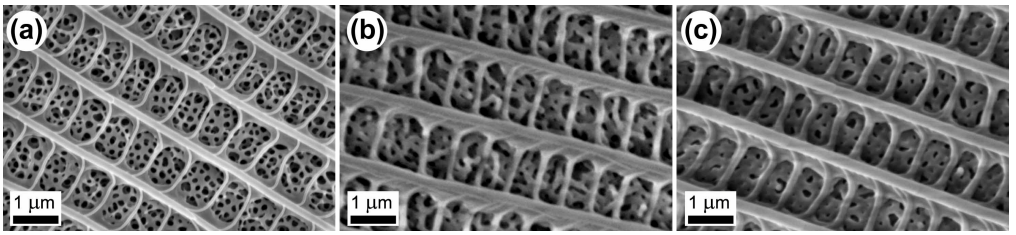


***Figure 1.*** *Scanning electron micrographs of Polyommatus icarus wing scales. (a): original condition, without deposition, (b): 20 nm, and (c): 40 nm of deposited $Al_2O_3$.*

For the vapour sensing experiment the untreated and the coated samples were laid into an air-proof aluminium cell which had gas inlet and outlet and a quartz window to provide UV transmittance. The optical reflectance measurements were done through the quartz window using a modular fibre optic spectrophotometer. The gas mixing equipment was based on digital flow controllers which set the vapour concentration by letting pass synthetic air and saturated volatile vapor (from gas bubblers containing the liquids) in the required ratio. During the measurements the colour of the wing in synthetic air was set as a reference, therefore in the vapour detection measurement the variations in the reflectance were followed. This means that the reflectance of the wing in air will be taken as 100% for the full wavelength range while the vapour mixture results a change in the optical properties of the wing, which generates a deviation of the reflectance spectra from the reference. The

deviation of the reflectance was recorded as a function of time while concentration of the vapours was increased in 20% steps. The temporal evolution of the optical reflectance variation can be represented as a 3D surface plot (Figs. 2b, c). The pore size of the photonic crystal structures in the studied butterfly wing was 200 nm or smaller, in the pepper-pot type nanoarchitecture of P. icarus there are circular air voids (Fig. 1a). We made experiments starting from thinner ALD-deposited layers: 5, 10, 20, 30 and 40 nm of $Al_2O_3$, respectively. The SEM image in Fig. 1 shows the differences in the P. icarus scale surface while no ALD layer is present (a), and after 20 respective 40 nm of $Al_2O_3$ deposition (b and c). We observed the photonic band gap shift for the pepper-pot type nanoarchitectures. On the blue butterfly wings even with the naked eye one can observe the change to a greenish hue, depending on the thickness. Fig. 2a shows the changes of the reflectance with increasing ALD layer thickness.

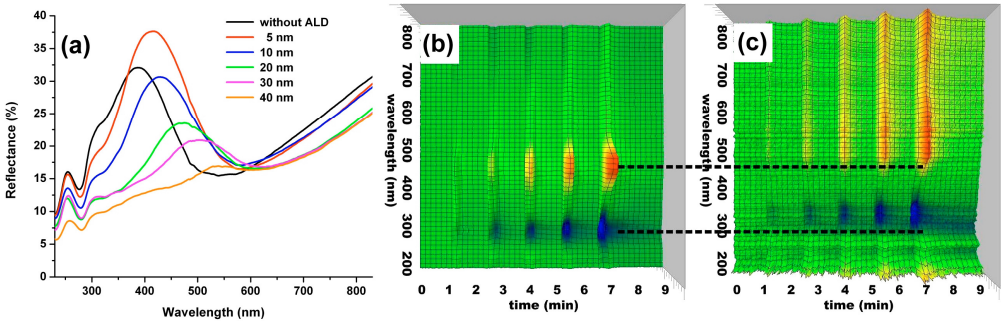


***Figure 2.*** *(a): Optical reflectance spectra of Polyommatus icarus wings in the original state (without ALD) and with increasing thickness of deposited $Al_2O_3$. On the right, signals on Polyommatus icarus wing in ethanol vapor can be seen comparing the uncoated (b), and 5 nm thick $Al_2O_3$ layer (c). (Green corresponds to the reflectance unchanged from that in ambient air, blue shades correspond to the negative change, while yellow-red, to the positive peaks.)*

The peak at 387 nm for the wing before ALD shifts towards the longer wavelengths which means the (red)shift of the spectral position (Fig. 2a). Therewith, the $Al_2O_3$ layer also changes the characteristic size of nanopores which is expected to influence the gas/vapour sensing properties. Comparing the spectral position of the signal, P. icarus wing was measured in ethanol vapour before (Fig. 2b) and after (Fig. 2c) a 5 nm $Al_2O_3$ deposition. The 3D colour graph is shown from the top, for the easier comparison of the wavelengths. One can see in the case of the modified sample that the positive and negative peaks are shifted towards the longer wavelengths. The red shift is now extended with the broadening of the positive peaks. The selectivity, i.e. the characteristic response for different vapours given by a certain photonic nanoarchitecture is preserved after the ALD modification.

Careful modification of the naturally occurring nanoarchitectures may be useful in several aspects: (i) within certain limits the reflectance maximum can be tuned to the desired position; (ii) the surface chemistry may be modified; (iii) the reflectivity can be improved by optimizing the filling fraction ratio.

# *Photonics Department*

**Head: Miklós FRIED, D.Sc., scientific advisor**

**Research Staff**

- Péter PETRIK, Ph.D.
- Miklós SERÉNYI, D.Sc.
- András DEÁK, Ph.D.
- Antal GASPARICS, Ph.D.
- Norbert NAGY, Ph.D.
- András HÁMORI, dr. Univ.
- Róbert HORVÁTH, Ph.D.
- Csaba MAJOR, Ph.D.
- György JUHÁSZ, dr. Univ.
- Péter KOZMA, Ph.D.
- Zsolt LACZIK, Ph.D. (on leave)
- Tivadar LOHNER, C.Sc.
- György KÁDÁR, D.Sc.
- Sándor KURUNCZI, Ph.D.
- János MAKAI, C.Sc. (part-time)
- Olivér POLGÁR, Ph.D.
- Miklós RÁCZ, Ph.D. (part-time)
- Ferenc RIESZ, C.Sc.
- Inna SZÉKÁCS, Ph.D.
- Gábor VÉRTESY, D.Sc.
- Csaba S. DARÓCZI, dr. Univ.

**Technical Staff**

- Rózsa Mária JANKÓNÉ, technician

**Ph.D. students / Diploma workers**

- Dániel PATKÓ, Ph.D. student
- Emil AGÓCS, Ph.D. student
- Bálint FODOR, Ph.D. student
- Eszter FÜLÖP, Ph.D. student
- Norbert ORGOVÁN, Ph.D. student
- Judit NÁDOR, Ph.D. student
- Krisztina JUHÁSZ, Ph.D. student
- Rita SALÁNKI, Ph.D. student
- Beatrix PÉTER, Ph.D. student

Magnetic Adaptive Testing (MAT) is a recently developed nondestructive magnetic measurement method, which is based on systematic measurement and evaluation of minor magnetic hysteresis loops. MAT seems to be a good method for replacing the destructive test measurements to predict the life expectancy of the neutron radiation fluence of nuclear reactor structural materials.

In the frame of a "National technology development" project: „*Equipment development for industrial size thin film optical mapping*" and an ENIAC JU project: "*E450EDL European 450mm Equipment Demo Line*" growing (30, 45, 60 and 90 cm) sample-size prototypes of optical mapping device are developed.

In the frame of an EU FP7 project (UNION, *Ultra-versatile Nanoparticle Integration into Organized Nanoclusters*) plasmonic, magnetic and semiconducting nanoparticles are assembled in homo and heteroclusters. The aims are to utilise the full control over the interaction-potential between different nanoparticles in order to achieve nanoparticle-assemblies with enhanced functionality. The envisaged field of application are: **theranostics** (therapy and diagnosis): magnetic and semiconducting nanoparticles are assembled into clusters and combined with lipid nanoparticles;

thermoelectrics: two different types of semiconducting nano crystals are co-assembled into highly organised micron sized clusters for further processing in thermoelectric device fabrication; lighting applications: plasmon-enhanced photoluminescence is targeted by combining plasmonic and semiconducting nanoparticles!
The Photonics Department incubated the „Lendület" project: „Advanced label-free biosensors for proteins and cells" financed by the Hungarian Academy of Sciences.

## Makyoh topography

### *(KMR_12-1-2012-0265, KMR_12-1-2012-0226)*

F. Riesz and J. P. Makai

In 2013, activities were concentrated on measurement theory, instrumental development as well as applications. The nonlinearity and related features of Makyoh-topography imaging was studied (continuation from previous years).
The Makyoh-topography set-up was re-assembled on breadboards, thus enhancing mechanical stability and facilitating flexible re-configuring and additions of parts. A LED-based light source was used to replace the old filament lamp. In addition, a translation stage was added to facilitate studying the flatness of large-area samples for neutron optics applications.
The flatness of Si substrates and the stress of thin films deposited onto them have been assessed for the company Mirrotron Ltd. for neutron optics applications. The surface profile of galvanic Ni(P) layers for neutron mirrors have also been measured. For in-house research, Makyoh topography was used to assess the overall deformation and surface/interface defects for process optimisation of wafer bond technology of various structures. This included also the measurement of highly structured wafers (Fig. 1) which is always a challenge for optical testing. For this, a new methodology which uses the wafer pattern itself as a reference was developed. In addition, curvature measurements as well as deformation measurements on micromachined membrane structures were performed for thin-film stress assessment.

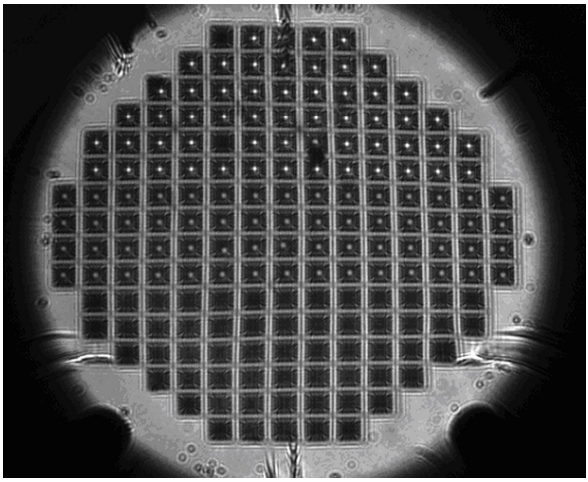

***Figure 1.*** *Makyoh-topography image of a structured wafer.*

# Optical characterization of materials for optoelectronics and biosensorics

## *(OTKA K81842, OTKA PD73084)*

P. Petrik, E. Agócs, B. Fodor, M. Janosov, A. Németh, S. Kurunczi, M. Fried, R. Horváth, Gy. Juhász, O. Polgár, and Cs. Major

Optical characterization and modelling of ultra thin protein and optoelectronic reference layers is of large importance in a broad range of organic and solid state applications from sensors through printed electronics to photovoltaics. Metrologies are mainly used and developed independently, however cross checking and validation using reference method is crucial for the reliable characterizations and model developments. In the Ellipsometry Laboratory of MFA optical models and evaluation methods have been developed for silicon nanoparticles embedded in insulator matrix.

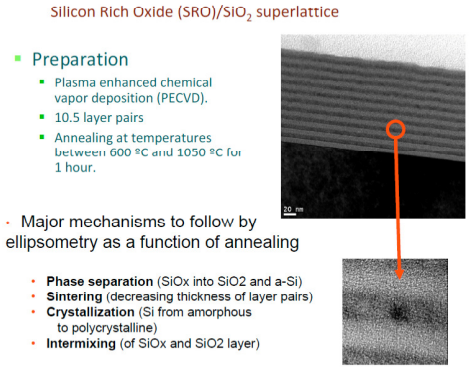


***Figure 1.*** *Silicon nanoparticles in SRO/$SiO_2$ superlattice.*

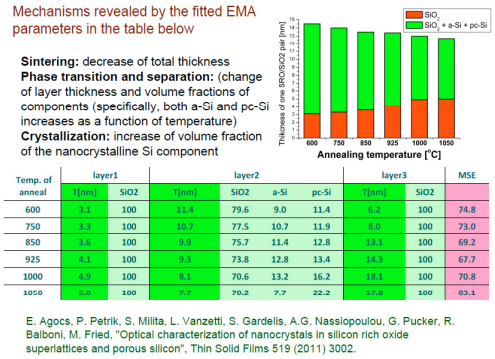


***Figure 2.*** *Structural evolution during annealing revealed by Spectroscopic Ellipsometry (measurements and optical modelling).*

# Complex characterization of degradation of ferromagnetic materials by Magnetic Adaptive Testing

## *(OTKA A08CK80173)*

G. Vértesy

Magnetic measurements are frequently used for characterization of changes in ferromagnetic materials, because magnetization processes are closely related to their microstructure. The recently developed method (Magnetic Adaptive Testing, MAT) is based on the systematic measurement and evaluation of minor magnetic hysteresis loops. This method was suggested as a highly promising non-destructive alternative of destructive tests for monitoring structural changes in ferromagnetic objects. MAT

introduces a large number of magnetic descriptors to diverse variations in non-magnetic properties of ferromagnetic materials, from which, those optimally adapted to the just investigated property and material, can be picked up.

The purpose of this work is to show that MAT can offer a solution even in such cases, when a non-monotonous correlation is found in a measured primary magnetic characteristic as function of the degradation parameters of the investigated material. As an example, plastic deformation was investigated in industrial steel specimens by this nondestructive magnetic method. It was shown that the *multi-parametric* character of MAT is able to solve the problem. Namely MAT can determine unambiguously the level of the steel deformation from combination of two (or more) parameters obtained from a single measurement, even though both the parameters are non-monotonous.

Flat samples of low carbon commercial steel (used for high pressure pipelines) were loaded by application of tensile stress. The samples were plastically deformed up to a certain strain value, and then relaxed to different ε strain values (between 0 and 10.2%). As it is seen in Fig. 1, definite correlation was found between the primary (most sensitive) MAT degradation functions and the plastic deformation. The degradation functions depend significantly on ε and they typically and mostly have a maximum at around 7% strain. It is evident, however, that based on Fig. 1 only, the plastic deformation of an unknown sample cannot be unambiguously determined, because the dependence of the MAT parameter on the plastic strain is not monotonous. For solving this problem the advantage of the multi-parametric feature of MAT was used, and other degradation functions were also considered. Fig. 2 shows auxiliary degradation functions. These are not as sensitive as those of Fig. 1, but on the other side, even though this function is also not monotonous in the whole region of the strain, it is monotonous in the important 2–10% strain region, and it is sensitive enough to help to recognize whether the high-value-descriptor of Fig. 1 belongs to the ascending or the descending part of the curve. By simultaneous analysis of both primary and auxiliary degradation functions, the remaining expected residual life time of the investigated sample can be determined.

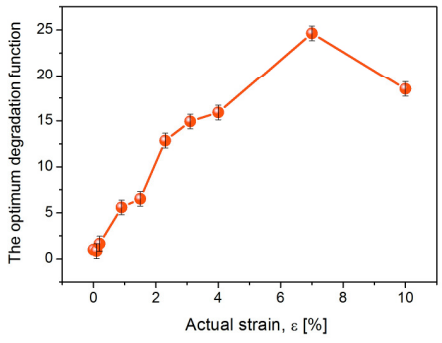


***Figure 1***. *The optimum (ε)-degradation.*

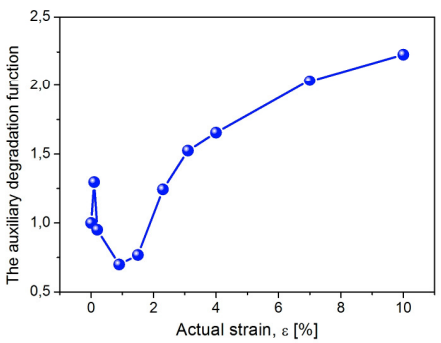


***Figure 2.*** *The auxiliary (ε)-degradation.*

# MeV energy $N^+$-implanted planar optical waveguides in sillenite type Bismuth Germanate crystals operating at 1.55 μm

*(OTKA K101223)*

I. Bányász, S. Berneschi, M. Bettinelli, M. Brenci, M. Fried, N.Q. Khánh, T. Lohner, G. Nunzi Conti, S. Pelli, P. Petrik, G. C. Righini, A. Speghini, A. Watterich, Z. Zolnai

Ion beam techniques are among the best methods for optical waveguide fabrication in crystalline and amorphous materials. It has better controllability and reproducibility than other techniques. The first articles reporting fabrication of waveguides by light ions ion implantation appeared between the end of 1960's and early 1980's.

Tellurite glasses have gained a widespread attention because of their potential as hosts of rare-earth elements for the development of fibre and integrated optic amplifiers and lasers covering all main telecommunication bands

Sillenite type Bismuth Germanate (BGO) crystals are good nonlinear optical materials. We have recently reported fabrication of planar waveguides in both eulytine and sillenite type bismuth germanate crystals using MeV energy $N^+$ ions operation in the 1550-nm telecommunication band.

Structure of the ion implanted planar waveguides is determined mainly by the energy and fluence of the implanted ions. Full-cascade SRIM (Stopping and Range of Ions in Matter) simulations were performed and compared with spectroscopic ellipsometric (SE) investigations to estimate the ion and damage depth distributions in the target, Figs. 3, 4. Results of the SRIM simulations for sillenite type BGO crystal can be seen in Figs. 1, 2. Peak of the $N^+$ distribution due to single energy irradiation at 3.5 MeV is at 2.2 μm. Two separate peaks appear when the lower irradiation energy is 2.5 MeV.

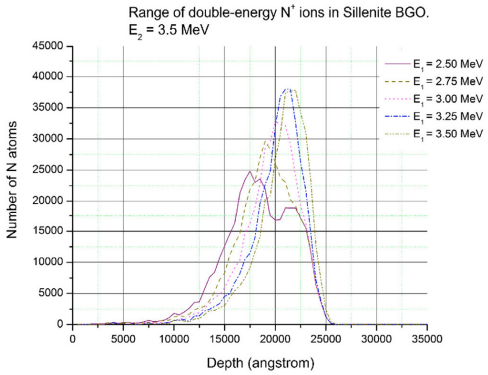


***Figure 1.*** *Depth-distributions of the implanted $N^+$ ions in sillenite type BGO crystal. Higher energy was 3.5 MeV in each case. Lower energy is indicated in the inset.*

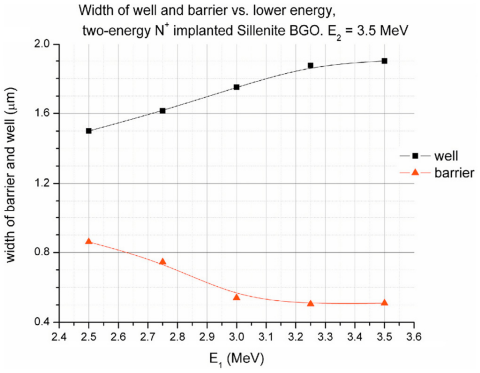


***Figure 2.*** *Width of the well and barrier layers vs. the lower energy of irradiation in the sillenite type BGO crystal.*

Functionality of the waveguides was tested by m-line (dark-line) spectroscopy and prism coupling technique. The accuracy is around 1 x $10^{-4}$ and 5 x $10^{-4}$ for measuring the effective refractive index ($n_{eff}$) and bulk refractive index, respectively. When the fluence of the 3.5 MeV $N^+$ irradiation was 10 x $10^{15}$ ions/cm$^2$, only three modes could be detected at k = 635 nm. Both single energy irradiation at 3.5 MeV and the combination of 3.5 + 3.1 MeV irradiation at 20 x $10^{15}$ ions/cm$^2$ resulted in the appearance of five modes at the same wavelength. Only the waveguide irradiated with the combination of 3.5 + 3.1 MeV irradiation at 20 x $10^{15}$ -ions/cm$^2$ had a mode at 1310 nm. All the detected modes were leaky.

Both spectroscopic ellipsometric and m-line spectroscopic results suggest that planar waveguides irradiated in the sillenite type BGO crystal have a complicated refractive index profile as a result of the crystal damage and the presence of the implanted $N^+$ ions. Because of the low number of modes, instead of the common methods, a multispectral method will be used to calculate the refractive index profiles of those waveguides.

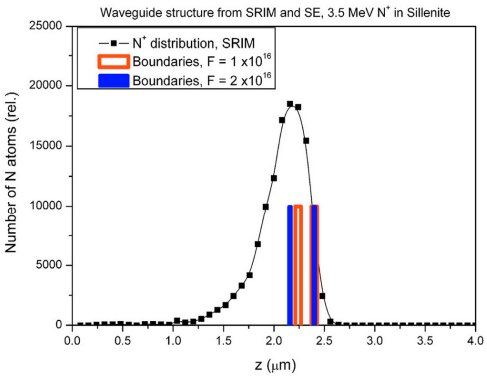


***Figure 3.*** *SRIM simulation and SE fit of the waveguide structure in sillenite BGO crystal. E = 3.5 MeV, fluences are 1 x $10^{16}$ and 2 x $10^{16}$ ions/cm$^2$.*

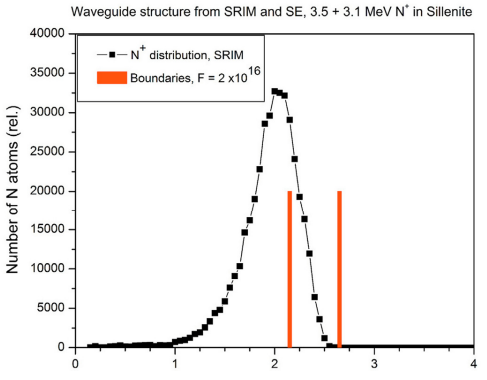


***Figure 4.*** *SRIM simulation and SE fit of the waveguide structure in sillenite BGO crystal. E = 3.5 + 3.1 MeV, fluence is 2 x $10^{16}$ ions/cm$^2$.*

No significant improvement with respect to the single energy irradiated waveguides could be found. Only slight decrease of the effective refractive indices with increasing difference of the irradiation energies was detected. Based on previous experience with the method and the material, it is hoped that thermal annealing of the ion beam irradiated planar waveguides up moderate temperatures (around 260 °C) could substantially re-structure waveguide and improve light confinement. Creation of a wider barrier via double energy irradiation did not improve waveguide quality in that material, as well.

# Development of optical metrology tool for in-line qualification of thin film solar cells

## *(KMR_12-1-2012-0225, EU FP7 FP7 SEA4KET 611332, ENIAC E450EDL)*

Cs. Major, Gy. Juhász, Z. Zolnai, N. Nagy, and M. Fried

We are involved in one Hungarian KMR_-12 project called „Ipari méretű vékonyréteg optikai térképezésre szolgáló berendezés fejlesztése” (with a Hungarian SME partner) and 2 EU-projects („SEA4KET” and the ENIAC-2012-2 “E450DL”) to develop “Imaging Optical Inspection Device With A Pinhole Camera”. We develop 30, 45, 60 and 90 cm wide prototypes.

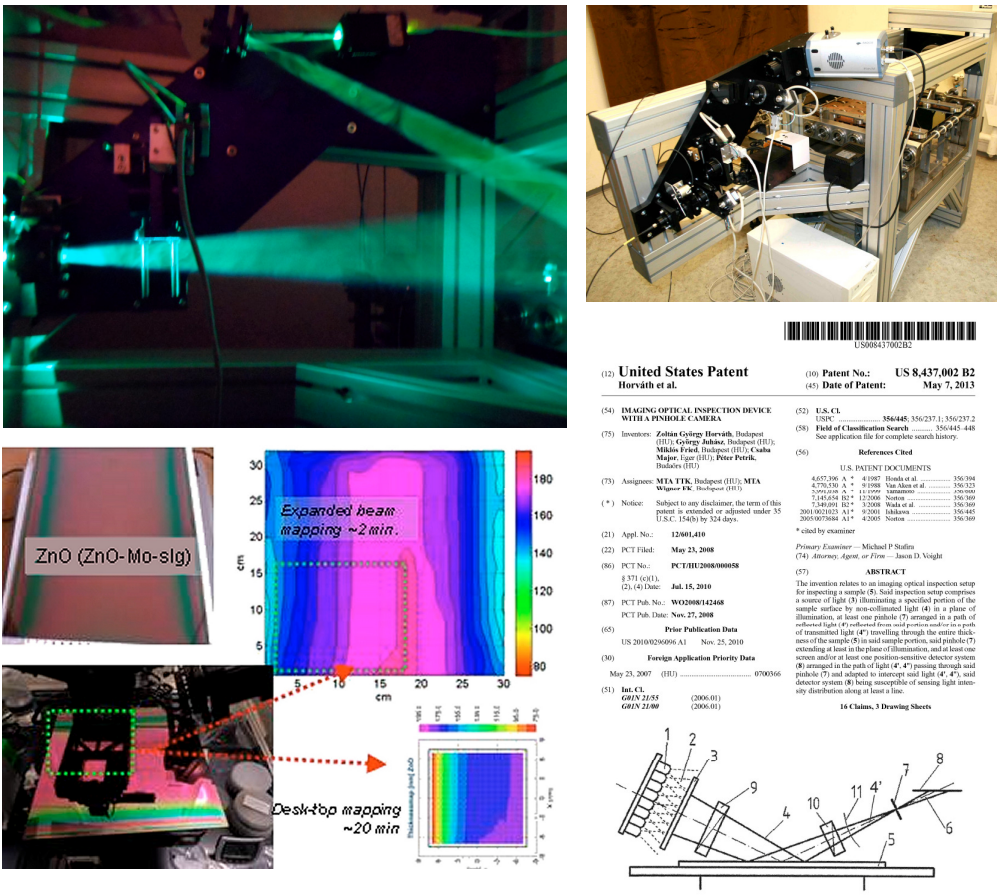


***Figure 1.*** *The 30 cm sample-size prototype (top pictures); Thickness map (of a ZnO/Mo/glass sample) measured by the prototype compared with the thickness map determined by a desktop device (bottom left); US 8,437,002 B2 patent (bottom right).*

# Ultra-versatile Nanoparticle Integration into Organized Nanoclusters

*(EU FP7 UNION 310250, OTKA PD105173, TET-12-CN-1-2012-0005)*

A. Deák, N. Nagy, E. Fülöp, and D. Zámbó

The project aims to utilise the full control over the interaction-potential between different nanoparticles in order to achieve nanoparticle-assemblies with enhanced functionality. Plasmonic, magnetic and semiconducting nanoparticles are assembled in homo and heteroclusters. The envisaged fields of application are

- **theranostics** (therapy and diagnosis): magnetic and semiconducting nanoparticles are assembled into clusters and combined with lipid nanoparticles
- **thermoelectrics**: two different types of semiconducting nano crystals are co-assembled into highly organised micron sized clusters for further processing in thermoelectric device fabrication
- **lighting applications**: plasmon-enhanced photoluminescence is targeted by combining plasmonic and semiconducting nanoparticles!

We are involved in the following main tasks:

- state-of-the-art preparation of high-quality nanoparticle samples and surface-functionalisation of these building blocks to enable the nanoscale assembly through modulating colloid interactions (Fig. 1)
- self-assembly and process monitoring by optical methods (Fig. 2)
- interfacial structure formation of nanoparticles and nanoparticle-clusters (Langmuir-Blodgett and capillary assembly) (Fig. 3)

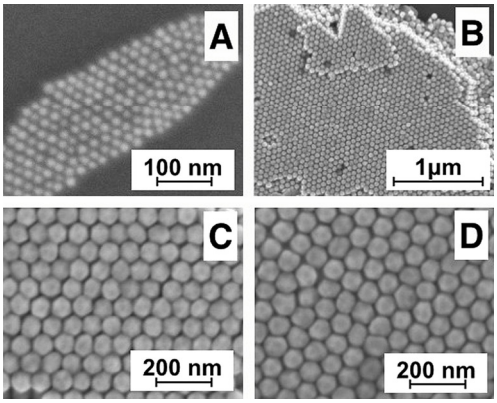


***Figure 1.*** *Representative SEM images of some of the CTAB-capped Au nanoparticles prepared. NP diameters (from SEM): (A): 25 nm, (B):* 75 nm, (C): 89 nm, and (D): 118 nm.

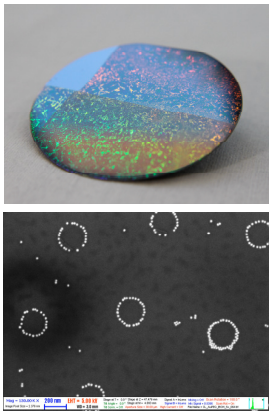

***Figure 2.*** *(a) Two partially overlapping Langmuir-Blodgett mono-layers of ~350 nm silica nanoparticles deposited on a 2" Si wafer. (b) PEG stabilised 15 nm gold nanoparticles arranged in a circular pattern using a microsphere monolayer template and capillary assembly.*

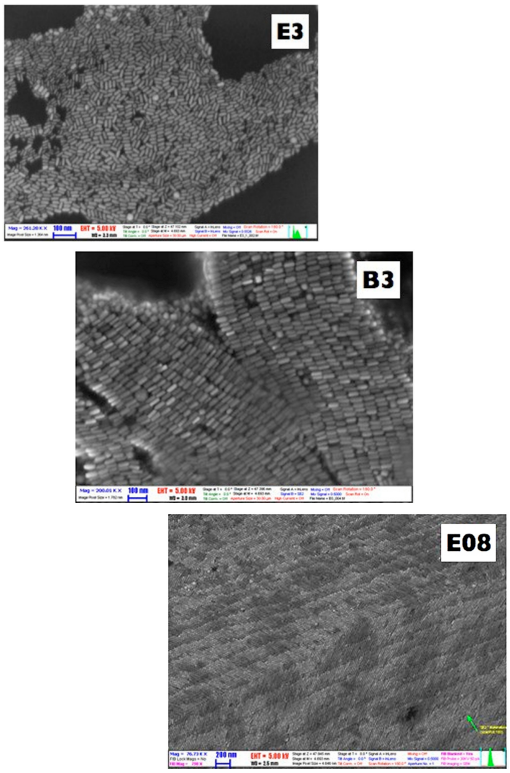


***Figure 3***. *Representative SEM images of selected Au nanorod samples prepared. Due to their highmonodispersity the nanorods tend to close-pack upon solvent evaporation. The nanorod dimensions and ARs are: (E3) L×W = 37×13 nm, AR = 2.85; (B3) L×W = 64×25 nm, AR =2.56; and (E08) L×W = 51×16 nm, AR = 3.18*

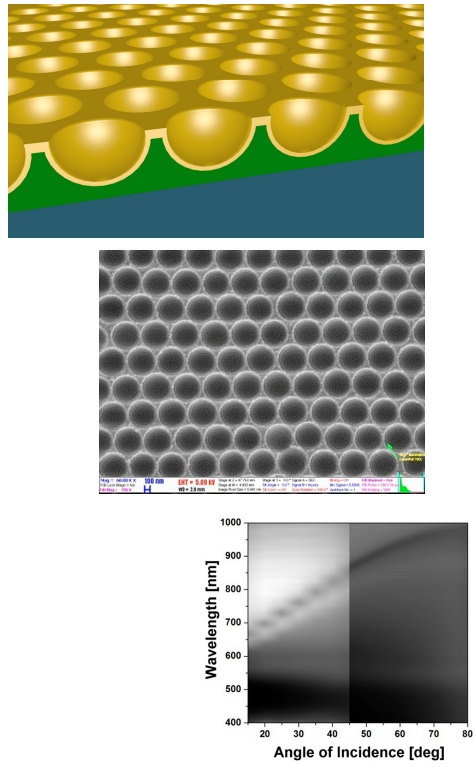


***Figure 4.*** *(a) Schematic structure of the gold coated inverse-sphere structure (b) SEM image of the sample (void diameter: ca. 450 nm, gold film thickness: 100 nm) (c) optical reflection spectra of the sample as a function of wavelength and incident angle.*

We target the site-selective surface-functionalization of asymmetric nanoparticles to study the self-assembly of these inhomogeneous objects. We mainly work with plasmonic nanoparticles (gold nanorods) and use PEG moieties to selectively block the tips of the nano rods during the assembly process.

In the framework of an ongoing project we develop plasmonic solar cells with colleagues from the Suzhou Institute of Nano-Tech and Nano-Bionics (China). Here we utilise nano structured plasmonic back-electrodes and plasmonic nanoparticles in a dye sensitised solar cell in order to achieve optimal light-distribution and light trapping in the active layer of the solar cell. We focus on the near-field enhancement of the dye absorption as well as on redistribution of the incoming energy due to scattering and diffraction.

# *Microtechnology Department*

**Head: Gábor BATTISTIG, Ph.D., senior research fellow**

**Research Staff**

- Zsófia BAJI, Ph.D.
- István BÁRSONY, corr.memb. of HAS
- Gábor BATTISTIG, Ph.D.
- László DÓZSA, Ph.D.
- Csaba DÜCSŐ, Ph.D.
- Zoltán FEKETE, Ph.D.
- Péter FÖLDESY, Ph.D.
- Péter FÜRJES, Ph.D.
- Zoltán HAJNAL, Ph.D.
- Nguyen Quoc KHÁNH, Ph.D.
- Zoltán LÁBADI, Ph.D.
- István LUKÁCSI, Ph.D.
- György MOLNÁR, Ph.D.
- Ákos NEMCSICS, D.Sc. (part time)
- Andrea Edit PAP, Ph.D. (part time)
- Anita PONGRÁCZ, Ph.D. (on leave)
- Vilmos RAKOVICS, Ph.D.
- Attila Lajos TÓTH, Ph.D.
- Erika TUNYOGI
- János VOLK, Ph.D.
- Zsolt ZOLNAI, Ph.D.

**Technical Staff**

- János FERENCZ (engineer)
- Levente ILLÉS (engineer)
- Csaba LÁZÁR (engineer)
- István RÉTI (engineer)
- Róbert HODOVÁN (engineer)
- András LÖRINCZ (engineer)
- Katalin VERESNÉ VÖRÖS (engineer)
- György ALTMANN (technician)
- Gabriella BIRÓ (technician)
- Sándor CSARNAI (technician)
- Tibor CSARNAI (technician)
- Magda ERŐS (technician)
- Károlyné PAJER (technician)
- Csilla ARIAS-SOTONÉ FARAGÓ (technician)
- Attila NAGY (technician)
- Magda VARGA (technician)

**Ph.D. students**

- Zsófia BÉRCZES
- Zoltán SZABÓ
- Ferenc BÍRÓ
- Máté TAKÁCS
- Róbert ERDÉLYI
- Gergely MÁRTON
- Tamás KÁRPÁTI

**Diploma workers**

- Kristóf PÉTERFI, B.Sc.
- Éva JELINEK, B.Sc.
- Hunor MENYHÁRT, B.Sc.
- Gergő János MIKULA, B.Sc.
- János RADÓ, B.Sc.
- Ágoston HORVÁTH, B.Sc.
- Kristóf KUBINA, M.Sc.
- Ádám LUTZ, M.Sc.
- Tamás PARDY, M.Sc.
- Ferenc TOLNER, M.Sc.
- Eszter TÓTH, M.Sc.

**The main task of the Microtechnology Department is the research and development of physical, chemical/biochemical sensors and integrated systems:**

- **MEMS** and MEMS related **technologies**, with special emphasis on CMOS compatibility.
- Development of novel microfluidic systems, their application in new fields of biochemistry, **BioMEMS**.
- **Sensor development** with special emphasis on micropellistor-type gas sensors, 3D force sensors, thermal sensors, gas flow sensors, etc.
- Development of Si and polymer based sensors for biomedical applications with special emphasis on **NeuroMEMS**.
- Development of semiconductor nanodevices, synthesis and charactirization of quasi-one-dimensional semiconducting nanostrucrures, their integratation into functional sensor, optoelectronic and photovoltaic devices - **NEMS**.

**Fundamental research on:**

- sensing principles;
- novel materials and nanostructures;
- novel 3D fabrication techniques;
- ion-solid interaction for supporting MEMS development.

**Device and structural characterization methods** widely used in our projects:

- Electrical characterization;
- Thermo-mechanical characterization;
- Scanning Microprobes;
- Ion beam analysis methods;
- SEM, TEM, EDX;
- Spectroscopic Ellipsometry.

The Microtechnology Department of MFA runs two 300 + 160 $m^2$ clean labs, respectively (Class 100-10000) comprising a complete Si-CMOS processing line and a mask shop, unique in Hungary. The facility is capable on 3" and 4" Si and glass wafers of manufacturing layers, patterned structures and devices with 1µm resolution.

**Main processes in the Microtechnology lab** (available also for our partners and customers):

- High temperature annealing, diffusion and oxidation;
- Rapid Thermal Treatment;
- Low Pressure Chemical Vapor Deposition of poly-Si, SiO2 and Si3N4 layers;
- Low Temperature Chemical Vapor Deposition;
- Ion implantation;
- Physical Vapor Deposition – Electron beam evaporation, DC and RF Sputtering;
- Atomic Layer Deposition;
- Reactive Ion Etching, Deep Reactive Ion Etching;

- Photolithography with back-side alignment and Nanoimprinting;
- E-beam lithography;
- Nanopatterning, deposition and etching by Focussed Ion-Beam;
- Wafer Bonding;
- Wet chemical treatments;
- Electro-chemical porous Silicon formation;
- Molecular Beam Epitaxy of III-V compound semiconductors;
- Mask design, laser pattern generator;
- Polymer (PDMS, SU8, Polyimide) structuring by photolithography and micromoulding techniques,
- Chip dicing, packaging especially for sensor applications;
- Materials and structural characterizations, Stylus Profiler, Electrochemical Impedance Spectroscopy, SEM, FIB, EDX, Atomic Force Microscopy;
- Electrical and functional characterization.


For detailed information please visit us at our web-site (http://www.mems.hu/) or contact us: dragon@mfa.ttk.hu

# MEMS

*Activity leader:* Cs. Dücső
*Group members:* Zs. Baji, I. Bársony, G. Battistig, L. Dózsa, P. Földesy, P. Fürjes, Z. Hajnal, Z. Lábadi, G. Molnár, A. E. Pap, V. Rakovics, A. L. Tóth, E. Tunyogi, Zs. Zolnai, F. Biró, T. Kárpáti, and M. Takács

*Activities are supported by*
- OTKA K109674 - Graphen based terahertz modulators (2013-2017)
- OTKA K91154 - Environmentally friendly semiconductors: iron silicide nanostructures (2010-2013)
- OTKA CNK77564 - Terahertz sensing for THz imaging (2010-2013)
- KMR-12-1-2012-0107 – Sensor for continuous monitoring of carbonhydrides dissolved in underground water (2012-2015)
- KMR_12-1-2012-0031 – Development of an embedded information system for the optimisation of energy-positive public lighting (2012-2014)

**Development of physical and chemical sensors**

This activity of the MEMS lab focused on the development of existing gas and force sensor chips and related characterization methods, targeting application in commercial sensor systems.

**Gas sensors**

Having successfully demonstrated the operation of micro-pellistor and conductivity (Taguchi-type) sensors, their long term properties in terms of thermo-mechanical stability and functionality were investigated. For marketable products it is required to achieve several years of operation time without loss of sensitivity.

Accelerated ageing tests revealed that degradation of the present catalyst results in a sensitivity drop of 10% within a few weeks, therefore substantial improvement of the catalyst is required to provide a stable sensor response. Although the slurry-like catalyst was traditionally widely used in commercial Pt coil based pellistors, this mixture proved to be non-compatible with the thin film based microsensor structure. Besides, the thermo-mechanical stability of the micro-hotplate could also be improved to meet life-time expectations.

Based on FEM calculations of alternative structures the micro-hotplate geometry and its vertical multilayer construction were further optimized. The aim was to achieve operational temperature above 500 °C with a power dissipation below 20 mW and to facilitate a minimum displacement of the membrane during temperature shocks. The most promising layer structures were realised and tested in pulsed mode heating cycles between room temperature and 500 °C. After the first few thousand stabilizing periodes, the best devices were able to withstand up to $8 \times 10^5$ cycles corresponding to ca. 5 years of operation time. Nevertheless, electromigration effect induced

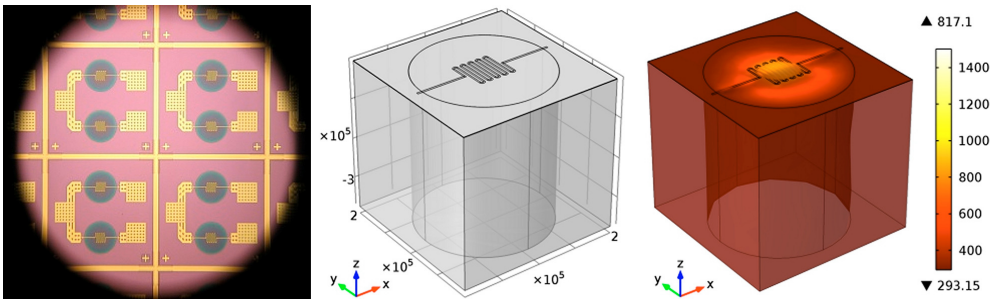


***Figure 1.*** *Microscopic view of 4 sensor chips containing two microheaters (left), 3D FEM structure (centre), and thermal distribution at 12 mW heating power (right).*

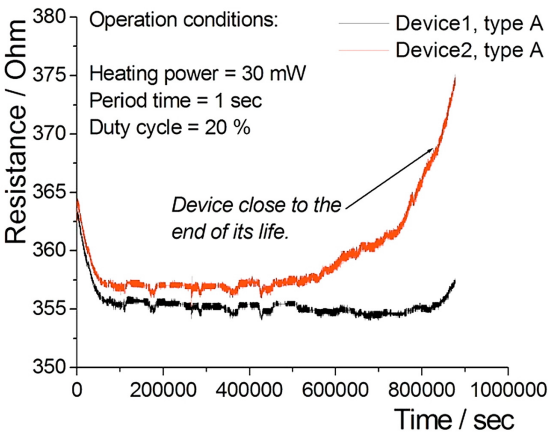


***Figure 2***. *Results of accelerated ageing tests.*

degradation of Pt filament must also be reduced, if continuous operation mode is selected. As the current density in the filament cannot be reduced without losing thermal isolation, we have started to investigate the effect of alternative adhesion layers on heater stability. Due to geometric and adhesion constraints application of conventional Pt based catalyst slurry droplets is far for being compatible with the thin film hotplate structure. Therefore, an appropriate thin film catalyst formation method must be elaborated. A laterally selective electrochemical process to provide a large surface was developed by formation of a thin (< 2 - 3 µm) porous alumina layer on the top of the hotplate. This layer is to support noble metal catalytic nano-particles to be deposited in a subsequent step. Beside sputtering and micro droplet methods for sensitizing the porous layer ALD (atomic layer deposition) is also considered. Optimization of pore size and porosity as well as testing alternative sensitizing techniques is the next step in process development. As a proof of concept, porous alumina catalyst support was covered with Pt by thermal decomposition of water dissolved $H_2[PtCl]_6$ droplets and devices were tested for hydrocarbon response.

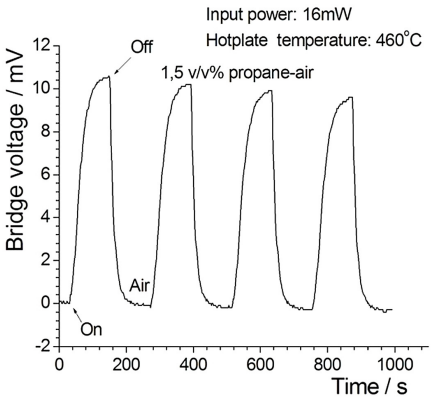


***Figure 3.*** *Sensor response to 60% LEL of propane.*

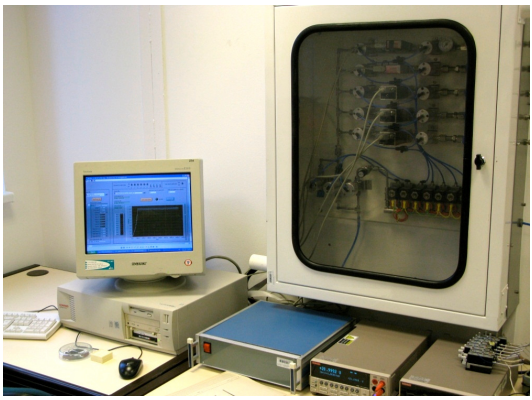

***Figure 4.*** *Gas sensor test setup.*

For functional characterization of gas sensor chips a new test station was developed capable of introducing 3 different gases in synthetic air if needed. Besides measuring response time accurately, the gas concentration range can arbitrarily be set between ppm and 20v%.

**3D micro-force sensor**

A high yield, reliable processing technology for manufacturing three dimensional force sensors was demonstrated. The basis of the process is the adaptation of the existing technology for SOI (silicon on insulator) wafers to provide uniform membrane geometry over the whole wafer. Thereby, the deviation of chip characteristics could be harmonized with industrial process requirements. As by this technique the size of a single element force sensor can be reduced to ca. 1.5 × 1.5 $mm^2$, we hope to extend the application area of the device to biomedical/surgery field as well.

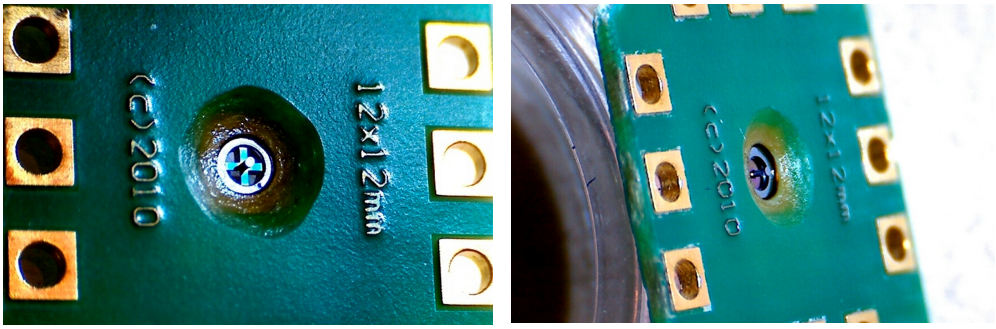


***Figure 5.*** *3D micro force measuring chips with perforated (left) and full membranes (right). Both versions are fabricated in SOI wafers and assembled in a PC board for testing. Size of the sensing structure: 1 mm diameter.*

For individual testing and quick feedback of characteristics an accurate 3D vectorial-force loading station was also constructed.

***Figure 6.*** *Setup for testing 3D micro-force sensor chip by an accurate force-vector load. Close-up view of the chip and the needle of the calibration force sensor are seen on the monitor of the system control PC.*

Sensor chips of alternative membrane structures were processed and assembled for characterization.

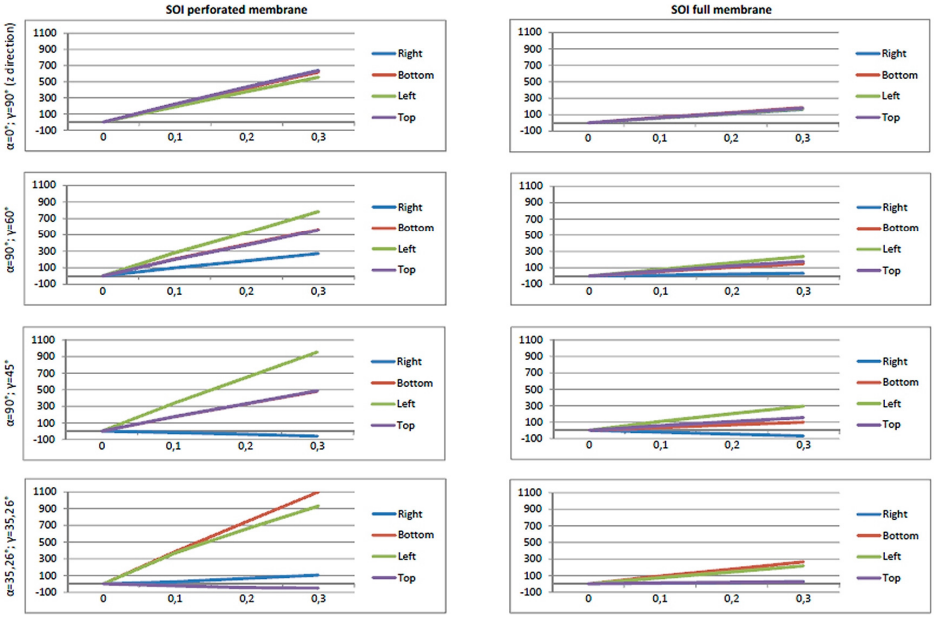


***Figure 7.*** *Sensitivity of different 3D force sensor structures fabricated from SOI wafers.* $\alpha$ *and* $\gamma$ *represent the angles in the spherical coordinate system: the angle in the x-y plane and the angle between the force vector and the x-y plane, respectively.*

# BioMEMS and Microfluidics

*Activity leader:* P. Fürjes
*Group members:* Zs. Baji, I. Bársony, Cs. Dücső, Z. Fekete, Z. Hajnal, and A. L. Tóth

*Activities are supported by:*
- OTKA K108366 - Creating microchannels by Proton Beam Writing and their applications in Lab-on-a-chip devices (2013-2017)
- ENIAC_08-1-2011-0006 - Chip Architectures by Joint Associated Labs for European diagnostics CAJAL4EU (2010-2013)

Significant numbers of the environmental or clinical analytic tests are targeting the quantitative or qualitative analysis of different molecules in air or liquid samples. The micro and nanotechnology based sensing principles enable the development and realisation of robust, user-friendly and cost-effective analytic platforms.
Recently significant efforts were devoted to set up a competitive infrastructure and acquire solid background knowledge in the Microtechnology Laboratory of MFA for supporting the development of biosensors, bio-interfaces and microfluidic systems. The related scientific fields involved micro- and nanofluidics, bio-analytical and medical diagnostics (BioMEMS) research. As proven by the numerous ongoing projects and also by the growing interest of industrial partners, this emerging field is highly challenging. The research field is most attractive for Ph.D., graduate and undergraduate students as well. Our main goal is to develop integrated systems for industrial and medical applications, as demonstrated successfully in several projects in cooperation with industrial partners like Tateyama Kagaku Ind. Corp. Ltd. (Toyama, Japan), NORMA Diagnostics, (Wien, Austria), 77 Elektronika (Budapest, Hungary), Micronit (Twente, The Netherlands).

- Besides the development of conventional micromechanical sensors, a reliable background was established at MFA for the research and development of bioanalytical and medical diagnostic systems in form of a complex laboratory for characterisation of microfluidic and BioMEMS devices.
- The established system technology is capable to fabricate complex micro- and nanofluidic systems in silicon/glass and polymer materials.
- A wide cooperative network and knowledge base in the topic was set up by the research projects we participated in.
- The scientific and processing results are directly transferred into higher education, which is represented by the number of students working in the laboratory on their TDK, B.Sc., M.Sc. or Ph.D. theses.

**Integrated bioanalitycal systems based on nanopore arrays**
The application of complex nanofabricated structures is increasingly demanded in the field of mechanical, chemical and biochemical transducers. As a result, innovative biosensing principles, new capabilities for medical applications are offered. Chemically modified nanonopore based sensors, e.g. can be applied to detect specific biomolecules electrochemically via transport modulation by molecule binding in

pores. Nanopore sensing was envisioned to provide a new generation, nanoelectronics-based high sensitivity, label-free medical diagnostic platform. The main targeted application was the diagnosis of cardiovascular diseases (CVD) through relevant biomarkers (primarily cardiac Troponin I (cTnI).

**Individual and fluidically integrated solid-state nanopore arrays**

The nanopore based sensors proposed in the CAJAL4EU project were fabricated by the combination of silicon micromachining and nanofabrication processes, applying Focused ($Ga^+$) Ion Beam (FIB) milling of nanopores in a Silicon-Nitride membrane. Gold coated Silicon-Nitride layers provided mechanically stable membranes with controlled pore geometries for bio-functionalization. To establish a reliable fabrication process the FIB drilling was characterized and improved to achieve accurate pore geometry by computer controlled nanomachining. The nanopore membranes were integrated into an electrochemically addressable fluidic system

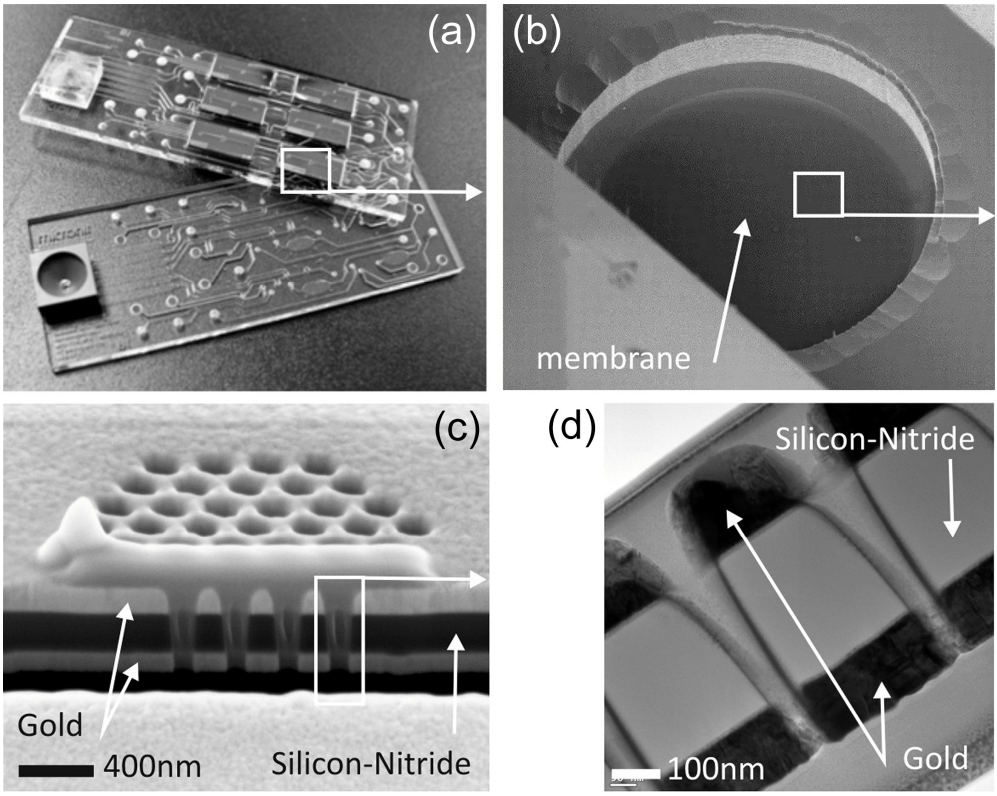


***Figure 1.*** *(a): Biosensor cartridge with integrated fluidic and electrical addressing of six nanopore chips for multiplexed measurements, (b): Gold/Silicon-Nitride/Gold multilayer structure of the individual nanopore chips in which the nanopores are milled by FIB, (c): SEM image of the FIB nanopore array, (d): TEM image of the nanopore cross section.*

comprising the fluidic channels and electrodes. The 3D fluidic channel system of the individual nanopore chips was micromachined in Si/glass heterostructure and bonded to the multichannel fluidic cartridge, designed and fabricated by 77 Elektronika and Micronit, accommodates six nanopore chips for multiplexed measurements.

**System integration and the development of the nanopore platform prototype**
A prototype of the integrated nanopore platform was designed and constructed interfacing of the disposable biosensor cartridge through a custom holder to the electrochemical measurement and microfluidic actuation systems.

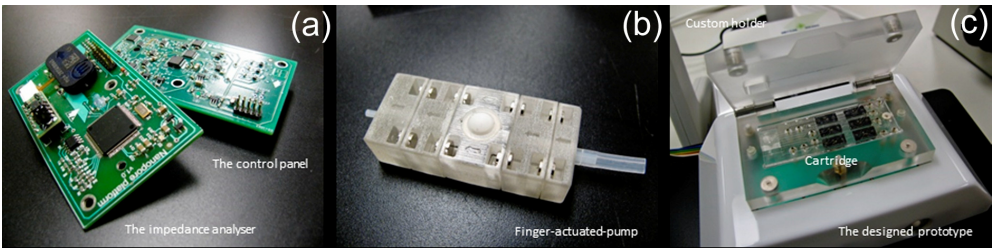


***Figure 2***. *Prototype of the nanopore platform: (a): impedance analyser, (b): finger-actuated micropump, (c): the complete system with the biosensor cartridge.*

The electrochemical read-out is facilitated by an AC electrochemical impedance analyzer - measuring nA currents in the range of 100kHz to 1Hz. The complete system is manufactured in a portable hand-held device format, which can be connected to any PC via micro-USB. The device control and the data evaluation are done through a user-friendly GUI. The prototype of the integrated nanopore platform is able to measure up to six independent markers sequentially just from a single sample. The required sample volume is 9µl from serum and 18µl from whole blood.

**Biomarker detection with biofunctionalized nanopores**
The high-throughput characterization of novel, extremely stabile, high affinity artificial bioreceptors (aptamers, spiegelmers) to comply with the specific requirements of nanopore sensing was developed by researchers of the Semmelweis University and the Budapest University of Technology and Economics. Receptors were characterized in terms of binding properties by using novel high throughput SPR imaging and optical bioassay methodologies. The spiegelmer receptor developed for cTnI enables the selective detection of cTnI in serum *without any additional reagents, which is a major breakthrough*. Extremely high sensitivities in serum samples were obtained for cTnI detection (LOD ca. 1 pg/ml) by nanopores. This is a *label-free troponin measurement method of unprecedented high sensitivity!*

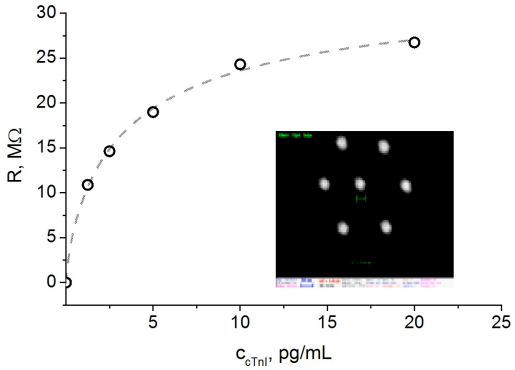


***Figure 3.*** *Typical calibration curve of cTnI in the high sensitivity range measured with a nanopore array of seven 30 nm diameter pores (inset) sensitized by spiegelmer receptor.*

The nanopore platform team achieved a significant progress beyond state of the art in terms of: (i) nanopore fabrication by FIB, (ii) on-chip fluidic integration of nanopores, (iii) discovery and implementation of novel highly stable, selective and cost-effective receptors (spiegelmers, PNAs) as well as novel high throughput methods for their characterization, (iv) bio-functionalization of gold-coated and SiNx nanopores, (v) development of high sensitivity label-free nanoelectronic detection methodology, (vi) design and fabrication of the complete range of hardware and software for autonomous use of nanopore diagnostic platforms.
The feasibility of the nanopore platform for diagnostic measurements was demonstrated with the selected cTnI biomarker. Furthermore, essential know-how was gathered for establishing the bio-functionalized nanopore sensing as universal platform for a wide range of biomarkers.

**Development and characterisation of functional passive microfluidic devices**
The rapid development of microscale medical diagnostic devices has pointed out the importance of microfluidics enabling quick and effective transport, preparation and analysis of liquid biological samples. In microscale, otherwise trivial sample preparation methods, such as effective mixing of fluids as well as the size-dependent separation of corpuscles and their filtering from the blood might become a challenge. A low cost and comfortable sample loading and on-chip transport is thus also an important question in medical application.

**Particle motion in microfluidic structures**
Besides microscale characterisation of the hydrodynamic behaviour of conventional fluids, the analysis of the real biological samples, the investigation of special properties of the fluid (blood) and the physical properties of the particles (cells) is also a critical requirement.
Computational fluid dynamics (CFD) simulations, trajectory modelling and laboratory measurements were carried out to characterise in detail the performance of various microfluidic mixer structures utilising chaotic advection. The mixing performance of Herring-Bone type chaotic mixers constructed with various geometric parameters was studied by FEM modelling. The developing particle distribution in

the microfluidic structures with different geometries were visualized by Poincare-maps. The results of the simulations showed that for improved performance of the mixer we should increase the number or the width of the grooves in the Herring-Bone structure. The results of simulations were verified experimentally by recording the particle trajectories by dark field microscopy. The experienced behaviour was in good agreement with the results of the simulations. The modelled trajectories of the individual particles confirmed the experimentally observed main hydrodynamic effects, pressure gradients and shear forces.

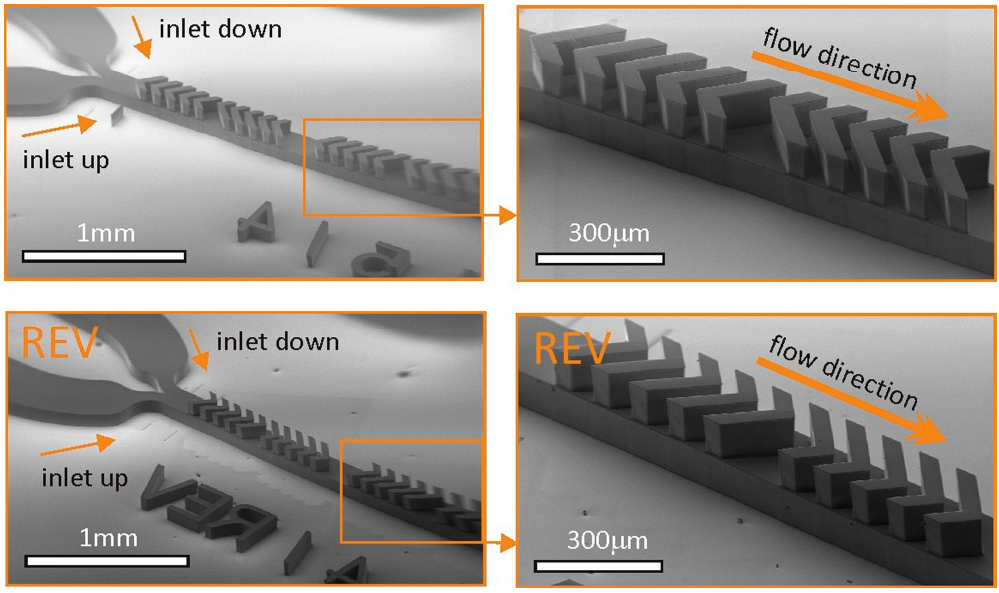


***Figure 4.*** *Multilayer SU-8 molding masters of different Herring-bone mixer designs for PDMS structuring.*

The behaviour of real particles (blood cells) in special microfluidic structures was characterised by both numerical modelling and measurements for analysis of the size dependent separation, especially the physical phenomenon of lateral migration. Based on the simulation results test structures were fabricated by fast prototyping and the main characteristics of the selected structures were studied.

**Surface modification of microfluidic structures**

Surface modification methods were also studied to improve both wettability and non-specific protein binding of PDMS. Triton X-100 surfactant and PDMS-PEO were added to the raw PDMS before polymerization. The influence of embedded molecules was analysed in terms of contact angles and functionality. Contact angle of the modified PDMS surfaces was decreased by up to 30% and 50% by PDMS-PEO and TX-100 surfactant molecules, respectively. This reflects the changing of the surface of PDMS from hydrophobic to hydrophilic. Moreover, we found in both cases that irreversible protein adsorption on the PDMS surface can be decreased by almost 100%.

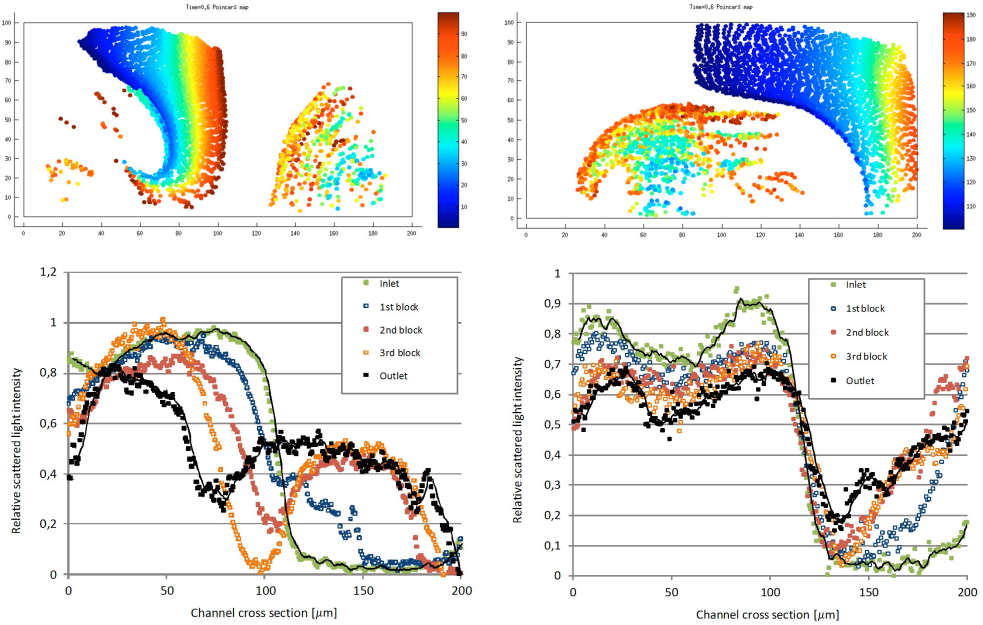


***Figure 5***. *The Poincare maps represent the particle mixing in the plane perpendicular to the channel direction and heading with the flow front in the Herring-Bone structure: forward–left/reverse-right (top images). The relative light intensity scattered from the fungi cells reflects the particle distribution in the cross section of the Herring-Bone mixer structure in different cross-sectional planes (bottom images).*

**Mechanical biosensors for particle and molecule detection**

Microcantilever structures were designed and fabricated by the application of recently developed surface micromachining process. The microfabricated test structures were characterised for mechanical stability, deformation, resonance frequency. Investigations definitely require the controlled actuation of the microstructures as well as a precise detection of deformation when applying optical, piezoelectric or piezoresistive read-out.

**Electromagnetic model of cellular flow in a microfluidic system**

Impedance based flow cytometry is a well-known cell-counting and characterising method in and wide spread use. Flow cytometry is powerful in counting, sorting or differentiating cells, or larger particles which have diverse characteristic physical properties. The electromagnetic field evolving in the sample fluid was characterised when particles are travelling in a microfluidic system containing platinum electrodes deposited on the borosilicate glass surface of the fluidic channel formed in crystalline silicon.

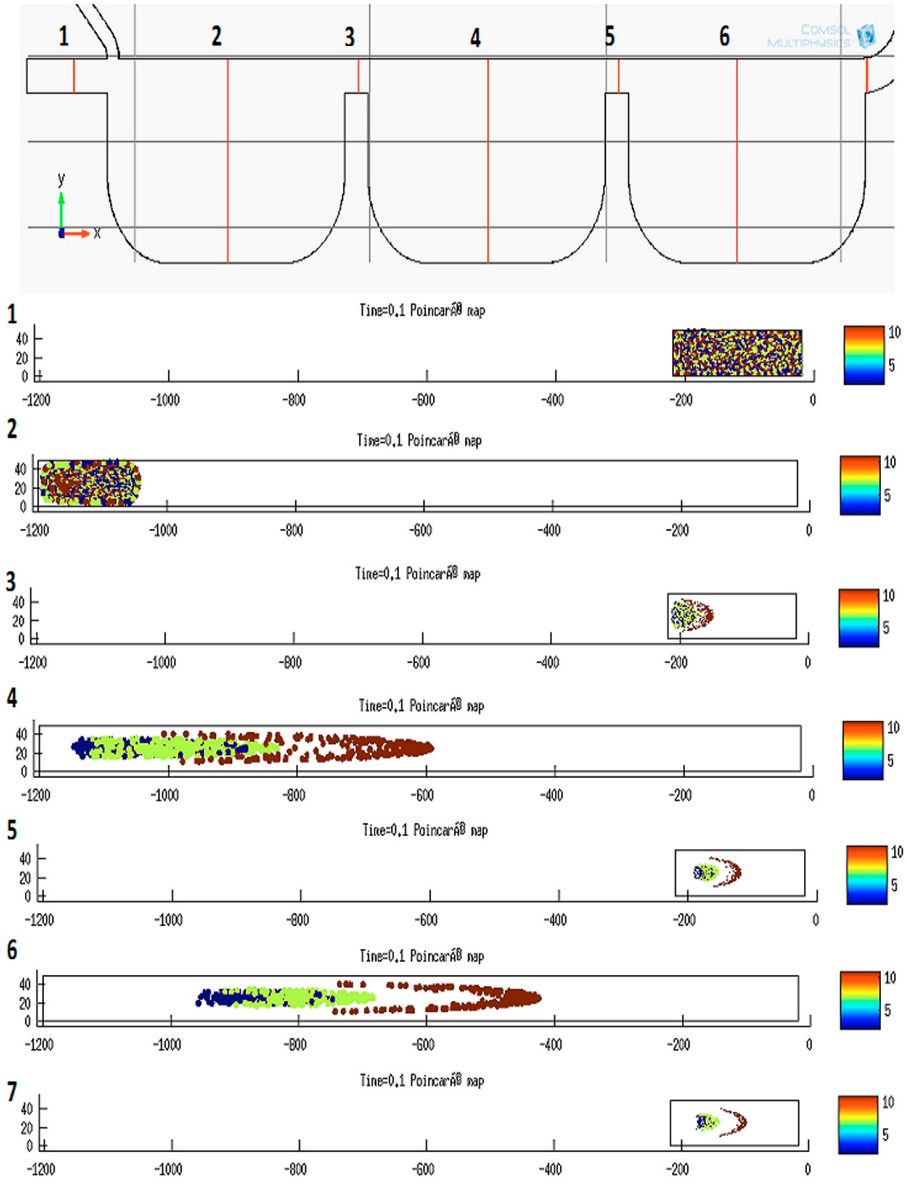


***Figure 6.*** *Size dependent particle separation due to the lateral migration effect was modelled by FEM simulation. The particle distributions (d= 2 (blue), 7 (green) and 15µm (red)) are plotted in different cuts perpendicular to the microchannel.*

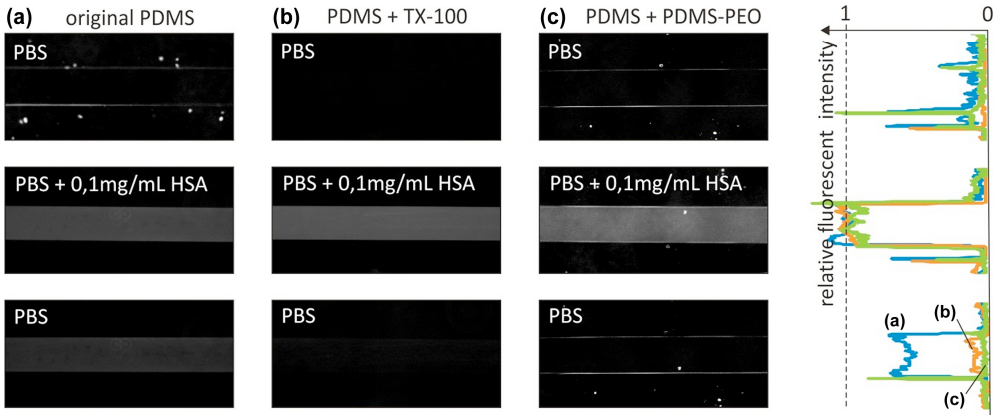


***Figure 7.*** *Fluorescence intensity change in the microchannel recorded after FITC labelled HSA solution (0.1mg/mL HSA in PBS) was injected and washed by PBS. Decreased protein absorption was achieved when the original PDMS surface (a) was modified by 0.2v/v% TX-100 (b), and by 0.2%v/v PDMS-PEO additives(c).*

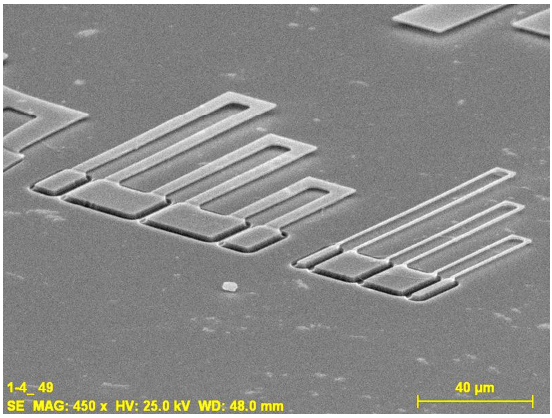


***Figure 8.*** *Polysilicon microcantilever array prepared by surface micromachining.*

2D and 3D simulations were implemented by Matlab and Comsol Multiphysics, respectively, applying simple Dirichlet-boundary for the electrodes and Neumann-boundaries on the channel walls defined as non-conducting elements. The impedance characteristics were computed as the single red blood cell travelled along the channel in physiologic saline water between the electrodes vs. different geometry parameters as channel width, electrode lengths, electrode distance from each other, or the distance of the biological cell from the electrodes. DC and AC impedance and lifting force acting on the biological cell were also computed.

We could conclude that for efficient cell detection and differentiation we should apply low input voltage. The cells have to be positioned by hydrodynamic focusing close to the electrodes being on the same side of the channel (till cell lysis occurs), however, if the electrodes are on the opposite sides, focusing should be in the middle region. Moreover, the channel height and the width of the electrodes should be decreased (just until danger of clogging occurs). The results were applied for optimization of the further geometric design of detector chips including microfluidic channels and platinum electrodes, too.

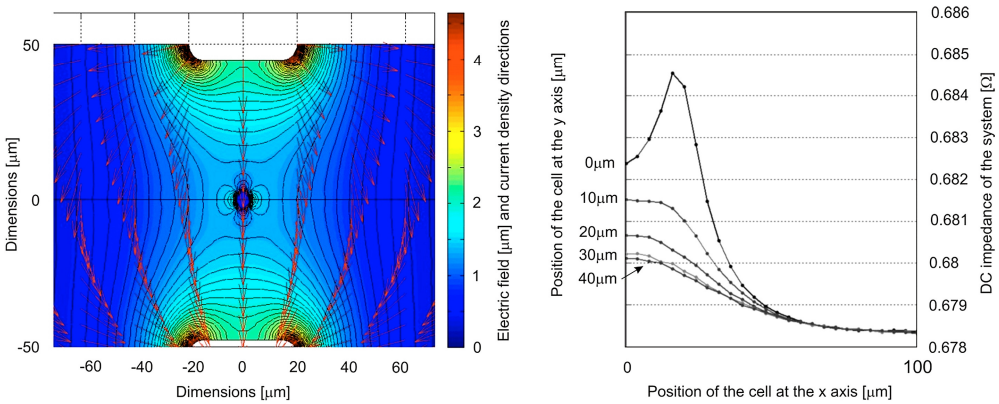


***Figure 9***. *Simulated electric field and current density evolving in a microfluidic channel (left) and DC impedance of the system as a function of the cell position (right).*

# NeuroMEMS

*Activity leader:* Z. Fekete
*Group members:* P. Fürjes, Z. Hajnal, Gy. Molnár, A. Pongrácz, A. L. Tóth, Z. Bérczes, and G. Márton,

*Activities are supported by:*
- Targeted research activity supported by Gedeon Richter Plc.

**Single-shaft microelectrodes combined with microdrives**

Exploring neural activity behind synchronization and time locking in brain circuits is one of the most important tasks in neuroscience. These questions are intensively studied by using multiple electrodes to measure activity concurrently in different brain areas. A robust silicon-based microelectrode array with anatomically designed site arrangement was designed in order to record neural activity of freely moving rats in several brainstem nuclei, concurrently. A microdrive allows precise electrode positioning (and free repositioning) during chronic experiments. When the recording of single-unit activities is crucial, this ability is extremely useful.

In our system, the probe is fixed on a PTFE block of the micropositioner. The self-lubricating PTFE block travels smoothly on two tightly fit rods, its position can be adjusted with a driving screw (300 μm/turn). A flexible cable connection of 50 μm thick polyimide provides sufficient freedom for the movements of the drive. The robust structure of the device allows very stable probe location, and excludes vibration.

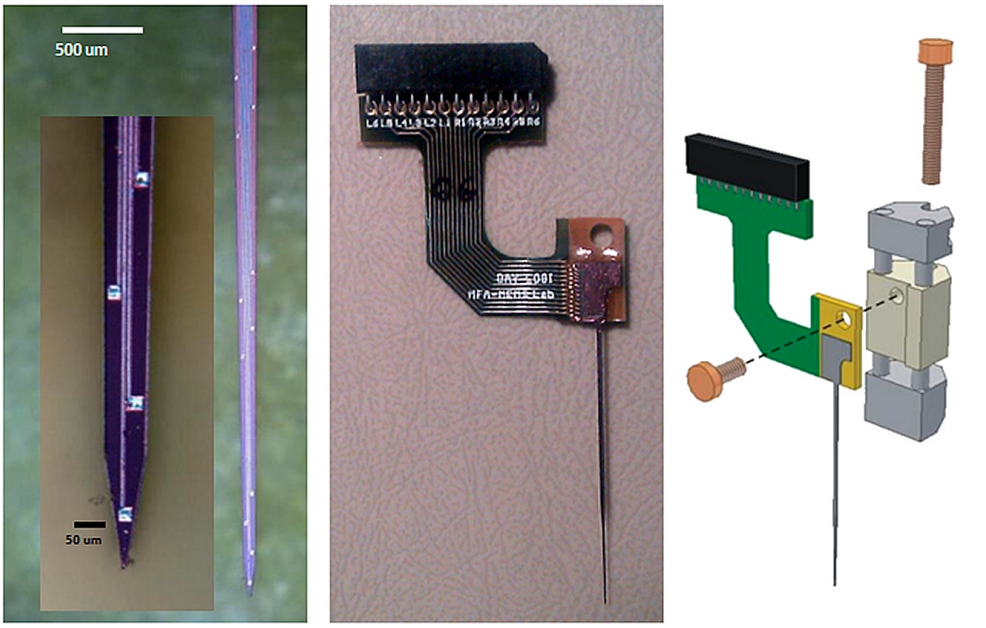


***Figure 1***. *Si microelectrode - microdrive system with flexible encapsulation.*

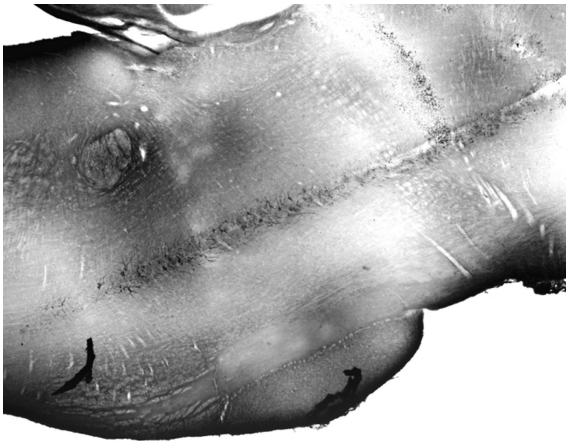

***Figure 2***. *Simultaneous long-term recording (up to 6 months) of single unit activity from three target areas.*

| | **Putative principal-like cells** | **Local inter-neurons** |
|---|---|---|
| DpMe | 23 | 8 |
| PPtg | 8 | 0 |
| PnO | 55 (37+18) | 24 |
| | 86 (~73%) | 32 (~27%) |
| | 135 after sorting →**118** | |

***Figure 3***. *Distribution of action potentials recorded in the target areas.*

**Neural microelectrodes with local drug delivery and simultaneous electrical recording functions**

The fabrication method, electrical and fluidic characterization and in vivo testing of the first silicon deep brain multielectrodes (up to 70mm long) with monolithically integrated fluidic channel were studied. Both the electrical and fluidic performance of the probe was investigated. Field potential, multi- and single unit activities were recorded. Measured and calculated hydrodynamic resistance of the microchannels showed good consistency. The typical volumetric flow rate values are in the 0.5–5 µl/min range at pressures below 200 kPa. The performed in vivo test proved that the fabricated hollow microprobes are applicable as stable drug delivery devices in neural implants. Simultaneous electrical recording is provided even in deep brain regions. This technology is robust and scalable. Custom made drug outlets and recording/stimulating sites can be integrated in order to fulfil requirements of special experiments. The proposed technology still preserves the freedom of further integration of microcomponents, e.g. fluidic actuators, micromixers, optical waveguides and biosensors, opening the door to more complex and delicate investigation of the central nervous system.

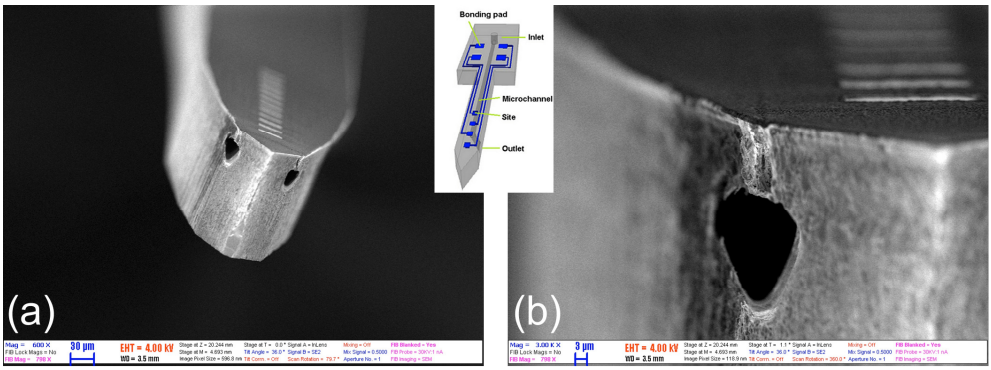


***Figure 4.*** *Micrograph of the first silicon deep brain multielectrode with monolithically integrated fluidic channel (a), and close-up SEM view of the fluidic outlet of a buried microchannel (b).*

**Surface enhancement of silicon microelectrode array by black-platinum**

Despite the broad spectrum of already published methods, impedance reduction of electrodes of neural microelectrode arrays (MEAs) is still an issue under active research. A key factor to be considered is whether these deposits are durable enough to withstand the penetration into the neural tissue. The durability of high surface area platinum electrodes during acute intracerebral measurements was investigated. Electrode sites with extremely rough surfaces were prepared by electrochemical deposition of platinum onto silicon-based MEAs from a lead-free platinizing solution. The close to 1000-fold increase in effective surface area lowered the impedance, its absolute value at 1 kHz dropped to about 7% and 18% of the original Pt electrodes in vitro and in vivo, respectively. 24-channel probes were subjected to 12 recording sessions, during which they were implanted into the cerebrum of rats.

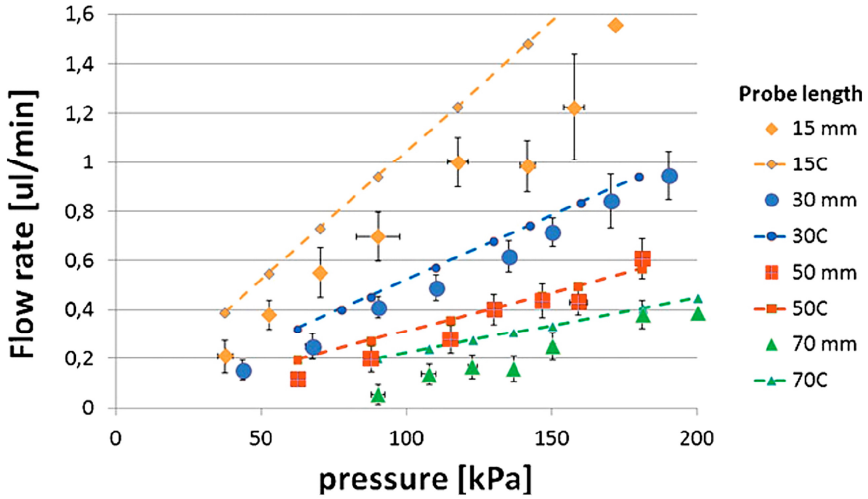


***Figure 5.*** *Measured and calculated flow rate vs. pressure characteristics of a hollow microprobe for different probe lengths.*

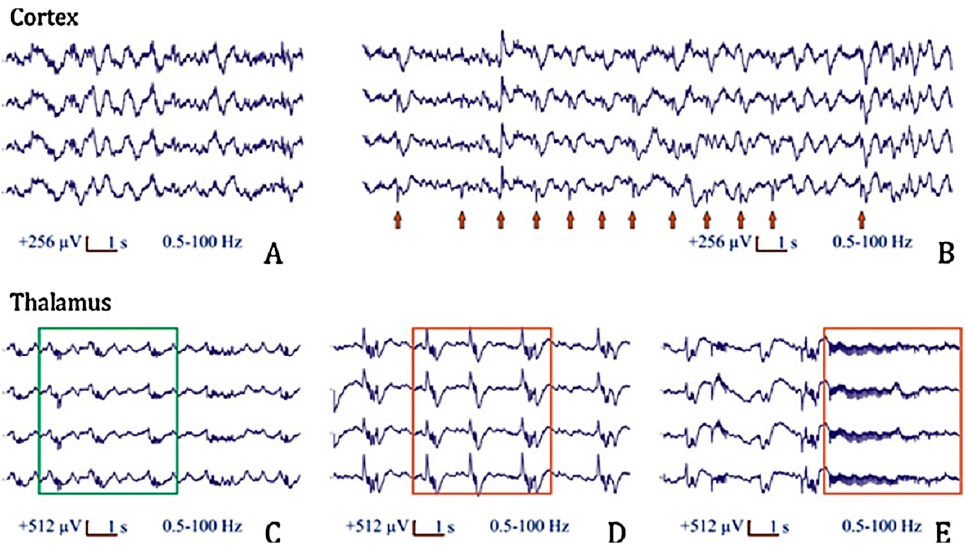


***Figure 6****. Local field potential signals in rat cortex, band-pass filtered at 0.5–100 Hz, showing slow wave activity before injection (A). Bicuculline caused elevated neural activity, which is indicated by interictal-like spikes on the local field potential signals. These local field potential spikes are marked by red arrows (B). In the thalamus, signals were recorded during normal activity (C), and under bicuculline-induced conditions, such as interictal-like spikes (D), and high-frequency epileptic-like events (E).*

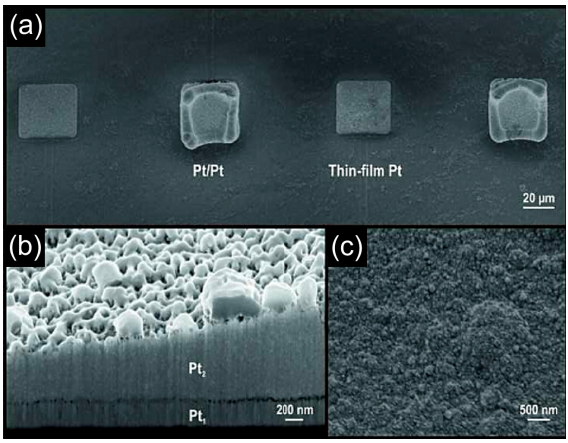


***Figure 7.*** *(a): Scanning electron microscopic images of four neighbouring electrode sites on the MEA, two of them coated with Pt/Pt, (b): A cross-sectional view of the Pt/Pt layer, sectioned by Focused Ion Beam (FIB). Pt1 is the original thin-film, Pt2 is the electrochemically deposited layer. (c): Surface microgram of deposited platinum (Pt/Pt electrode).*

Although the effective surface area of the platinized sites mostly decreased, it remained more than two orders of magnitude higher than the average effective surface area of the sputtered original platinum thin-film electrodes. Sites with electrochemical deposits proved to be superior, e.g. they provided less thermal and 50 Hz noise, even after 12 penetrations into the intact rat brain.

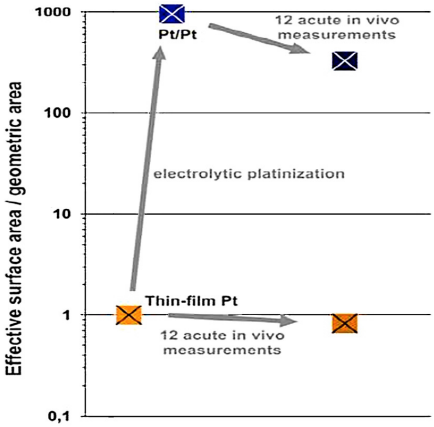


***Figure 8.*** *The variation of average effective surface area with electrolytic platinum deposition and multiple acute use of the MEAs.*

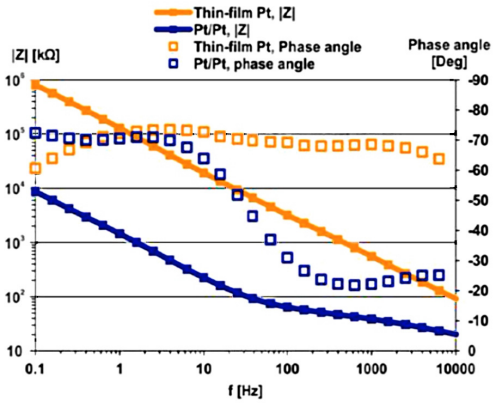


***Figure 9.*** *Average EIS spectra of original thin-film Pt and Pt/Pt electrodes on a probe.*

**Mechanical interaction between single-shaft silicon microelectrodes and rat dura-matter**

Due to the rapid development in micro- and nanofabrication technologies, several types of medical implants were proposed and applied successfully in neurosurgery. In order to determine the safety margins and design rules for newly emerging techniques, in vivo mechanical characterisation is essential to be performed. In our

work, experimental investigation is presented focusing on the interaction between rat brain tissue and single-shaft silicon microprobes fabricated by deep reactive ion etching. Physical parameters like penetration force and dimpling were studied in terms of insertion speed (mm/min range) and microprobe cross-section. Insertions were performed through intact *dura* and *pia* matter.

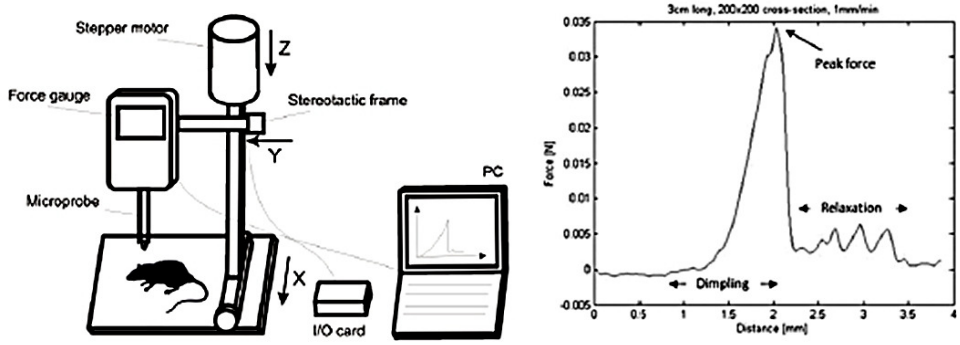


***Figure 10.*** *Schematic representation of the experimental setup for in vivo testing of penetration mechanics (left) and a typical force vs. distance curve (rights).*

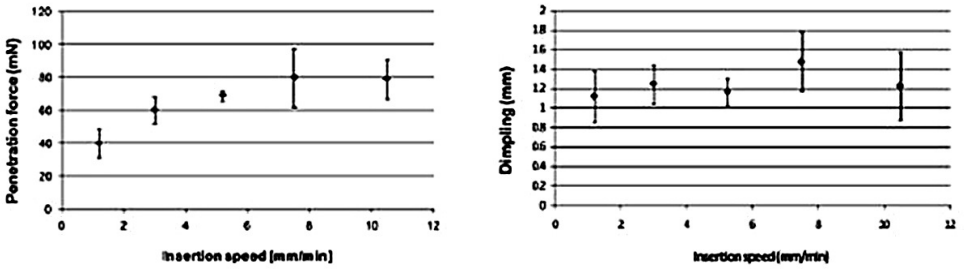


***Figure 11.*** *Measured penetration force and dimpling at various insertion speed with a probe cross-section of 200 × 200 μm$^2$.*

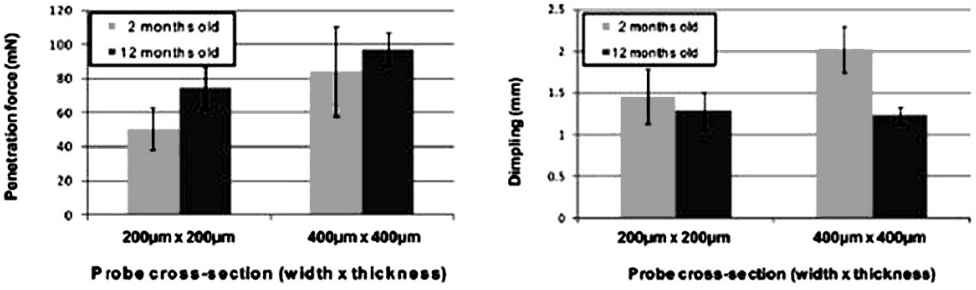


***Figure 12.*** *Measured penetration force and dimpling as a function of rodent age in case of two different probe-cross-sections.*

**Polymer-based microelectrode arrays for electrophysiology**

Polymers attract increasing attention as bulk materials for microelectrode arrays, applied in experimental electrophysiology and clinical use. Their fabrication costs are relatively low, and their flexibility allows smoother coupling with the soft neural tissue than do rigid substrates. Sufficient biocompatibility of the applied materials is essential in this field. Several types of polymers, such as SU-8 photoresist, Polyimide (PI) and Parylene C meet this criterion. Polymer-based device components for neural interfacing show great heterogeneity in structure and function. In order to obtain electrical connection with the central nervous system, cerebral implants are available. Interfaces with peripheral nerves can be constructed with sieve, cuff and transverse probes. Microfabricated polymer structures are commonly applied for electrocorticography (ECoG) as well, which is a widely used method for the localization of epileptogenic zones. At the Department of Microtechnology, we have developed various microtechnology related processes which are required to create – among others – such structures. We use silicon wafers as substrates. The key components of the process flows are SU-8 lithography, patterning metal layers with lift-off technology and reactive ion etching of polyimide. Utilizing these methods, e.g. PI – Pt – SU-8 three-layer structures can be formed. We constructed various, custom-designed, polymer-based probes for both in vitro and in vivo electrophysiological applications.

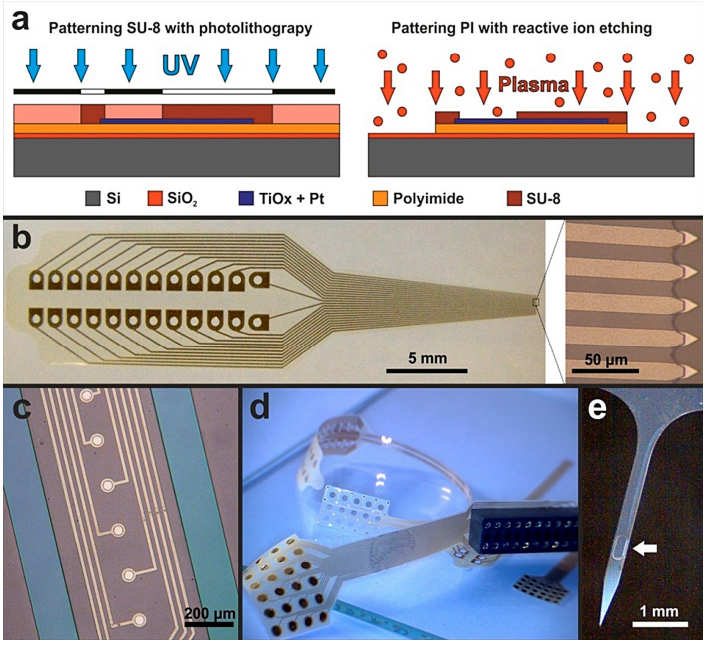


***Figure 13.*** *(a): patterning of SU-8 and polyimide layers in microfabrication. (b): examples of polymer-based neural probes manufactured by our group: a "spiky" electrode array for in vitro analysis of brain wafers. (c): an intracerebrally implantable extracellular array. (d): electrodes designed for electrocorticography. (e): a probe with a microwell, which can contain e.g. bioactive molecules.*

# NEMS

*Activity leader:* J. Volk
*Group members:* Zs. Baji, G. Battistig, Cs. Dücső, P. Földesy, N. Q. Khánh, I. Lukács, Gy. Molnár, A. L. Tóth, Zs. Zolnai, R. Erdélyi Z. Szabó, and I. Bársony

*Activities are supported by:*
- OTKA K109674 – Graphene-based terahertz modulators (2013-2017)
– EU FP7-ICT-2013-10- 611019 - High-resolution fingerprint sensing with vertical piezoelectric nanowire matrices (PiezoMAT) (2013-1015)

**Investigation of quasi-one-dimensional compound semiconductor nanostructures**
The semiconductor nanodevice activity focussed on the synthesis and characterization of quasi-one-dimensional semiconducting nanostrucrures, as well as on their integration into functional sensor, optoelectronic and photovoltaic devices. The explored research fields include the electrical characterization of hydrothermally grown high aspect ratio ZnO nanowires, the mechanical characterization of vertical nanorods, the synthesis and characterization of hierarchical ZnO nanostructures, as well as a new research topic related to $TiO_2$ atomic wires.

**Characterization of Field Effect Transistor Based on Hydrothermally Grown ZnO Nanowire**
Since the last decade zinc oxide nanowires (ZnO NW) became potential candidates in sensor applications. The transducer in most cases of chemical and biosensors is a ZnO NW based Field Effect Transistor (FET). In such application for obtaining an acceptable noise/signal ratio it is important to fabricate good contacts to the NW. The other essential point is its gating behaviour, which determines the sensitivity of the sensor. We have prepared the FETs based on hydrothermally synthesized ZnO NW, and characterized them observing the above aspects electrically.
Synthesis of ZnO NWs was carried out from Zn foil in solution of sodium hydroxide and ammonium persulfate (W1), or from sputtered ZnO seed in aqueous solution of zinc nitrate/ hexamethylenetetramine (W2). In some cases the NWs were annealed at 200 or 600 °C in air for 30 min. Contact formation of the NWs with Al or Ti/Au was realized by using e-beam lithography, metal deposition and lift-off.

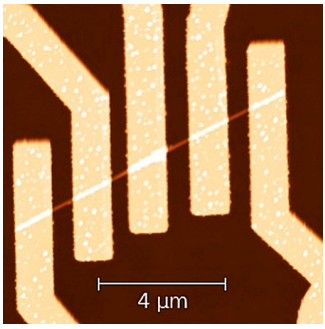


The AFM image of a NW having multiple contacts is presented here. By means of I-V measurement on each contact pair, one can determine the contact and wire resistance (Transfer Length Method), respectively, as depicted on the right side of the figure. These parameters can also be obtained by four-wire measurement, where the voltage drop between the inner contact pair was measured while forcing a constant current through the outer contacts.

***Figure 1.*** *AFM image of contacted ZnO NW.*

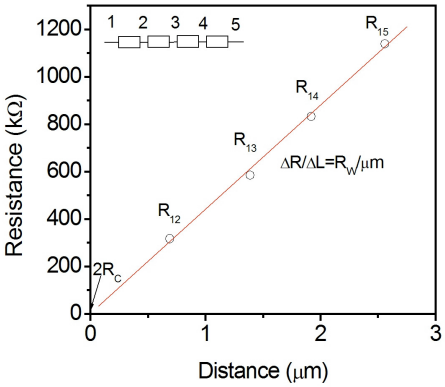


***Figure 2.*** *TLM measurement of Ti contacted ZnO NW.*

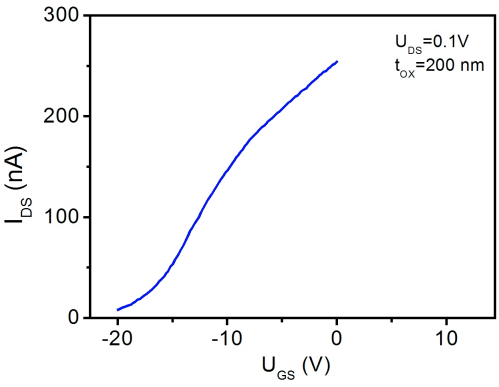


***Figure 3.*** *$I_{DS}$-$V_{GS}$ characteristics of Ti contacted ZnO NW.*

Using degenerately doped Si substrate as global back gate, the $I_{DS}$ vs. $V_{GS}$ function can be recorded, from which one can deduce the values of transconductance ($g_m$), surface mobility ($\mu$), carrier concentration ($n_i$), and threshold voltage ($V_{th}$).
The results are summarized in the table below. The non-annealed W1 wire is rather metallic, presumably due to high charge carrier concentration in the NWs, which causes low contact resistance, but makes the gating impossible. The gating effect is significant only for the W1 NW annealed at 600 °C, probably due to the out-diffusion of hydrogen incorporated into ZnO during the synthesis process. The W2 NWs are superior to W1 ones, because they can be gated without post annealing. Furthermore, their typical thickness is less than that of the W1 NW's, which enhances the sensitivity of the NW-based sensor via a complete depletion of the conducting channel.

***Table I.*** *Parameters of ZnO NW based FETs*

| Samp./$T_a$/Contact | Spec. $R_c$ (x$10^{-7}$ Ωcm$^2$) | Spec. $R_w$ (mΩcm) | $V_{th}$ (V) | $g_m$ (nS) | μ (cm$^2$/Vs) | Carrier conc. (x$10^{18}$ cm$^{-3}$) |
|---|---|---|---|---|---|---|
| W1 RT Ti | 2.5 | 3 | - | - | - | - |
| W1 RT Al | 3.0 | 3 | - | - | - | - |
| W1 200 °C Al | 4.4 | 2.6 | - | - | - | - |
| W1 600 °C Ti | 110 | 130 | -17.8 | 20 | 17.6 | 4.0 |
| W1 600 °C Al | 72 | 113 | -13.1 | 98 | 22.7 | 6.7 |
| W2 RT Ti | 340 | 40 | - | - | - | - |
| W2 RT Al | 326 | 10 | -11.8 | 34 | 52.4 | 14 |

**Bending strength analysis of vertical ZnO nanowires**

For the practical applications of vertical nanowires in Nano-ElectroMechanical Systems (NEMS) it is pivotal to maintain mechanical strength, since they are often exposed to heavy duty use during operation. Aqueous chemical method is widely used for the growth of ZnO nanostructures, since various morphologies in a predefined fashion can fairly easily be achieved. However, 'as prepared' wet

chemically grown NWs show poor mechanical behaviour compared to their counterparts synthesized by physical methods at higher temperatures.
To overcome this latter problem, while retaining the benefits of aqueous chemical growth, we applied different heat treatments right after the synthesis in order to improve the mechanical properties. The effect of annealing temperature and annealing atmosphere was studied by our *in-situ* static bending setup inside the SEM. The arrangement is composed of a nanomanipulator robotic arm equipped with a calibrated AFM probe, which was used to bend the NWs at their free end until fracture occurred. The maximal strain generated at the root of the NWs right before the fracture was estimated by analysis of the videos captured during the manipulation. The most significant improvement in the robustness was achieved by applying an annealing temperature of 700 °C for 2 hours in oxygen atmosphere. Hence the maximal strain increased from 1.2 % to 3.8 % and the magnitude of the load needed to fracture the NWs became almost half an order of magnitude larger.

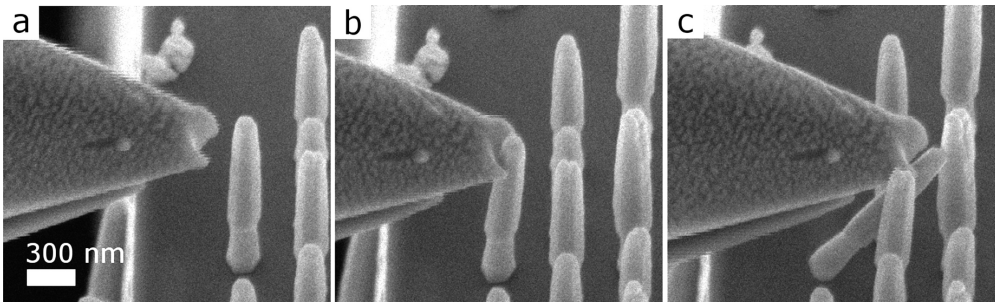


***Figure 4.*** *Scanning electron micrographs showing the steps leading to the fracture of a ZnO nanowire of poor mechanical properties: positioning the tip(U-shaped) of the AFM probe close to the nanowire before manipulation (a), bending of the nanowire by the lateral load at its free tip (b), and fracture at its root (c).*

Another quantitative way of the mechanical characterisation of vertical nanowires can be done by atomic force microscopy (AFM), since during scanning both cantilever deflections and torsions are monitored by a position-sensitive photodetector. The obtained normal and lateral force signals can provide information about normal and lateral forces acting on the tip. However, in the normally used indirect calibration methods many error sources exist. To apply a known lateral force on the AFM probe we used a sheet of pyrolytic graphite which is levitated by a strong magnetic field, as a reference spring. Due to the direct nature of this detection method, the applied loads and hence the elastic moduli of nanostructures can be determined with high confidence, without the need for detailed information (e.g. geometry, resonant frequency) of the cantilever. The proposed technique was successfully applied for the quantitative characterization of NW fractures.

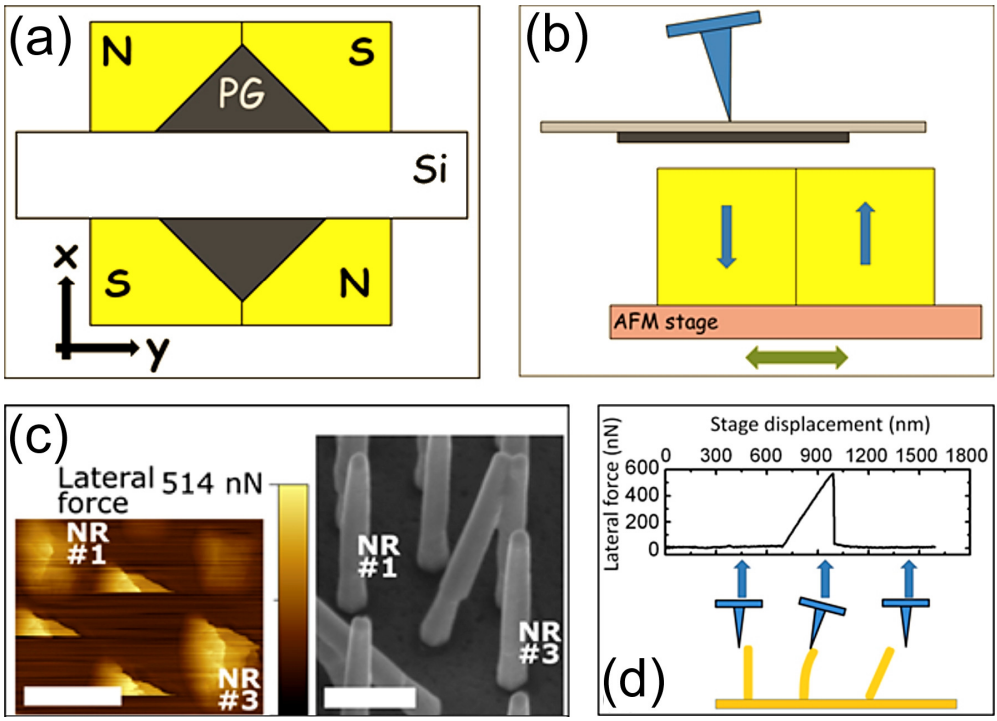


***Figure 5.*** *Scheme of the D-LFC method: (a): the pyrolytic graphite sheet - Si wafer assembly is levitated by a strong magnetic field (top-view), (b): the diamagnetic levitation spring system mounted on the AFM stage to calibrate the lateral PSPD output, (c): typical lateral force map recorded during fracture events with the corresponding SEM image, and (d): the recorded bending curve.*

**Investigation of hierarchical ZnO nanostructures for dye-sensitized solar cells**

Dye-sensitized solar cells (DSSCs) are attracting considerable attention, as they may offer a promising alternative for silicon-based solar cells. This is because of their reasonably high power generation efficiency that comes at a low cost without environmental risks. The most efficient DSSCs apply $TiO_2$ nanoparticles. ZnO, however, is also often considered as a good candidate, too, since its more than one order of magnitude higher bulk electron mobility. Moreover, there is a great variety of fabrication techniques available for micro- and nanostructured ZnO.

In order to maximize the specific surface and thereby the dye uptake of the nanostructure, a novel synthesis route was demonstrated for the preparation of hierarchical ZnO structures. The fabrication technique combines a self-assembled nanosphere photolithography technique with multiple steps of low temperature hydrothermal ZnO growth.

The investigated nanostructure geometries include as grown random ZnO nanowires (NW), short and long regular pillars (SP, LP), short pillars covered by a porous ZnO layer (SP+PL) and long pillars with shorter or longer side branches (LP+short-SB, LP+long-SB), as well as ZnO thin film (TF) for reference. The specific surface area

was deduced from the absorbance spectra of the dye solutions after selective etching of ZnO nanostructure in NaOH water-ethanol solution. Assuming a uniform monomolecular coverage on the surface, effective roughness factors up to $10^6$ were achieved. Some selected nanostructures were also used to fabricate solid electrolyte DSSC cell. The photoelectric characterizations revealed that the higher specific surface results in an enhanced short circuit current but too long side-braches can lead to smaller fill-factor and open-circuit voltage.

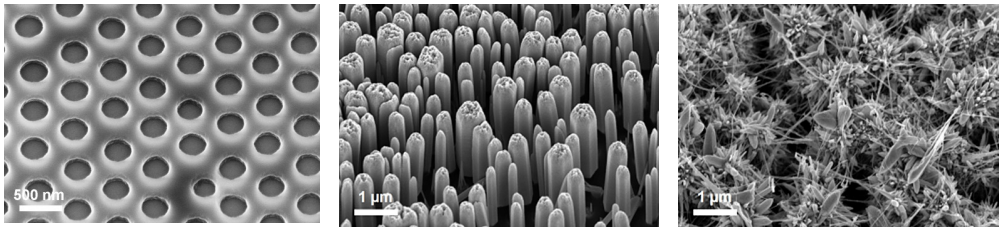


***Figure 6.*** *(a): SEM images of developed photoresist, (b): hydrothermally grown ZnO pillars, and (c): ZnO pillars with hydrothermally grown side branches.*

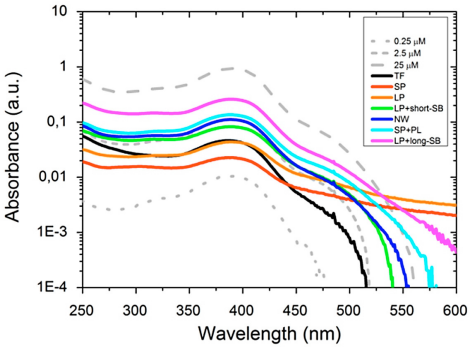


***Figure 7.*** *Absorbance spectra of the calibration series (grey dashed lines) and the resolved dye solutions (colour lines).*

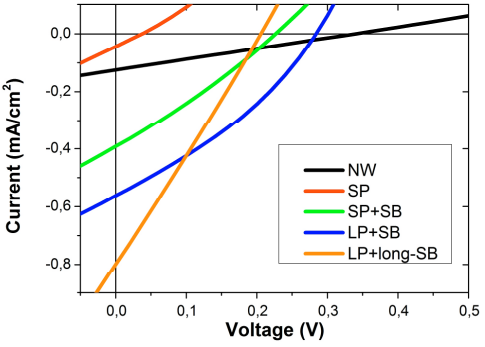


***Figure 8.*** *Current-voltage curve of photovoltaic cells built with different nanostructure geometries.*

**Structural Characterization and Contact Formation on Ultra-thin Anatase $TiO_2$ Nanowires**

Wide band gap semiconductor titanium dioxide ($TiO_2$) is known as a versatile material with a wide range of applications. Nanostructures of $TiO_2$ in various crystal modifications are used among others in photocatalytic and photovoltaic applications. Recently, a new concept based on Dirac-states inside the conduction band of ultra-thin, n-type anatase $TiO_2$ nanowire (NW) was proposed to prepare high speed and good on-off ratio field effect transistors. To this end, we have characterized the structure of the $TiO_2$ NWs grown by non-hydrolytic solution approach. Then we successfully prepared contacts to such NWs, as first step to prove the above concept.

**Structural characterization**

The $TiO_2$ NWs first have been analysed by Transmission Electron Microscopy (TEM). The length of the wires was found to vary in the range of 10–40 nm, while their thickness is estimated to be around 3-3.5 nm. The picture shows the high resolution image (HRTEM) of the individual $TiO_2$ NW. The lattice fringes of the single crystalline NW are well resolved. The wire diameter is not uniform, but fluctuates about 25% along the longitudinal axis. The phase analysis using electron diffraction reveals that the crystal structure of our $TiO_2$ NWs is not rutile, but anatase, which was confirmed by X-ray diffraction analysis.

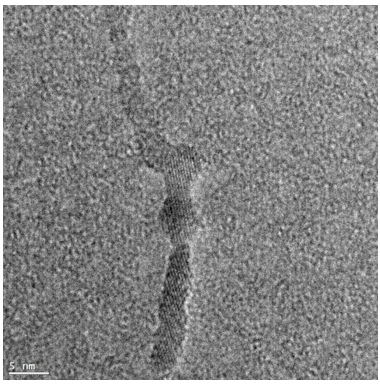

***Figure 9.*** *High resolution TEM image of $TiO_2$ NW.*

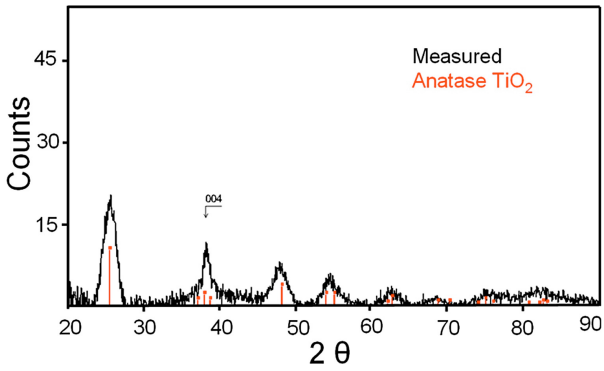


***Figure 10.*** *XRD of the $TiO_2$ NW. (The pattern of anatase $TiO_2$ is also shown (red).)*

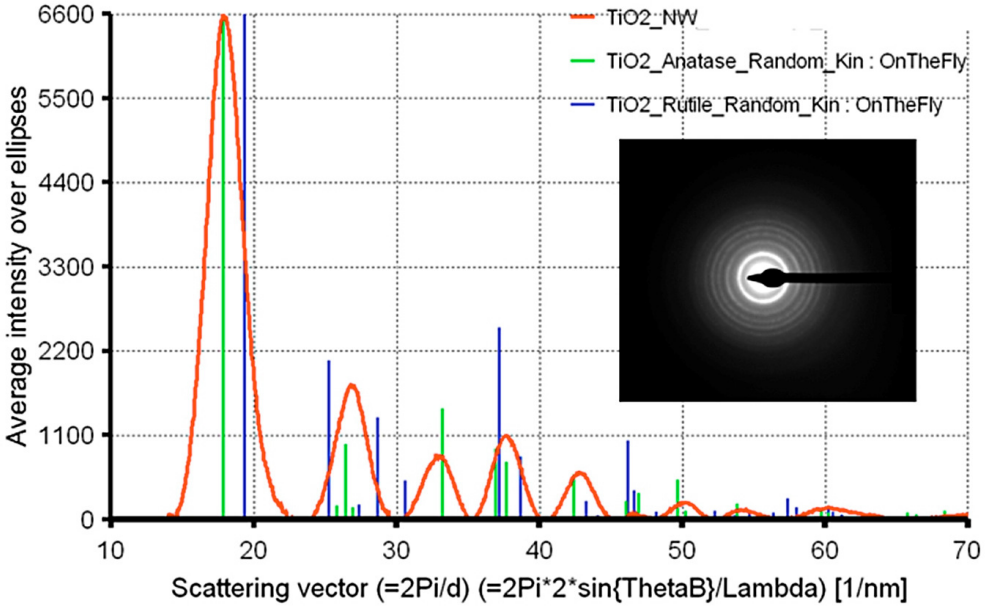


***Figure 11.*** *Phase analysis of electron diffraction.*

**Contact preparation**

The $TiO_2$ NWs surface-stabilized by oleic acid was dispersed in cyclohexane, and deposited on top of the 100 nm thermal silicon-dioxide coated chip. The lithography of the PMMA e-resist layer was used for the formation of a pair of contacts with a gap of ca. 25 nm in two steps. The first one was the usual e-beam lithography to form a PMMA stripe with the width of 100 nm, which is the resolution limit of our system. In the second step oxygen plasma was applied to adjust the desired width by an optimized treatment time. This dry etch is gentle enough to prevent the collapse of final, very thin PMMA stripe, which could occur due to capillary force in the case of normal use of developer. The figure shows the AFM image of the $TiO_2$ NW contacted with 5 nm thick Cr layer. The thickness of the NW measured by AFM is about 3 nm, as confirmed by the TEM.

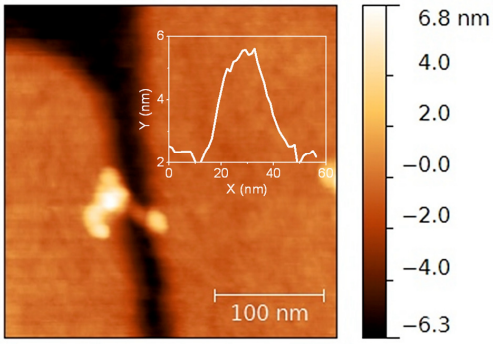


***Figure 12.*** *AFM image of $TiO_2$ NW contacted by 5 nm thick Cr layer. The line-cut across the nanowire is shown in the inset.*

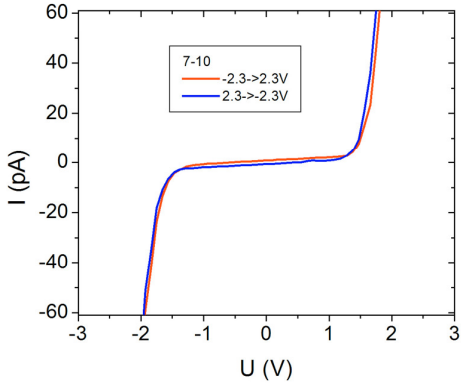


***Figure 13.*** *I-V characteristics of Cr contacted $TiO_2$ NW.*

Preliminary I-V characterization was carried out on the Cr contacted NW. The device shows back-to-back Schottky behaviour, presumably due to the fact that the work function of Cr (4.5 eV) is higher than the electron affinity of $TiO_2$ (4.2 eV), thus forming a Schottky-junction at both $Cr/TiO_2$ interfaces.

# *Nanobiosensorics "Lendület" Group*

**Head: Róbert HORVÁTH, Ph.D., senior scientist**

**Research Staff**

- Róbert HORVÁTH, Ph.D.
- Sándor KURUNCZI, Ph.D.
- Inna SZÉKÁCS, Ph.D.

**Ph.D. students / Diploma workers**

- Krisztina JUHÁSZ, Ph.D. student
- Judit NÁDOR, Ph.D. student
- Norbert ORGOVÁN, Ph.D. student
- Dániel PATKÓ, Ph.D. student
- Beatrix PÉTER, Ph.D. student
- Rita SALÁNKI, Ph.D. student
- Enikő FARKAS, M.Sc. student
- Boglárka KOVÁCS, M.Sc. student
- András SAFTICS, M.Sc. student
- Ágnes DOBOS, B.Sc. student
- Gabriella GULYÁS, B.Sc. student
- Bálint KOVÁCS, B.Sc. student

The Nanobiosensorics Group was established in the framework of the Lendület Program of the Hungarian Academy of Sciences. The research program funds outstanding young researchers in Hungary in order to establish their own independent research groups. The research profile of the Nanobiosensorics Group is the development and application of label-free optical biosensors, the mathematical modeling of the relevant biological and biophysical processes. In 2013, the group made important steps in the development of its unique research infrastructure and in creating its personal and collaborative network as well. The established – in Hungary not yet conducted - research lines are promising. In several topics (instrumental development, monitoring microvesicles, flagellin based functional layers, modeling) the group could achieve strategic results, which were published in important international journals (*Analytical Chemisty, Biosensors and Bioelectronics, Nature Scientific Reports, Sensors and Actuators B, International Journal of Molecular Sciences*), or are under submission.

The group has established a unique cell culture sensorics laboratory, making possible to launch a new and promising research line in Hungary, the "label-free biosensorics of living cells". They have installed an EPIC multichannel biosensor prototype and an M4 Holomonitor. In collaboration with the Semmelweis and Eötvös Universities the Nanobiosensorics Group first characterized the adhesion properties of microvesicles secreted by living cells and the surface adhesion kinetics of human monocytes using label-free optical biochips. Their results on measuring the structural order of nanometer scale biological layers (lipid bilayers [53], proteins [83]) are similarly important. These results can find further applications in medical diagnostics.

# Cell secreted microvesicle label-free research

*(EU FP7 OPTIBIO 231055, OTKA PD73084, "Lendület" grant of HAS, TÁMOP)*

D. Patkó, B. György*, A. Németh*, K. E. Szabó-Taylor*,
A. Kittel**, E. I. Buzás*, and R. Horváth

*Semmelweis Univ., Dep. of Genetics, Cell- and Immunobiology, Budapest, Hungary
**Institute of Experimental Medicine, HAS, Budapest, Hungary

In 2013 we have introduced for the first time a novel label-free optical method, the Grating Coupled Interferometry (GCI), to study EVs (Extracellular Vesicles) secreted by live cells. GCI was applied for on-line monitoring the interaction of these cell-derived EVs with extracellular matrix molecules. The GCI technique is completely label-free; the vesicles were investigated in their native state and their interaction was followed with extremely high resolution.

It is important to stress that EVs represent novel diagnostic biomarkers of various diseases. They are highly abundant in various biological fluids including blood plasma, urine, cerebrospinal fluid, synovial fluid, saliva, breast milk, etc. Their levels, protein compositions and microRNA signatures were shown to associate with numerous pathologies, including tumors, autoimmune disorders, cardiovascular diseases, infections. However, their routine clinical analysis is limited, and thus, there is an urgent need for the development of new techniques for the analysis of EVs.

Further applications of this novel technique include studying EV surface molecules by investigating the binding of EVs to antibody-coated surfaces as well as investigation of receptor-ligand interactions in the field of EVs. The GCI technique can be especially advantageous for the above applications since it not only offers superior sensitivity with excellent time resolution, but contains no moving parts, built up from cheap and potentially highly miniaturizable components. The technique is equally suitable for handheld devices as well as for high through screening instruments, facilitating industrial and diagnostic applications as well [121].

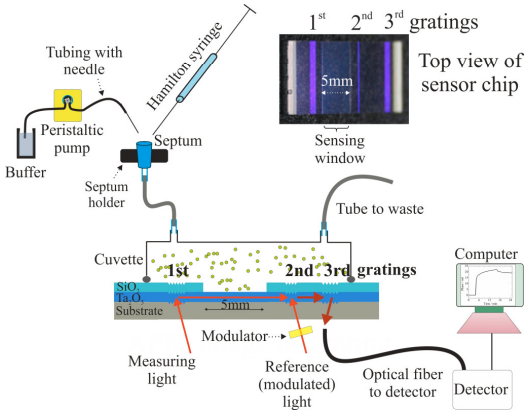


***Figure 1.*** *Schematic cross-sectional illustration of the GCI sensor [121].*

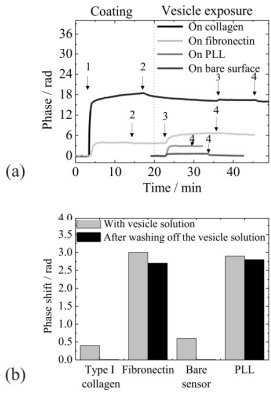


***Figure 2.*** *In situ phase changes of the GCI sensor [121].*

# In-situ and label-free optical monitoring of the adhesion and spreading of primary monocytes isolated from human blood: Dependence on serum concentration levels

*("Lendület" grant of HAS)*

N. Orgovan*, R. Salánki, N. Sándor**, Zs. Bajtay***, A. Erdei**,***, B. Szabó*, and R. Horváth

*Department of Biological Physics, ELTE, Budapest, Hungary
**MTA-ELTE Immunology Research Group, Budapest, Hungary
***Department of Immunology, ELTE, Budapest, Hungary

Adhesion and spreading of primary monocytes isolated from human blood were monitored utilizing optical waveguide lightmode spectroscopy (OWLS); a highly sensitive label-free biosensor technique using evanescent optical waves generated at a biocompatible surface [Biosens Bioelectron 54, pp.339-344 (2014)]. Appropriate development on a custom built setup enabled the OWLS cuvette to be operated as a 1.5 ml mini-incubator, controlling both temperature and $CO_2$ levels (Fig. 1). The incubator-equipped OWLS is readily applicable for delicate and long-term studies on sensitive primary cells, demonstrated here through monitoring the serum dependence of the adhesion and spreading of human monocytes. Moreover, the custom-built setup enables the simultaneous monitoring of the position and overall width of the OWLS resonant peaks. This unique feature makes it possible to distinguish the refractive index variations induced by the adsorption of secreted material from refractive index changes provoked by cellular spreading. A definite attachment and spreading activity was observed on the substratum (glassy silica–titania), when the serum level of the culturing medium was 0.0–0.01% (Fig. 2). Increasing serum concentration resulted in a steep fall in monocyte surface adhesion and spreading. 1.0% serum level practically abolished all spreading activity measured by OWLS (Fig. 2), and the number of attached cells was significantly decreased, too. Serum addition to fully spread cells provoked a reduction in the cell–substratum contact area, clearly detectable by the biosensor. Cell spreading was inhibited by pre-coating the sensor surface with considerable amounts of serum proteins. These findings suggest that monocyte spreading is inhibited by the adsorption of serum biomolecules to the substratum, rather than by soluble factors present in the serum. All of these results were obtained completely noninvasively with real time monitoring; demonstrating the capabilities of OWLS to sensitively monitor the adhesion properties of immune cells isolated from human blood.

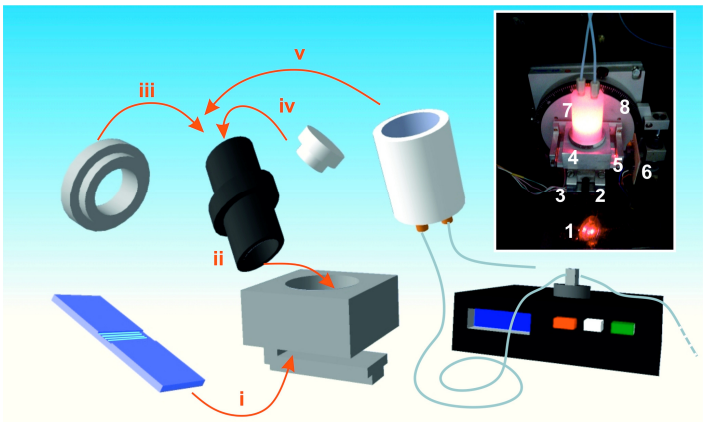


***Figure 1.*** *Simple modification on our custom built OWLS setup allowed us to operate the OWLS cuvette as a mini-incubator. In this drawing only the parts enabling $CO_2$ control are depicted. Roman numbers indicate the order of assembly: (i) and (ii) the waveguide (sensor chip with optical grating) and the cuvette is inserted to the holder, (iii) the cuvette is fixed with a screw, then (iv) plugged and (v) capped, the cap being connected to the $CO_2$-infusion control unit (bottom left corner). Inset: photograph of the assembled mini-incubator OWLS cuvette mounted on the goniometer. 1. Mirror reflecting the laser light, 2. track into which the cuvette holder can be fixed, 3. heating module fastened to the back of the metallic cuvette holder, 4. cuvette holder, 5. sensor chip guiding the in-coupled light, 6. photodiode measuring the intensity of in-coupled light, 7. cap for $CO_2$-infusion, and 8. high- precision goniometer [Biosens Bioelectron 54, pp.339-344 (2014)].*

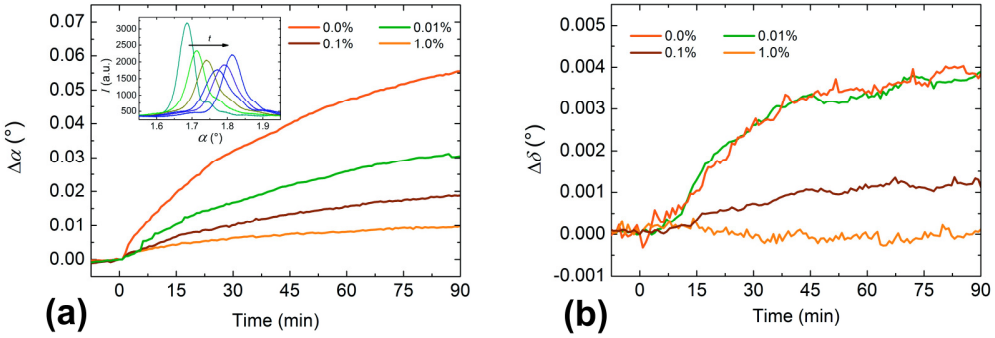


***Figure 2.*** *OWLS responses provoked by monocyte adhesion and spreading in the presence of various serum concentrations (expressed as % FBS dilution). All of the four experiments were carried out on the same day with monocytes of the same donor. Image **(a):** shift of the position of the resonance peak (Δα) as a function of time. Inset: temporal evolution of the overall shape of the resonance peak. Image **(b):** temporal evolution of the width of the resonance peak provoked by monocyte spreading [Biosens Bioelectron 54, pp.339-344 (2014)].*

# Dependence of cancer cell adhesion kinetics on integrin ligand surface density measured by a high-throughput label-free resonant waveguide grating biosensor

*("Lendület" grant of HAS)*

N. Orgovan*, B. Péter, Sz. Bősze**, J. J. Ramsden***,****, B. Szabó*, and R. Horváth

*Department of Biological Physics, ELET, Budapest, Hungary
**Research Group of Peptide Chemistry, HAS, ELTE, Budapest, Hungary
***Clore Laboratory, University of Buckingham, UK
****Centre for Molecular Recognition, Collegium Basilea (Institute of Advanced Study), Basel, Switzerland

A novel high-throughput label-free resonant waveguide grating (RWG) biosensor, the Epic® BenchTop (BT), was utilized to determine the dependence of cell spreading kinetics on the average surface density ($\nu_{RGD}$) of integrin ligand RGD-motifs [Scientific Reports, 4:4034. 8 p. (2014)].

$\nu_{RGD}$ was tuned over four orders of magnitude by co-adsorbing the biologically inactive PLL-g-PEG and the RGD-functionalized PLL-g-PEG-RGD synthetic copolymers from their mixed solutions onto the sensor surface. Using highly adherent human cervical tumor (HeLa) cells as a model system, cell adhesion kinetic data of unprecedented quality were obtained (Fig. 1a).

Spreading kinetics were fitted with the logistic equation (Fig. 1b) to obtain the spreading rate constant ($r$) and the maximum biosensor response ($\Delta\lambda_{max}$), which is assumed to be directly proportional to the maximum spread contact area ($A_{max}$). $\Delta\lambda_{max}$ increased with increasing RGD surface density until saturation at high densities (Fig. 2a).

Interpreting this behaviour with a simple kinetic mass action model (Fig. 2b), a heterogeneous (2D) dissociation constant of 1753 $\mu m^{-2}$ (corresponding to a homogeneous (3D) dissociation constant of ~30 μM) was obtained for the binding between RGD-specific integrins embedded in the cell membrane and PLL-g-PEG-RGD.

All of these results were obtained completely noninvasively without using any labels.

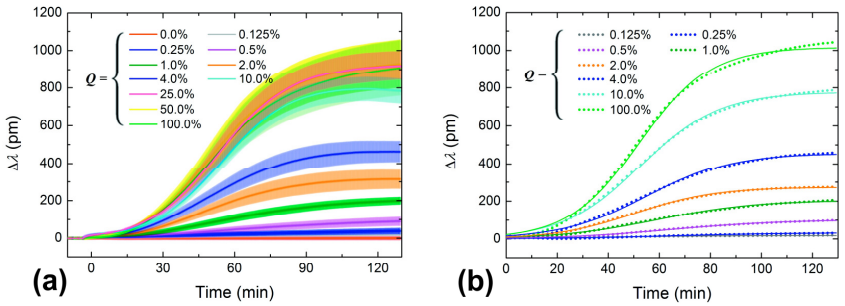


***Figure 1.*** *Spreading curves obtained at different RGD densities and their fits.* ***(a):*** *Spreading curves of HeLa cells measured using the RWG imager. The surface density of integrin ligand RGD-motifs was fine-tuned by co-adsorbing the generally cell repellent and protein-resistant PLL-g-PEG copolymer and its cell adhesive, functionalized counterpart, PLL-g-PEG-RGD, from their mixed solutions. HeLa cells in serum-free buffer were seeded on the coated sensor surfaces (at epoch t=0 min) and their spreading was monitored for approximately 2 h. Measurements were done in triplicate, data are presented as mean ± standard deviation.* ***(b):*** *Individual spreading curves registered by the RWG sensor and their fits (Eq. 5) can be hardly distinguished, which demonstrates the superior quality of the data (only one series of curves is shown, and some data and the corresponding fits have been omitted from this figure to avoid crowding and overlaps). Dots represent data, solid curves are the fits [Scientific Reports, 4:4034. 8 p. (2014)].*

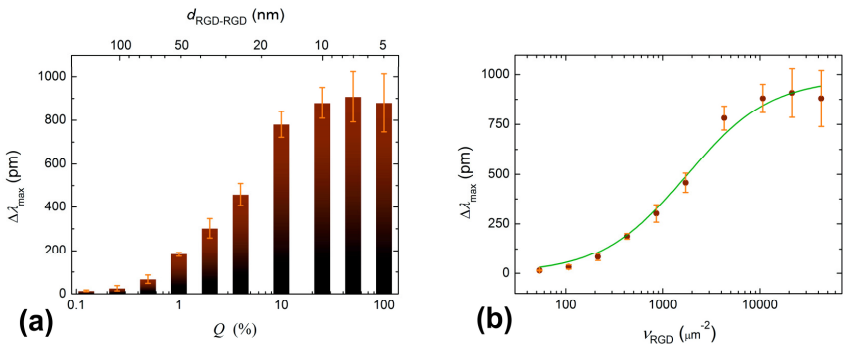


***Figure 2.*** ***(a):*** *Maximum biosensor response ($\Delta\lambda_{max}$) as a function of Q (bottom axis) and the $d_{RGD-RGD}$ average interligand distance (top axis). The values were obtained by fitting the individual spreading curves and averaging the parameters obtained from triplicate fits. Error bars represent the standard deviation from the mean $\Delta\lambda_{max}$ values.* ***(b):*** *$\Delta\lambda_{max}$ as a function of the average number of ligands per unit contact area $\nu_{RGD}$ (dots) was fitted with a kinetic mass action model (solid line) describing the steady-state of single-step monovalent binding, which yielded a 2D dissociation constant of $^{2D}K_d$=1753±243 $\mu m^{-2}$ for the binding between integrins embedded in their the cell membrane and the RGD motifs. Error bars on the dots represent the standard deviation from the mean $\Delta\lambda_{ma}$ value [Scientific Reports, 4:4034. 8 p. (2014)].*

# Immobilization methods for label free bioassays

*("Lendület", OTKA PD73084, FP7-ICT4-P3SENS)*

S. Kurunczi, A. Saftics, A. Hainard*, K. Juhász, D. Patkó, N. Orgován, N. Turck*, J. C. Sanchez*, and R. Horváth

*Department of Human Protein Sciences, Medical University Center, Geneva University, Geneva, Switzerland

Immobilization of biomolecules and receptors on the sensing surface is a key step in biosensing experiments. Methods of immobilization can be classified into 4 main groups: physical adsorption, covalent coupling, affinity immobilization and grafting into hydrogel layer. Our laboratory actively works on this field by developing specific protocols for different assay. We have got experience with silane chemistry (APTES, GOPS, MPTS, HMDS, etc.), and the subsequent application of cross-linking reagents [Applied Surface Science, 257 (2010) 319-324], [J. Chem Phys, 130 (2009) 011101].
Dextran is a polysaccharide that has been routinely used in various biosensor chips. Advantageous properties are the high immobilization capacity in the 3D network and low non-specific binding. We developed our dextran surface on OWLS chips which can be adapted to different surfaces. Carboxymethylated dextran prepared in our laboratory from different molecular weights is grafted on the silylated sensor surface. Development is currently on the way for dextran layers controlling the cellular adhesion.
Polyethylene imine (PEI) based immobilization of antibodies has been recently described and the concept was proved on the label free assay of C-Reactive Protein (CRP) [85]. An advantageous property of such PEI layer is the flexibility and hydrophilicity of these extended molecule loops. This interfacial PEI is simple, inexpensive using aqueous solutions and there is no need for thermal curing neither plasma treatment.

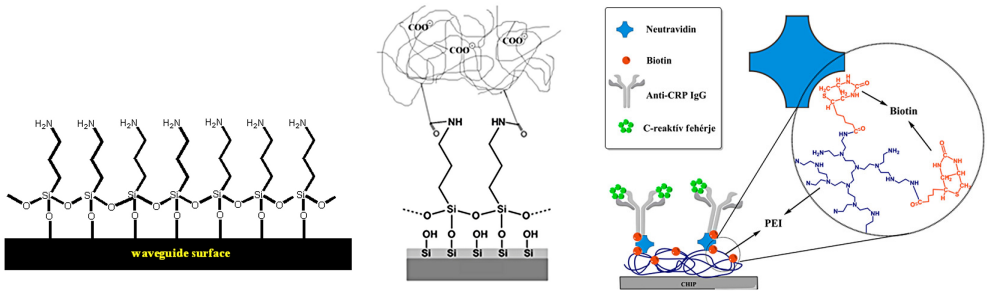


***Figure 1.*** *Schematic illustrations of the various surface immobilization chemistries.*

# *Complex Systems Department*

**Head: György SZABÓ, D.Sc., scientific advisor**

**Research Staff**

- István BORSOS
- Imre EÖRDÖGH, dr. Univ., engineer
- Zoltán JUHÁSZ, Ph.D., researcher
- Géza ÓDOR, D.Sc., scientific advisor
- Károly SZÁSZ, engineer
- Attila SZOLNOKI, D.Sc., scientific advisor
- Jeromos VUKOV, Ph.D., researcher
- Michael Gastner Ph.D., guest researcher

**Ph.D. students / Diploma workers**

- Levente VARGA Ph.D. student
- Kinga BODÓ, ELTE B.Sc.
- Zoltán DOMOKOS, ELTE B.Sc.
- József NYITRAI, BME B.Sc.

The main scientific activity of the department is the application of concepts and tools of statistical physics to investigate complex non-equilibrium systems. The most successful topics belong to the field of evolutionary game theory. In international collaboration they studied what happens to different social dilemmas if the participants/players are separated into two weakly interacting networks. In addition, following the trends in human experiments they extended these models to human features (e.g., emotion and fraternity) with the possibility of various punishments. They studied what happens if different dynamics/delays are built into the models. It turned out that all of the features mentioned above enforce the appearance of cooperative behaviour in the societies.

For multi-agent evolutionary games the potential games play a distinguished role due to their intimate relation to the many-particle models of statistical physics and the straightforward applicability of the laws of thermodynamics and other well developed methods.

The scientific results achieved by the members of this group in 2013 have been published in 15 articles that appeared in ranked international journals, and their previous papers were cited about 1250 times during the last year. Some of their articles are available in the list of TOP 10 most cited papers for several journals.
The research of evolutionary games is related strongly to the project “Fundamental Questions in Evolutionary Biology” supervised by Martin Nowak (Harvard University) and supported financially by the Templeton Foundation. Nine papers are published in collaboration with Slovene and Chinese researchers.

# Diverging fluctuations in a spatial five-species cyclic dominance game

*(OTKA TK101490, J. Templeton Foundation No. RFP-12-22)*

J. Vukov, A. Szolnoki, and G. Szabó

A five-species predator-prey model is studied on a square lattice where each species has two prey and two predators on the analogy to the rock-paper-scissors-lizard-Spock game. The evolution of the spatial distribution of species is governed by site exchange and invasion between the neighbouring predator-prey pairs, where the cyclic symmetry can be characterized by two different invasion rates. Fig. 1 illustrates how we distinguish two types of invasion rates ($p_1$ and $p_2$).

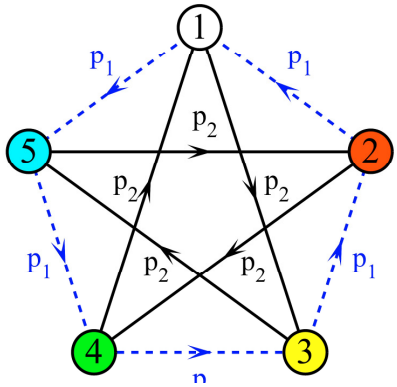


***Figure 1.*** *Food web of cyclic predator-prey system with five species. The directed dashed (blue) and solid (black) lines represent possible invasions.*

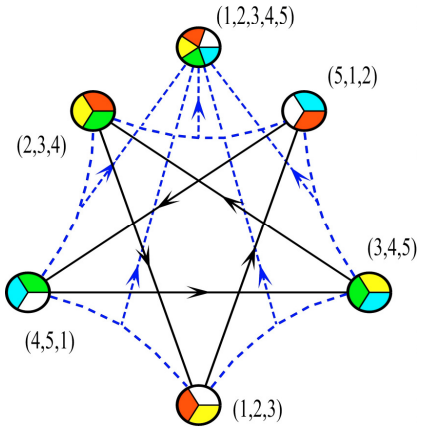


***Figure 2.*** *Flow diagram without the five homogeneous states for $p_1=p_2$. The invasion processes between the three-species are indicated by directed solid lines. Dashed lines refer to transitions when the confrontation of two three-species solutions leads to the emergence of the symmetric five-species phase.*

The curiosity of this model is illustrated in Fig. 2 indicating that three cyclically dominant species can form stable strategy associations. Furthermore, Monte Carlo simulations have indicated that we can deduce a complex food web describing the invasion processes between these strategy associations that exhibits similar symmetries as it is shown in the food webs of Fig. 2. It is found that if the competing

three species associations have two common species then they invade cyclically each other when these associations are separated by an interface in the spatial systems. On the other hand, if all the five species are present along the interface then we can observe the expansion of the five-species solution. These features are summarized qualitatively in Fig. 2 and quantitatively in Fig. 3.

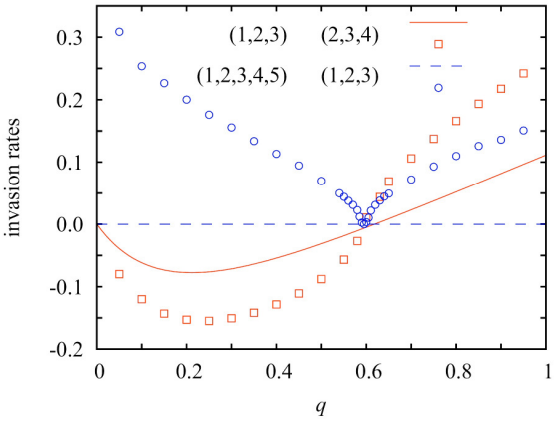


***Figure 3.*** *MC results for the average invasion velocities between the phases $v^{(123)}$ versus $v^{(234)}$ (squares) and $v^{(12345)}$ versus $v^{(123)}$ (circles) as a function of $p_1/p_2$ for a high value of spatial mixing. Lines illustrate the mean-field predictions between two stationary solutions as indicated in the legend.*

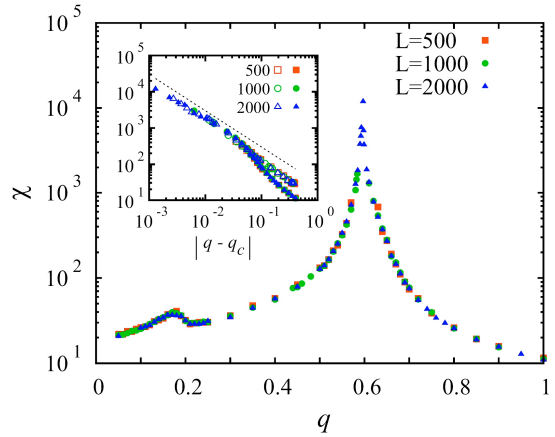


***Figure 4.*** *Fluctuation $\chi$ in dependence of $q$ at $p_m$=0.7 migration rate. Data obtained for different linear sizes are indicated by colored symbols as explained in the legend. The fluctuations diverge at the critical point $q_c$=0.5957(3). Inset shows power-law behavior with an exponent $\gamma$=1.0(1), marked by dotted line. In the inset, open (solid) symbols represent $\chi$ values obtained below (or above) the critical point.*

Fig. 3 illustrates that at a particular value of the ratio of invasion rates, namely ($p_1/p_2$= golden ratio) the invasion rates vanish and the system behaviour becomes similar to those described by the so-called voter model exhibiting extremely slow domain growth. In the vicinity of this critical point the fluctuation $\chi$ of species concentrations diverges (see Fig. 4).

Additionally we have performed a mean-field analysis of time-dependent composition on the analogy of the method used in the description lattice vibration. This calculation shows the appearance of a zero-frequency mode explaining the reason of diverging fluctuation within the framework of population dynamics.

# Spectral analysis and slow spreading dynamics on complex networks

*(OTKA T77629, FuturICT.hu TAMOP- 4.2.2.C -11/1/ KONV-2012-0013)*

G. Ódor, and Z. Domokos

The susceptible-infected-susceptible (SIS) model is one of the simplest memory-less systems for describing information or epidemic spreading phenomena with competing creation and spontaneous annihilation reactions. The effect of quenched disorder on the dynamical behaviour has recently been compared to quenched mean-field (QMF) approximations in scale-free networks. QMF can take into account topological heterogeneity and localization effects of the activity (IPR) in the steady state by spectral decomposition analysis of the adjacency matrix. Therefore, it can provide predictions on possible rare-region effects, thus on the occurrence of slow dynamics. We compared QMF results of SIS with simulations on various large dimensional graphs. In particular, we showed that for Erdős-Rényi graphs this method predicts correctly the occurrence of rare-region effects. It also provides a good estimate for the epidemic threshold ($\lambda_c$)in case of percolating graphs.

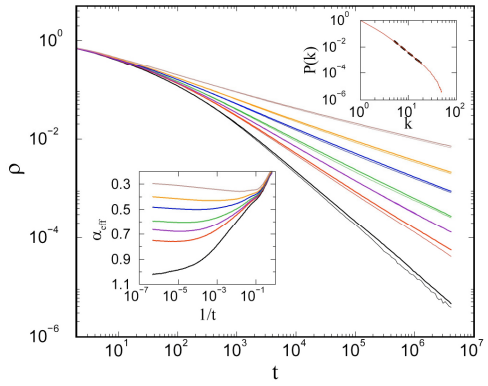


***Figure 1.*** *Density decay as a function of time for the SIS on BA graph with network sizes: N = $10^5$ (thin lines), N = $10^6$ (thick lines). Different curves correspond to λ = 2.4, 2.45, 2.47, 2.5, 2.55, 2.6, 2.7 (from bottom to top curves). (Left inset) Local slopes of the same data. (Right inset) Degree distribution of the aging BA graph for N = 4x$10^6$ nodes.*

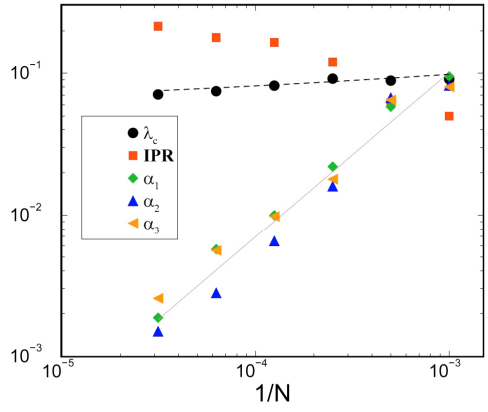


***Figure 2.*** *Finite size scaling of QMF SD results of the SIS on generalized BAT with N = 1000, 2000, 4000, 8000, 16 000, 32 000 nodes. Bullets: $\lambda_c$, boxes: IPR, rhombs: $\alpha_1$, up-triangles: $\alpha_2$, left-triangles: $\alpha_3$. (Line) Least-squares fitting with the form 1/N.*

Griffiths phases emerge if the graph is fragmented or if we apply a strong, exponentially suppressing weighting scheme on the edges. The latter model describes the connection time distributions in the face-to-face experiments. In case of a generalized Barabási-Albert type of network with aging connections, strong rare-region (Fig. 2.) effects and numerical evidence for Griffiths Phase dynamics (Fig. 1.) are shown. The dynamical simulation results agree well with the predictions of the spectral analysis applied for the weighted adjacency matrices.

## The Self Organising Cloud algorithm

***(OTKA K81954)***

Z. Juhász

We have developed a new unsupervised self-learning algorithm deduced from the Self Organising Map and Multidimensional Scaling principles. Our aim was to construct a simultaneous clustering and visualising method for structural analysis of large folksong corpora. After validating the method on a Hungarian test corpus containing variants of known folksong types, we applied the method for contour analysis of a large folksong database representing the folk music of native Central Andean people. The resulting topographic map of the learned feature vectors (melody contour type vectors learned by the algorithm) are shown in the figure. The method provides a feedback between the learning and mapping functions, resulting in a very visual map of the feature vectors.

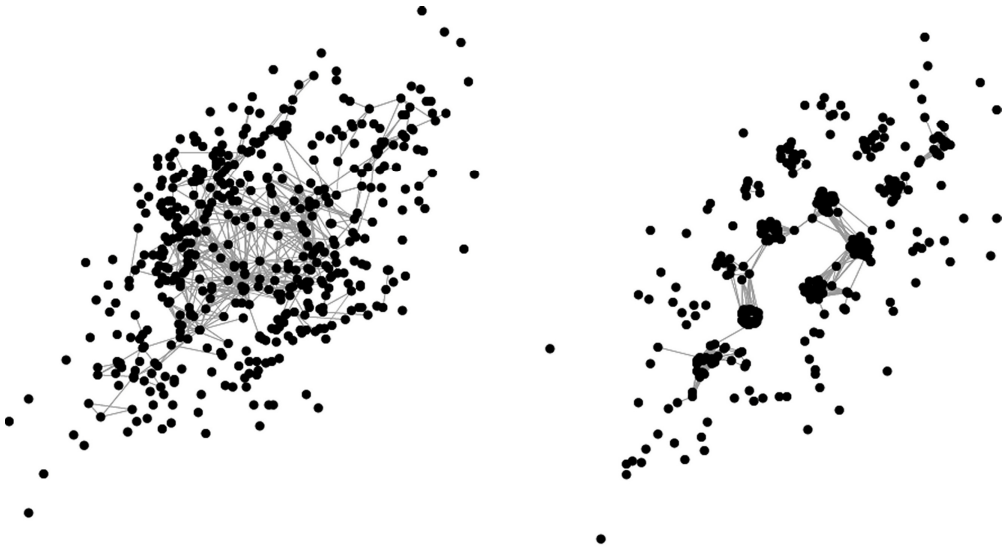

***Figure 1***. *Musical maps of Central-Andean folk music. The points correspond to 500 contour types of 1300 melodies. Left: non-cooperative, Right: cooperative learning.*

# *MFA Seminar Talks*

2013.01.23 **István TAMÁSKA**
(MTA TTK MFA, Budapest, Hungary): *"Structural and optical characterization of novel photonic crystal type nanoarchitectures of biological extraction, and fabrication of biologically inspired artificial nanoarchitectures"*

2013.02.08 **Zsófia BAJI**
(MTA TTK MFA, Budapest, Hungary): *"Compound semiconducting layers for photovoltaic purposes"*

2013.02.20 **Jeromos VUKOV**
(MTA TTK MFA, Budapest, Hungary): *"The art of blackmailing – or game strategies of zero-determinant"*

**Due to reconstruction of the MFA conference room, the series of regular scientific seminars was technically interrupted for six months.**

2013.09.26 **József GYULAI**
(MTA TTK MFA, Budapest, Hungary): *"Retrospection from – somewhat more than – half of career (Experiences and councils for friends)"*

2013.10.02 **Zsolt TÓTH**
(Szeged University): "Fabrication of thin films by laser-assisted evaporation in vacuum
and in reactive background gas atmosphere"

2013.10.02 **Zsuzsanna PÁPA**
(PhD student, Szeged University): *"Spectroscopic ellipsometry investigation of scattering and depolarizing thin films"*

2013.10.09 **Péter FÖLDESY**
(MTA TTK MFA, Budapest, Hungary): *"THz sensing by field-effect transistors"*

2013.10.09 **Yu.P. YAKOVLEV**
(Yoffe Inst, Saint Petersburg): *"Ultrafast (bandwidth 2-10 GHz) photodiodes for the 1.0-2.4 micrometer spectral range"*

2013.10.15 **Emil AGÓCS**
(MTA TTK MFA, Budapest, Hungary): *"Characterization of silicon based nanocrystalline structures by spectroscopic ellipsometry"*

2013.10.16 **József GYULAI**
(MTA TTK MFA, Budapest, Hungary): *"Retrospection from – somewhat more than – half of career (II) (Experiences and councils for friends)"*

2013.11.06 **Antal KOÓS**
(MTA TTK MFA, Budapest, Hungary): *"Fabrication of carbon nanostructures by the CVD method: from carbon nanotubes to graphene"*

2013.11.13 **Róbert HORVÁTH**
(MTA TTK MFA, Budapest, Hungary): *"Initial results and future goals of the Nano-bio-sensorics Group"*

2013.11.20 **György KÁDÁR**
(MTA TTK MFA, Budapest, Hungary): *"Retrospection… Publish or perish (defeat? or success?)"*

2013.12.04 **Norbert ORGOVÁN**
(MTA TTK MFA, Budapest, Hungary): *"Monitoring of the adhesion of living cells by optical bio-sensors"*

2013.12.11 **Dániel PATKÓ**
(MTA TTK MFA, Budapest, Hungary): *"Development and application possibilities of a high sensibility dual channel interferometric biosensor"*

## *Research and Development Partners, Foreign Visitors*

**ACHILLES, Tolias** *(Robert Bosch Gmbh, Germany)*
**ALM, Kersti** *(PHIAB, Lund, Sweden)*
**ATKINSON, Irina** *(Ilie Murgulescu Research Institute, Romania)*
**BARDET, Benjamin** *(Tours University, France)*
**BÍRÓ, Domokos** *(Sapientia Hungarian University, Tirgu-Mures, Romania)*
**CALAME, Michele** *(University of Basel, Switzerland)*
**CARYEL, Frederic** *(University of Tours, France)*
**COTTIER, Kaspar** *(Creoptix GmbH, Switzerland)*
**CRACIUN, Valentin** *(INFLPR Institute, Bucharest, Romania)*
**DEFFORGE, Thomas** *(Tours University, France)*
**DEMIN, Victor** *(Emanuel Institute of Biochemical Physics, Russian Academy of Sciences, Moscow, Russia)*
**DHAR, Ajay** *(National Physical Laboratory, New Delhi, India)*
**DICKMA, Ronald** *(Universidade Federal Minas Gerais, Brazil)*
**DMITRY, Gnatyuk** *(Institute of Ultra High Frequency Semiconductor Electronics, Russian Academy of Sciences, Russia)*
**DORCIOMAN, Gabriela** *(INFLPR Institute, Bucharest, Romania)*
**DOVBESHKO, Galina** *(Institute of Physics, National Academy of Science of Ukraine, Kiev, Ukraine)*
**DRAGANITS, Gerhard** *(Zeiss, Austria)*
**DUSZA, Jan** *(IMR SAS, Slovak Republic)*
**EVGENY, Klimov** *(Institute of Ultra High Frequency Semiconductor Electronics, Russian Academy of Sciences, Russia)*
**FESENKO, Olena** *(Institute of Physics, National Academy of Science of Ukraine, Kiev, Ukraine)*
**FRANGIS, N.** *(Aristotle University of Thessaloniki, Greece)*
**GALKIN, Nikolaj** *(Institute for Automation and Control Processes, Vladivostok, Russia)*
**GAUTIER, Gael** *(University of Tours, France)*
**HONG, Suk-Lyun** *(Sejong University, Seoul, Korea)*
**HWANG, Chan-Yong** *(Korea Research Institute of Standards and Science, Daejeon, Korea)*
**IVANOV, Stefan** *(Boyadjiev MTA-BME Műszaki Analitikai Kémiai Kutatócsoport, Bolgaria)*
**KELLING, Jeffrey** *(HZDR, Dresden, Germany)*
**KIM, Han-Soo** *(LG Chemicals, Korea)*
**KIM, Won-Dong** *(Korea Research Institute of Standards and Science, Daejeon, Korea)*
**KIM, Yong-Sung** *(Korea Research Institute of Standards and Science, Daejeon, Korea)*
**KIM, Yung Suk** *(KOTRA, Korea)*

**KUMAR, Avanish** *(Srivastava National Physical Laboratory, New Delhi, India)*
**KUMAR, Mahaveer** *(Jain IIT, Madras, India)*
**KVASHNIN, Dmitrii** *(Emanuel Intitute of Biochemical Physisc, Russian Academy of Sciences, Moscow, Russia)*
**LAMBIN, Philippe** *(Facultes Universitaires Notre-Dame de la Paix, Namur, Belgium)*
**LEE, Byong-Taek** *(Soonchunhyang University, Korea)*
**LEE, In-Ho** *(Korea Research Institute for Standards and Science, Daejeon, Korea)*
**MAKARONA, Eleni** *(IMEL, Democretos, Athen, Greece)*
**MIHAIU, Susana** *(Ilie Murgulescu Research Institute, Romania)*
**MÜLLER, Joseph** *(Robert Bosch Gmbh, Germany)*
**MYKOLA, Dmitruk** *(Institute for Physics of Semiconductors, NAS of Ukraine, Ukraine)*
**PARK, Duck-Gun** *(Korea Atomic Energy Research Institute, Taejeon, Korea)*
**PERC, Matjaz** *(University of Maribor, Slovenia)*
**POPESCU, Andrei** *(INFLPR Institute, Bucharest, Romania)*
**RAWAL, Amit** *(Indian Institute of Technology, India)*
**SCHONENBERGER, Christian** *(University of Basel, Switzerland)*
**SHVAB, Ruslan** *(IMR SAS, Slovak Republic)*
**SOUCEK, Pavel** *(Masaryk University, Brno, Czech Republic)*
**STOEMENOS, J.** *(Aristotle University of Thessaloniki, Greece)*
**SUZUKI, Gorou** *(Director of Sales branch & ITM company, Tateyama, Japan)*
**SZABÓ, Pavol** *(UEF SAV, Slovak Republic)*
**TSUKUDA, Masahiko** *(Toyama National College of Technology, Toyama, Japan)*
**USHIODA, Sukekatsu** *(National Institute for Materials Science Tsukuba, Ibaraki, Japan)*
**VERNHOUT, Peter** *(AIST-NT BV, Apeldoorn, Netherlands)*
**VOLODYMYR, Romanyuk** *(Institute for Physics of Semiconductors, NAS of Ukraine, Ukraine)*
**VOUROUTIS, N.** *(Aristotle University of Thessaloniki, Greece)*
**WATANUKI, Osama** *(Toteyama Kagaku, Toyama, Japan)*
**WATANUKI, Osamu** *(Director of R&D, Tateyama, Japan)*
**WITTMAN, Marion** *(Biogen Idec Ltd, USA Boston, USA)*
**YAKOVLEV, Yuri** *(Ioffe Institute, Sankt-Peterburg, Russia)*
**YAMASHITA, Ichiro** *(Toyama National College of Technology, Toyama, Japan)*
**YOKITA, Osamu** *(Toyama National College of Technology, Toyama, Japan)*
**ZHURAVEV, Konstantin** *(Novosibirsk Sci. Acad., Russia)*

# *MFA Publications in 2013*

1. **Agócs E**, Nassiopoulou AG, Milita S, Petrik P: "Model dielectric function analysis of the critical point features of silicon nanocrystal films in a broad parameter range", *Thin Solid Films 541: 83-86 (2013), IF:1.604*
2. **Allazadeh MR**, Balázsi Cs: "Reinforced aluminum matrix composite application in friction material", *Recpatcorrsci 3: online (2013)*
3. **Allazadeh MR**, Marangoni RD, Lovell MR: "Liquid Level Sensor for High Temperature Molten Salt in Confined Container", *Front Sensors 2: (1) 27-37 (2013)*
4. **Baji Zs**, Lábadi Z, Molnár Gy, Pécz B, Tóth AL, Tóth J, Csík A, Bársony I: "Post-selenization of stacked precursor layers for CIGS", *Vacuum 92: 44-51 (2013), IF:1.530*
5. **Baji Zs**: "Compound semiconductor layers for optoelectronic and photovoltaic purposes", *qtab95p. 2013. (Dissertation: PhD)*
6. **Balázsi Cs**, Gergely G, Balázsi K, Chang-Hoon C, Hye-Young S, Je-Yong C, Seong-Gon K: "Bone formation with nano-hydroxyapatite from eggshell", *Mater Sci Forum 729: 25-30 (2013)*
7. **Balázsi Cs**, Lukács IE, Balázsi K: "Chemical sensors based on nano-hexagonal tungsten oxide: Synthesis and characterization", *Nato Sci Peace Secur Ser B Phys Biophys 2013: 125-138 (2013)*
8. **Balázsi Cs**, Tapasztó O, Károly Z, Kun P, Balázsi K, Szépvölgyi J: "Structural and mechanical properties of milled $Si_3N_4$/cnts composites by spark plasma sintering method", *Mater Sci Forum 729: 31-36 (2013)*
9. **Balázsi K**, Lukács IE, Gurbán S, Menyhárd M, Bacáková L, Vandrovcová M, Balázsi Cs: "Structural, mechanical and biological comparison of TiC and TiCN nanocomposites films", *J Eur Ceram Soc 33: (12) 2217-2221 (2013), IF:2.360*
10. **Balázsi K**, Vandrovcová M, Bacáková L, Balázsi Cs, Bertóti I, Davin F, Radnóczi Gy: "Mechanical behavior of bioactive TiC nanocomposite thin films", *Mater Sci Forum 729: 296-301 (2013)*
11. **Balázsi K**, Vandrovcová M, Bacáková L, Balázsi Cs: "Structural and biocompatible characterization of TiC/a:C nanocomposite thin films", *Mat Sci Eng C-Bio S 33: (3) 1671-1675 (2013), IF:2.404*
12. **Bányász I**, Berneschi S, Fried M, Lohner T, Conti GN, Righini GC, Pelli S, Zolnai Zs: "M-line spectroscopic, spectroscopic ellipsometric and microscopic measurements of optical waveguides fabricated by MeV-energy $N^+$ ion irradiation for telecom applications", *Thin Solid Films 541: 3-8 (2013), IF:1.604*
13. **Bányász I**, Zolnai Zs, Fried M, Lohner T, Berneschi S, Righini GC, Pelli S, Nunzi-Conti G: "Single- and double energy $N^+$ ion irradiated planar optical waveguides in Er: Tungsten-tellurite oxide glass and sillenite type Bismuth Germanate crystals working up to telecommunications wavelengths", *Nucl Instrum Meth B 307: 299-304 (2013), IF:1.266*
14. **Bányász I**, Zolnai Zs, Pelli S, Berneschi S, Fried M, Lohner T, Nunzi-Conti G, Righini GC: "Single- and double-energy $N^+$ - Irradiated planar waveguides in eulytine and sillenite type BGO crystals", *Proceedings of SPIE 8627: 862705 (2013)*

15. **Beck A**, Frey K, Schay Z, Borkó L, Sajó I, Sáfrán G, Kruse N, Teschner D: "Manganese-promoted cobalt oxide in PROX reaction", *In: 11th European Congress on Catalysis: EuropaCat-XI2013. pp.150*
16. **Beke D**, Szekrényes Z, Balogh I, Czigány Zs, Kamarás K, Gali A: "Preparation of small silicon carbide quantum dots by wet chemical etching", *J Mater Res 28: (1) 44-49 (2013), IF:1.713*
17. **Beke D**, Szekrényes Z, Pálfi D, Róna G, Balogh I, Maák PA, Katona G, Czigány Zs, Kamarás K, Rózsa B, Buday L, Vértessy B, Gali A: "Silicon carbide quantum dots for bioimaging", *J Mater Res 28: (2) 205-209 (2013), IF:1.713*
18. **Bíró F**, Dücső Cs, Hajnal Z, Pap AE, Bársony I: "Optimisation of Low Dissipation Micro-hotplates - Thermo-mechanical Design and Characterisation", *In: P E Raad, M Rencz, B Wunderle, A Poppe(Eds.), Proc. of the 19th International Workshop on THERMal INvestigation of ICs and Systems: THERMINIC 2013., Berlin: Brandenburgische Technische Universität, Cottbus, 2013. pp.116-121., (ISBN:978-1-4799-2271-0)*
19. **Biró LP**, Lambin P: "Grain boundaries in graphene grown by chemical vapor deposition", *New J Phys 15: Art. Nr 035024 (2013), IF:4.063*
20. **Bosi M**, Attolini G, Pécz B, Zolnai Zs, Dobos L, Martínez O, Jiang L, Taysir S: "Structural characterization of 3C-SiC grown using methyltrichlorosilane" *in Silicon Carbide and Related Materials 2012, Mater Sci Forum 740-742: 291-294 (2013)*
21. **Charnovych S**, Szabó IA, Tóth AL, Volk J, Trunov ML, Kökényesi S: "Plasmon assisted photoinduced surface changes in amorphous chalcogenide layer", *J Non-Cryst Solids 377: 200-204 (2013), IF:1.597*
22. **Czigány Zs**: "Fullerénszerű nanoszerkezetek jellemzése transzmissziós elekronmikroszkópiával", *qtab95p. 2013. (Dissertation: DSc)*
23. **Czigány Zs**: "HRTEM Image Simulation of Model Structures for Fullerene-Like Nanotructures", *In: Proceedings of MC2013 Microscopy Congress 2013. pp.601-602*
24. **Czigány Zs**: "P-doped random C20 fullerite - model structure for fullerene-like CPx", *Phys Status Solidi B Basic Solid State Phys 250: (2)334-337 (2013), IF:1.489*
25. **Csanády A**, Barna P, Csordás-Pintér A: "Magyar részvétel a kvázikristályokkal kapcsolatos kutatásokban a 80-as és 90-es években", *Anyagok Világa XI: (1)1-35 (2013)*
26. **Daróczi CsS**: "MFA Summer School and MFA Open Day", In: Menyhárd M, Daróczi CsS(Eds.), *MTA TTK MFA Yearbook 2012., Budapest: MTA MFA, 2013. pp.20-22*
27. **Desfours C**, Calas-Etienne S, Horváth R, Martin M, Gergely Cs, Cuisinier F, Etienne P: "Development and characterization of ultra-porous silica films made by the sol-gel method. Application to biosensing", *Appl Phys A-Mater in press: in press (2013), IF:1.545*
28. **Dobos L**, Pécz B, Tóth L, Horváth ZsJ, Horváth ZE, Tóth AL, Poisson MA: "Annealing of Cr/Au metallizations on p-GaN", *In: 19th International Vacuum Congress IVC-19: Electronic Material and Processes, Paris: 2013. pp.514-515*
29. **Dobrik G**, Tapasztó L, Biró LP: "Selective etching of armchair edges in graphite", *Carbon 56: 332-338 (2013), IF:5.868*
30. **Dózsa L**, Molnár Gy, Zolnai Zs, Dobos L, Pécz B, Galkin NG, Dotsenko SA, Bezbabny DA, Fomin DV: "Formation and characterization of semiconductor $Ca_2Si$ layers prepared

on p-type silicon covered by an amorphous silicon cap", *J Mater Sci 48: (7) 2872-2882 (2013), IF:2.163*

31. **Erenburg SB**, Trubina SV, Zhuravlev KS, Malin TV, Pécz B: "Diffusion and Deformations in Heterosystems with GaN/AlN Superlattices, According to Data from EXAFS Spectroscopy", *Bull Russ Acad Sci Phys 77: (9)1147-1150 (2013)*
32. **Fekete Z**, Hajnal Z, Márton G, Fürjes P, Pongrácz A: "Fracture analysis of silicon microprobes designed for deep-brain stimulation", *Microelectron Eng 103: 160-166 (2013), IF:1.224*
33. **Fekete Z**, Pongrácz A, Márton G, Fürjes P: "On the fabrication parameters of buried microchannels integrated in in-plane silicon microprobes", *Mater Sci Forum 729: 210-215 (2013)*
34. **Fekete Z**: "Technology of ultralong deep brain fluidic microelectrodes combined with etching-before-grinding", *Microsyst Technol in press: in press (2013), IF:0.827*
35. **Fogarassy Zs**, Dobrik G, Varga LK, Biró LP, Lábár JL: "Growth of Ni layers on single crystal sapphire substrates", *Thin Solid Films 539: 96-101 (2013), IF:1.604*
36. **Földesy P**: "Képalkotás sok száz Giga- és Teraherz frekvenciatartományban", *Fizikai Szemle LXIII: (12) 405-409 (2013)*
37. **Frigeri C**, Nasi L, Serényi M, Khánh NQ, Szekrényes Zs, Kamarás K, Csík A: "From nanovoids to blisters in hydrogenated amorphous silicon", *In: Borisenki VE, Gaponenko SV, Gurin VS, Kam CH(Eds.), Physics, chemistry and applications of nanostructures: Proceedings of International Conference Nanomeeting 2013., New Jersey City: World Scientific, 2013. pp.176-179. (ISBN:9789814460170)*
38. **Frigeri C**, Serényi M, Csík A, Szekrényes Zs, Kamarás K, Nasi L, Khánh NQ: "Evolution of the structure and hydrogen bonding configuration in annealed hydrogenated a-Si/a-Ge multilayers and layers", *Appl Surf Sci 269: 12-16 (2013), IF:2.112*
39. **Frigeri C**, Serényi M, Khánh NQ, Csík A, Nasi L, Erdélyi Z, Beke DL, Boyen HG: "Hydrogen behaviour in amorphous Si/Ge nano-structures after annealing", *Appl Surf Sci 267: 30-34 (2013), IF:2.112*
40. **Furlan A**, Gueorguiev GK, Czigány Zs, Darakchieva V, Braun S, Correia MR, Högberg H, Hultman L: "Structure and properties of phosphorus-carbide Thin Solid Films", *Thin Solid Films 548: 247-254 (2013), IF:1.604*
41. **Galkin KN**, Galkin NG, Dózsa L, Dotsenko SA, Chernev IM, Vavanova SV, Dobos L, Pécz B: "Growth, structure, optical and electrical properties of Si/2D $Mg_2Si$/Si(111) double heterostructures and Schottky diodes on their base", *Phys Status Solidi C Curr T Solid State Phys 10: (12) 1720-1723 (2013)*
42. **Gergely G**, Molnár A, Gácsi Z: "The Role of Pb Impurity in SAC Solder Alloy", *Mater Sci Forum 752: 42-47 (2013)*
43. **Gergely G**, Sahin FC, Göller G, Yücel O, Balázsi Cs: "Microstructural and mechanical investigation of hydroxyapatite-zirconia nanocomposites prepared by spark plasma sintering", *J Eur Ceram Soc 33: (12) 2313-2319 (2013), IF:2.360*
44. **Gergely-Fülöp E**, Nagy N, Deák A: "Reversible Shape Transition: Plasmonic Nanorods in Elastic Nanocontainers", *Mater Chem Phys 141: (1) 343-347 (2013), IF:2.072*

45. **Gubicza J**, Lábár JL, Luu-Manh Q, Nguyen-Hoang N, Nguyen-Hoang L: "Evolution of size and shape of gold nanoparticles during long-time aging", *Mater Chem Phys 138: (2-3)449-453 (2013), IF:2.072*
46. **Gumprecht T**, Petrik P, Roeder G, Schellenberger M, Pfitzner L, Pollakowski B, Beckhoff B: "Characterization of thin ZnO films by Vacuum ultra-violet reflectometry", *Mater Res Soc SP 1494: 65-70 (2013)*
47. **Gyulai J**, Tapasztó L, Horváth ZE, Nemes-Incze P, Osváth Z, Biró LP: "Ions and Carbon nanostructures", *Radiat Eff Defect S 168: (6) 412-417 (2013), IF:0.502*
48. **Gyulai J**: "A mikro- és a nanovilág az anyagtudományok tükrében - Nanomedicina és nanokémia", *Természet Világa 144: (11) 483-485 (2013)*
49. **Härkönen E**, Díaz B, Swiatowska J, Maurice V, Seyeux A, Fenker M, Tóth L, Radnóczi Gy, Marcus P, Ritala M: "$Al_xTa_yO_z$ mixture coatings prepared using atomic layer deposition for corrosion protection of steel", *Chem Vapor Depos 19: (4-6) 194-203 (2013), IF:1.316*
50. **Härkönen E**, Potts SE, Kessels WMM, Díaz B, Seyeux A, Swiatowska J, Maurice V, Marcus P, Radnóczi Gy, Tóth L, Kariniemi M, Niinistö J, Ritala M: "Hydrogen-argon plasma pre-treatment for improving the anti-corrosion properties of thin $Al_2O_3$ films deposited using atomic layer deposition on steel", *Thin Solid Films 534: 384-393 (2013), IF:1.604*
51. **Hegedüs Z**, Gubicza J, Kawasaki M, Chinh NQ, Fogarassy Zs, Langdon TG: "The influence of impurity content on thermal stability of low stacking fault energy silver processed by severe plastic deformation", *Mater Sci Forum 729: 222-227 (2013)*
52. **Hegedüs Z**, Gubicza J, Kawasaki M, Chinh NQ, Lábár JL, Langdon TG: "Stability of the ultrafine-grained microstructure in silver processed by ECAP and HPT", *J Mater Sci 48: (13)4637-4645 (2013), IF:2.163*
53. **Hegedüs Z**, Gubicza J, Kawasaki M, Chinh NQ, Süvegh K, Fogarassy Zs, Langdon TG: "High temperature thermal stability of ultrafine-grained silver processed by equal-channel angular pressing", *J Mater Sci 48: (4) 1675-1684 (2013), IF:2.163*
54. **Holczer E**, Fekete Z, Fürjes P: "Surface modification of PDMS based microfluidic systems by tensides", *Mater Sci Forum 729: 361-366 (2013)*
55. **Holfelder I**, Beckhoff B, Fliegauf R, Honicke P, Nutsch A, Petrik P, Roeder G, Weser J: "Complementary methodologies for thin film characterization in one tool - a novel instrument for 450 mm wafers", *J Anal Atom Spectrom 28: (4) 549-557 (2013), IF:3.155*
56. **Horváth A**, Guczi L, Kocsonya A, Sáfrán G, La Parola V, Liotta LF, Pantaleo G, Venezia AM: "Sol-derived AuNi/$MgAl_2O_4$ catalysts: Formation, structure and activityin dry reforming of methane", *Appl Catal A-Gen 468: 250-259 (2013), IF:3.410*
57. **Horváth R**, Kobzi B, Keul H, Moeller M, Kiss É: "Molecular Interaction of a New Antibacterial Polymer with a Supported Lipid Bilayer Measured by an in situ Label-Free Optical Technique", *Int J Mol Sci 14: (5) 9722-9736 (2013), IF:2.464*
58. **Horváth ZGy**, Juhász Gy, Fried M, Major Cs, Petrik P: "Imaging optical arrangement with a pinhole camera", *NSZO: G01N21/00, G01N21/55, Patent: US 8,437,002 B2, PCT/HU2008/000058 (2008), US 12/601,410 (2013)*

59. **Horváth ZsJ**, Basa P, Jászi T, Molnár KZ, Pap AE, Molnár Gy: "Charging behavior of silicon nitride based non-volatile memory structures with embedded semiconductor nanocrystals", *Appl Surf Sci 269: 23-28 (2013), IF:2.112*
60. **Horváth ZsJ**, Basa P, Molnár KZ, Jászi T, Pap AE, Molnár Gy, Dobos L, Tóth L, Pécz B: "Charging Behaviour of Metal-Nitride-Oxide-Semiconductor Memory Structures with Embedded Si or Ge Nanocrystals", *Nanosci Nanotech Lett 5: (4) 513-517 (2013), IF:0.886*
61. **Horváth ZsJ**, Basa P, Molnár KZ, Molnár Gy, Jászi T, Pap AE: "Effect of location of Si or Ge nanocrystals on the memory behavior of MNOS structures", *Physica E 51: 104-110 (2013), IF:1.522*
62. **Horváth ZsJ**, Molnár KZ: "Effect of current levels on memory behaviour of MNOS structures - limits of computer simulation", *In: Anikó Szakál(Eds.), ICCC 2013, Proceedings of IEEE 9th International Conference on Computational Cybernetics., Tihany: IEEE Hungary Section, 2013. pp.303-307. (ISBN:978-1-4799-0061-9; 978-1-4799-0060-2)*
63. **Hvizdos P**, Dusza J, Balázsi Cs: "Tribological properties of Si3N4-graphene nanocomposites", *J Eur Ceram Soc 33: (12) 2359-2364 (2013), IF:2.360*
64. **Jenei P**, Gubicza J, Yoon EY, Kim HS, Lábár JL: "High temperature thermal stability of pure copper and copper - Carbon nanotube composites consolidated by High Pressure Torsion", *Compos Part A-Appl S 51: 71-79 (2013), IF:2.744*
65. **Jenei P**, Yoon EY, Gubicza J, Kim HS, Lábár JL, Ungár T: "Microstructure and thermal stability of copper - Carbon nanotube composites consolidated by high pressure torsion", *Mater Sci Forum 729: 228-233 (2013)*
66. **Jiang LL**, Perc M, Szolnoki A: "If Cooperation Is Likely Punish Mildly: Insights from Economic Experiments Based on the Snowdrift Game", *PloS ONE 8: e64677 (2013), IF:3.730*
67. **Juhász Z**: "A probabilistic study of culture-dependent note association paradigms in folk music", *In: Third International Workshop on Folk Music Analysis (FMA2013), Amsterdam: 2013. pp.78-80*
68. **Kádár Gy**: "A hullámfüggvény tudattól független redukciója", *Fizikai Szemle 63: (1) 11-14 (2013)*
69. **Kárász Z**, Földesy P, Fiath R, Rodríguez-Vázquez A: "Tunable low noise amplifier implementation with low distortion pseudo-resistance for in vivo brain activity measurement", *IEEE Sens J PP: (99) (2013), IF:1.475*
70. **Károly Z**, Bartha C, Mohai I, Balázsi Cs, Sajó IE, Szépvölgyi J: "Deposition of silicon carbide and nitride-based coatings by atmospheric plasma spraying", *Int J Appl Ceram Tec 10: (1) 72-78 (2013), IF:1.153*
71. **Kárpáti T**, Kulinyi S, Végvári R, Ferencz J, Nagy A, Pap AE, Battistig G: "Packaging of a 3-axial piezoresistive sensor with backside contacts", *Microsyst Technol, in press: in press (2013), IF:0.827*
72. **Kárpáti T**, Pap AE, Kulinyi S: "Prototype MEMS Capacitive Pressure Sensor Design and Manufacturing", *Period Polytechn Electr Eng 57: (1) 3-7 (2013)*
73. **Kárpáti T**: "Szilícium alapú 3 dimenziós erőmérők kialakítása és tokozása: (1. rész)", *Elektronet 22: (7) 36-37 (2013)*

74. **Kárpáti T**: "Szilícium alapú 3 dimenziós erőmérők kialakítása és tokozása: (2. rész)", *Elektronet 22: (8) 28-29 (2013)*
75. **Kertész K**, Piszter G, Jakab E, Bálint Zs, Vértesy Z, Biró LP: "Color change of Blue butterfly wing scales in an air - Vapor ambient", *Appl Surf Sci 281: 49-53 (2013), IF:2.112*
76. **Kertész K**, Piszter G, Jakab E, Bálint Zs, Vértesy Z, Biró LP: "Selective optical gas sensors using butterfly wing scales nanostructures", *Key Eng Mater 543: 97-100 (2013)*
77. **Kertész K**, Piszter Gábor, Vértesy Z, Biró LP, Bálint Zs: "Színek harmóniája: a boglárkalepkék szerkezeti kék színének fajfelismerési szerepe: I. RÉSZ", *Fizikai Szemle 63: (7-8): 231-235 (2013)*
78. **Kertész K**, Piszter Gábor, Vértesy Z, Biró LP, Bálint Zs: "Színek harmóniája: a boglárkalepkék szerkezeti kék színének fajfelismerési szerepe: II. RÉSZ", *Fizikai Szemle 63: (9) 293-298 (2013)*
79. **Kiss AK**, Lábár JL: "A method for complete characterization of the macroscopic geometry of grain boundaries", *Mater Sci Forum 729: 97-102 (2013)*
80. **Kiss-Pataki B**, Horváth ZE, Tiusanen J, Caglar B, Vértesy Z: "Többfalú szén nanocsövek eloszlásának vizsgálata polimer kompozitokban mikroszkópos módszerekkel", *In: Székely Tünde(Eds.), RODOSZ XIII., Kolozsvár: 2013. pp. in press*
81. **Koncz P**, Horváth A, Balázsi K, Sahin FC, Göller G, Onüralp Y, Balázsi Cs: "Correlation between milling parameters, structural and mechanical properties of nanostructured austenitic Y2O3 strengthened steels", *Mater Sci Forum 729: 409-414 (2013)*
82. **Kotis L**: "Ionbombázás hatásainak vizsgálata Auger elektron spektroszkópiai mélységi feltérképezéssel", *qtab102p. 2013. (Dissertation: PhD)*
83. **Kovács N**, Patkó D, Orgován N, Kurunczi S, Ramsden JJ, Vonderviszt F, Horváth R: "Optical anisotropy of flagellin layers: in-situ and label-free measurement of adsorbed protein orientation using OWLS", *Anal Chem 85: (11) 5382-5387 (2013), IF:5.695*
84. **Kun P**, Tapasztó O, Czigány Zs, Balázsi Cs: "Preparation and characterization of multilayer graphene by mechanical milling and related applications for ceramic composites", *Mater Sci Forum 729: 252-259 (2013)*
85. **Kurunczi S**, Hainard A, Juhász K, Patkó D, Orgován N, Truck N, Sanchez JC, Horváth R: "Polyethylene imine-based receptor immobilization for label free bioassays", *Sensor Actuat B Chem 181: 71-76 (2013), IF:3.535*
86. **Kvetková L**, Duszová A, Kasiarová M, Dorcáková F, Dusza J, Balázsi Cs: "Influence of processing on fracture toughness of $Si_3N_4^+$ graphene platelet composites", *J Eur Ceram Soc 33: (12) 2299-2304 (2013), IF:2.360*
87. **Lambin P**, Vancsó P, Nemes-Incze P, Márk GI, Biró LP: "Electronic structure of a disordered grain boundary in graphene", *In: Borisenki VE, Gaponenko SV, Gurin VS, Kam CH(Eds.), Physics, chemistry and applications of nanostructures: Proceedings of International Conference Nanomeeting 2013., New Jersey City: World Scientific, 2013. pp.203-206., (ISBN:9789814460170)*
88. **Lohner T**, Csíkvári P, Petrik P, Hárs G: "Spectroellipsometric characterization of nanocrystalline diamond layers", *Appl Surf Sci 281: 113-117 (2013), IF:2.112*
89. **Lohner T**: "A spektroszkópiai ellipszometria és az ionsugaras analitika néhány alkalmazása az anyagtudományban", *qtab193p. 2013. (Dissertation: DSc)*

90. **Mándi G**, Nagy N, Palotás K: "Arbitrary tip orientation in STM simulations: 3D WKB theory and application to W(110)", *J Phys Condens Mat 25: (2013), IF:2.355*
91. **Márk GI**, Vancsó P, Biró LP: "Lehet-e tökéletes nanoelektronikai eszközöket készíteni tökéletlen grafénből?", *Fizikai Szemle 58: (11) 381-385 (2013)*
92. **Márton G**, Fekete Z, Fiath R, Baracskay P, Ulbert I, Juhász Gy, Battistig G, Pongrácz A: "In vivo measurements with robust silicon-based multielectrode arrays with extreme shaft lengths", *IEEE Sens J 13: (9) 3263-3269 (2013), IF:1.475*
93. **Menyhárd M**, Daróczi CsS(Eds.), "MTA TTK MFA Yearbook 2012", *Budapest: MTA MFA, 2013. 148p.*
94. **Menyhárd M**: "Detection of nanoparticles by means of reflection electron energy loss spectroscopy depth profiling: Journal of Physics D: Applied Physics", *J Phys D Appl Phys 46: (41) (2013), IF:2.528*
95. **Misják F**, Yamasaki J, Yamamoto Y, Lábár JL, Tanaka N, Radnóczi Gy: "Spontaneous barrier layer formation in $SiO_2$/Cu-Mn alloy film interface", *In: Reinhard Rachel(Eds.), MC 2013 Regensburg: Universitätsverlag Regensburg, 2013. pp. 579-580, Material Science*
96. **Molnár Gy**, Dózsa L, Vértesy Z, Horváth ZsJ: "Iron silicide nanostructures prepared by e-gun evaporation and annealing on Si(001)", *In: Torchinska TV(Eds.), XXI International Materials Research Congress, Symposium 6B, Low-Dimensional Semiconductor Structures: MRS Symposium Proceedings Volume 1534 Symposium 6B (Online Proceedings)., Pittsburgh: Materials Research Society, 2013. Paper imrc12-1534-s6b-p007. 1534*
97. **Molnár Gy**, Dózsa L, Vértesy Z, Horváth ZsJ: "New optoelectronic materials: Effects of annealing upon the formation of epitaxial iron silicide nanostructures on Si(001)", *Physica E 51: 79-86 (2013), IF:1.522*
98. **Molnár Gy**, Dózsa L, Vértesy Z, Horváth ZsJ: "Thickness dependent growth of epitaxial iron silicide Nanoobjects on Si(001)", *In: Alexander D Pogrebnjak(Eds.), International Conference Nanomaterials: Applications and Properties, Kiev, Vol.2, No.2, pp.02PCN21-1-02PCN21-4 (2013)*
99. **Molnár Gy**: "Epitaxy in solid-phase thin film reactions: Nucleation-controlled growth of iron silicide nanostructures on Si(001)", *J Mater Res 28: (13)1724-1728 (2013), IF:1.713*
100. **Molnár KZ**, Turmezei PJ, Horváth ZsJ, Kovács B: "Retention Behaviour of MNOS Memory Devices with Embedded Si or Ge Nanocrystals - Computer Simulation", *Nan Mat Appl Prop 2: (4) (2013)*
101. **Molnár KZ**, Turmezei PJ, Horváth ZsJ: "Charging behaviour of MNOS and SONOS memory structures with embedded semiconductor nanocrystals - Computer simulation", *In: Torchinska TV(Eds.),*
102. **Morgiel J**, Grzonka J, Mania R, Zimowski SL, Lábár JL, Fogarassy Zs: "Relation between microstructure and hardness of nano-composite CrN/$Si_3N_4$ coatings obtained using CrSi single target magnetron system", *Vacuum 90: (1) 170-175 (2013), IF:1.530*
103. **Nagy K**, Misják F, Szommer P, Lobotka P, Radnóczi Gy: "Composition dependence of morphology, electrical and mechanical properties of sputtered Cu-Mn alloy films", *In: Reinhard Rachel(Eds.), MC 2013 Regensburg: Universitätsverlag Regensburg, 2013. pp.567-568, Material Science*

104. **Nagy N**, Deák A, Hórvölgyi Z, Bársony I: "Eljárás maszk kialakítására görbült felületű test felületén és alkalmazásával felületi struktúra létrehozása orvosi implantátumon", *Patent: B01J 13/22, A61F 2/02, 229026, P0900530 (2009/2013) Hungary*
105. **Nemes-Incze P**, Vancsó P, Osváth Z, Márk GI, Jin X, Kim YS, Hwang C, Lambin P, Chapelier C, Biró LP: "Electronic states of disordered grain boundaries in graphene prepared by chemical vapor deposition", *Carbon 64: 178-186 (2013), IF:5.868*
106. **Nemes-Incze P**: "Nanostructures based on graphene and functionalized Carbon nanotubes", *qtab107p. 2013. (Dissertation: PhD)*
107. **Nemouchi F**, Carron V, Lábár JL, Vandroux L, Morand Y, Morel T, Barnes JP: "Formation of NiGe through germanium oxide on Ge(001) substrate", *Microelectron Eng 107: 178-183 (2013), IF:1.224*
108. **Neuróhr K**, Csík A, Vad K, Molnár Gy, Bakonyi I, Péter L: "Near-substrate composition depth profile of direct current-plated and pulse-plated Fe-Ni alloys", *Electrochim Acta 103: 179-187 (2013), IF:3.777*
109. **Ódor G**, Kelling J, Gemming S: "Ageing of the 2+1 dimensional Kardar-Parisi-Zhang model", *arXiv:1312.6029 (2013)*
110. **Ódor G**: "Rare regions of the susceptible-infected-susceptible model on Barabási-Albert networks", *Phys Rev E Stat Nonlin 87: (4) 042132 (2013), IF:2.313*
111. **Ódor G**: "Slow dynamics of the contact process on complex networks", *EPJ Web Conf 44: 04005 (2013)*
112. **Ódor G**: "Spectral analysis and slow spreading dynamics on complex networks", *Phys Rev E Stat Nonlin 88: (3) 032109 (2013), IF:2.313*
113. **Oh S**, Nagata T, Volk J, Wakayama Y: "Improving the performance of inorganic-organic hybrid photovoltaic devices by uniform ordering of ZnO nanorods and near-atmospheric pressure nitrogen plasma treatment", *J Appl Phys 113: (2013), IF:2.210*
114. **Olowojoba G**, Sathyanarayana S, Caglar B, Kiss-Pataki B, Mikonsaari I, Hübner C, Elsner P: "Influence of process parameters on the morphology, rheological and dielectric properties of three-roll-milled multiwalled Carbon nanotube/epoxy suspensions", *Polymer 54: (1)188-198 (2013), IF:3.379*
115. **Orlov LK**, Melnikova AA, Orlov ML, Alyabina NA, Ivina NL, Neverov VN, Horváth ZsJ: "Features of electronic transport in relaxed Si/Si1-XGeX heterostructures with high doping level", *In: Torchinska TV(Eds.), XXI International Materials Research Congress, Symposium 6B, Low-Dimensional Semiconductor Structures,: MRS Symposium Proceedings Volume 1534 Symposium 6B (Online Proceedings)., Pittsburgh: Materials Research Society, 2013. Paper imrc12-1534-s6b-p008. 1534*
116. **Orlov LK**, Nikova AAM, Orlov ML, Alyabina NA, Ivina NL, Neverov VN, Horváth ZsJ: "Features of electronic transport in relaxed $Si/Si_{1-x}Ge_x$ heterostructures with high doping level", *Physica E 51: 87-93 (2013), IF:1.522*
117. **Osváth Z**, Lefloch F, Bouchiat V, Chapelier C: "Electric field-controlled rippling of graphene", *Nanoscale 5: (22)10996-11002 (2013), IF:6.233*
118. **Park DG**, Angani CS, Kishore MB, Vértesy G, Lee DH: "Review paper: Application of the Pulsed Eddy Current Technique to Inspect Pipelines of Nuclear Plants", *J Magn 18: (3) 342-347 (2013), IF:0.326*

119. **Park DG**, Angani CS, Rao BPC, Vértesy G, Lee DH, Kim KH: "Detection of the Subsurface Cracks in a Stainless Steel Plate using Pulsed Eddy Current", *J Nondestruct Eval 32: (4) 350-353 (2013), IF:1.091*
120. **Park DG**, Song H, Kishore MB, Vértesy G, Lee DH: "Detection of Gamma-Irradiation Effect on DNA and Protein Using Magnetic Sensor and Cyclic Voltammetry", *J Nanosci Nanotechno 13: (11) 7250-7253 (2013), IF:1.149*
121. **Patkó D**, György B, Németh A, Szabó-Taylor KE, Kittel A, Búzás EI, Horváth R: "Label-free optical monitoring of surface adhesion of extracellular vesicles by grating coupled interferometry", *Sensor Actuat B Chem 188: 697-701 (2013), IF:3.535*
122. **Pécz B**, Baji Zs, Lábadi Z, Kovács A: "ZnO layers deposited by Atomic Layer Deposition", *J Phys Conf Ser 471: (1) (2013)*
123. **Pécz B**, Tóth L, Barna Á, Tsiakatouras G, Ajagunna AO, Kovács A, Georgakilas A: "Structural characteristics of single crystalline GaN films grown on (111) diamond with AlN buffer", *Diam Relat Mater 34: 9-12 (2013), IF:1.709*
124. **Perc M**, Gómez-Gardenes J, Szolnoki A, Floría LM, Moreno Y: "Evolutionary dynamics of group interactions on structured populations: a review", *J R Soc Interface 10: (80) 20120997 (2013), IF:4.907*
125. **Petrik P**, Agócs E: "High sensitivity optical characterization of thin films with embedded Si nanocrystals", *ECS Trans 53: (4) 43-52 (2013)*
126. **Petrik P**, Fried M: "Ellipsometry of semiconductor nanocrystals", *In: Maria Losurdo, Kurt Hingerl(Eds.), Ellipsometry at the Nanoscale., Heidelberg: Springer Verlag, 2013. pp.583-606, (ISBN:978-3-642-33955-4)*
127. **Petrik P**, Gumprecht TE, Nutsch A, Roedera G, Lemberger M, Juhász Gy, Polgár O, Major Cs, Kozma P, Janosov M, Fodor B, Agócs E, Fried M: "Comparative measurements on atomic layer deposited $Al_2O_3$ thin films using ex situ table top and mapping ellipsometry, as well as X-ray and VUV reflectometry", *Thin Solid Films 541: 131-135 (2013), IF:1.604*
128. **Petrik P**, Pollakowski B, Zakel S, Gumprecht T, Beckhoff B, Lemberger M, Lábadi Z, Baji Zs, Jank M, Nutsch A: "Characterization of ZnO structures by optical and X-ray methods", *Appl Surf Sci 281: 123-128 (2013), IF:2.112*
129. **Pongrácz A**, Fekete Z, Márton G, Bérces Zs, Ulbert I, Fürjes P: "Deep-brain silicon multielectrodes for simultaneous neural recording and drug delivery", *Sensor Actuat B Chem 189: 97-105 (2013), IF:3.535*
130. **Pramatarova LD**, Hikov TA, Krasteva NA, Petrik P, Dimitrova RP, Pecheva EV, Radeva EI, Agócs E, Tsvetanov IG, Presker RP: "Protein adsorption on detonation nanodiamond/Polymer composite layers", *Mater Res Soc SP 1479: 51-56 (2013)*
131. **Radnóczi Gy**, Misják F, Bíró D, Barna PB: "The impact of electron microscopy on revealing phase separation mechanisms in alloy thin films", *In: Reinhard Rachel(Eds.), MC 2013Regensburg: Universitätsverlag Regensburg, 2013. pp.363-364, Material Science*
132. **Rakovics V**, Réti I: "Near infrared luminescence of CdS:Cu thin films prepared by chemical bath deposition", *In: Róbert Brunner(Eds.), Proceedings of 8th Solid State Surfaces and Interfaces: Extended Abstract Book., Bratislava: Comenius University, 2013. pp.151-153, (ISBN:978-80-223-3501-0)*

133. **Riesz F**: "Non-linearity and related features of Makyoh (magic-mirror) imaging", *J Optics-UK 15: (7) (2013), IF:1.990*
134. **Saftics A**, Agócs E, Fodor B, Patkó D, Petrik P, Kolari K, Aalto T, Fürjes P, Horváth R, Kurunczi S: "Investigation of thin Polymer layers for biosensor applications", *Appl Surf Sci 281: 66-72 (2013), IF:2.112*
135. **Sathyanarayana S**, Olowojoba G, Weiss P, Pataki B, Mikonsaari I, Hübner C, Henning F: "Compounding of MWCNTs with PS in a Twin-Screw Extruder with Varying Process Parameters: Morphology, Interfacial Behavior, Thermal Stability, Rheology, and Volume Resistivity", *Macromol Mater Eng 298: (1) 89-105 (2013), IF:2.338*
136. **Schmidt S**, Czigány Zs, Greczynski G, Jensen J, Hultman L: "Influence of inert gases on the reactive high power pulsed magnetron sputtering process of Carbon-nitride thin films", *J Vac Sci Technol A 31: (1) (2013), IF:1.432*
137. **Schmidt S**, Goyenola C, Gueorguiev GK, Jensen J, Greczynski G, Ivanov IG, Czigány Zs, Hultman L: "Reactive high power impulse magnetron sputtering of $CF_x$ thin films in mixed Ar/$CF_4$ and Ar/$C_4F_8$ discharges", *Thin Solid Films 542: 21-30 (2013), IF:1.604*
138. **Serényi M**, Csík A: "Hidrogéntertalmú amorf szilícium/germánium multirétegek strukturális stabilitása - I. rész", *Fizikai Szemle 63: (6) 194-197 (2013)*
139. **Serényi M**, Csík A: "Hidrogéntertalmú amorf szilícium/germánium multirétegek strukturális stabilitása - II. rész", *Fizikai Szemle 63: (7-8) 222-225 (2013)*
140. **Serényi M**, Frigeri C, Szekrényes Zs, Kamarás K, Nasi L, Csík A, Khánh NQ: "On the formation of blisters in annealed hydrogenated a-Si layers", *Nanoscale Res Lett 8: (2013), IF:2.524*
141. **Skakalova V**, Kranshenninikov A, Tapasztó L: "Graphene, nanotubes and related materials", *Phys Status Solidi C Curr T Solid State Phys 10: (7-8) 1161-1162 (2013)*
142. **Sulyok A**, Tóth AL, Zommer L, Menyhárd M, Jablonski A: "Simulation of the backscattered electron intensity of multi layer structure for the explanation of secondary electron contrast", *Ultramicroscopy 124: 88-95 (2013), IF:2.470*
143. **Szabó Gy**, Szolnoki A, Czakó L: "Coexistence of fraternity and egoism for spatial social dilemmas", *J Theor Biol 317: 126-132 (2013), IF:2.351*
144. **Szabó Z**, Volk J, Gergely-Fülöp E, Deák A, Bársony I: "Regular ZnO nanopillar arrays by nanosphere photolithography", *Photonic Nanostruct 11: (1) 1-7 (2013), IF:1.792*
145. **Szekeres A**, Alexandrova S, Petrik P, Fodor B, Bakalova S: "Ellipsometric study of crystalline silicon hydrogenated by plasma immersion ion implantation", *Appl Surf Sci 281: 105-108 (2013), IF:2.112*
146. **Szijjártó GP**, Pászti Z, Sajó I, Erdőhelyi A, Radnóczi Gy, Tompos A: "Nature of the active sites in Ni/$MgAl_2O_4$-based catalysts designed for steam reforming of ethanol", *J Catal 305: 290-306 (2013), IF:5.787*
147. **Szívós J**, Sáfrán G, Serényi M, Gergely-Fülöp E: "Direct nanopatterning and nano-scale mask fabrication with UV laser", *In: IX. Országos Anyagtudományi Konferencia 2013. pp.*
148. **Szívós J**, Sáfrán G: "Nanoscale Patterning og Magnetic Thin Films", *In: Doctoral School of Molecular- and Nanotechnologies(Eds.), Proceedings of the PhD Mini Symposium 2013., Veszprém: Faculty of Information Technology, University of Pannonia, Regional Centre of the HAS, 2013. pp.32-35, (ISBN:978-615-5044-84-7)*

149. **Szívós J**, Serényi M, Gergely-Fülöp E, Sáfrán G: "Nanoscale masking with UV excimer laser for bit patterned media", *In: Proceedings of MC2013 Microscopy Congress 2013. pp.607-608*

150. **Szolnoki A**, Perc M: "Correlation of Positive and Negative Reciprocity Fails to Confer an Evolutionary Advantage: Phase Transitions to Elementary Strategies", *Phys Rev X 3: 041021 (2013), IF:6.711*

151. **Szolnoki A,** Perc M: "Decelerated invasion and waning-moon patterns in public goods games with delayed distribution", *Phys Rev E Stat Nonlin 87: 054801 (2013), IF:2.313*

152. **Szolnoki A**, Perc M: "Effectiveness of conditional punishment for the evolution of public cooperation", *J Theor Biol 325: 34-41 (2013), IF:2.351*

153. **Szolnoki A**, Perc M: "Information sharing promotes prosocial behaviour", *New J Phys 15: 053010 (2013), IF:4.063*

154. **Szolnoki A**, Xie NG, Ye Y, Perc M: "Evolution of emotions on networks leads to the evolution of cooperation in social dilemmas", *Phys Rev E Stat Nonlin 87: 042805 (2013), IF:2.313*

155. **Szolnoki A**: "Komplex viselkedés társadalmi dilemmákban", *Természet Világa 144: (II) 98-102 (2013)*

156. **Tabi T**, Balázsi Cs, Petrik A, Kovács JG, Kovács NK, Rákos K: "Megújuló erőforrásból előállított lebontható polimerek alkalmazása a gyors prototípusgyártásban", *Műanyag és Gumi 50: (10) 389-394 (2013)*

157. **Tamáska I**, Kertész K, Vértesy Z, Bálint Zs, Kun A, Shen-Horn Y, Biró LP: "Color Changes upon Cooling of Lepidoptera Scales Containing Photonic Nanoarchitectures", *Key Eng Mater 543: 18-21 (2013)*

158. **Tamáska I**, Kertész K, Vértesy Z, Bálint Zs, Kun A, Yen S, Biró LP: "Color changes upon cooling of lepidoptera scales containing photonic nanoarchitectures, and a method for identifying the changes", *J Insect Sci 13: Art Nr. 87. (2013), IF:0.875*

159. **Tamáska I**, Vértesy Z, Deák A, Petrik P, Kertész K, Biró LP: "Optical properties of bioinspired disordered photonic nanoarchitectures", *Nanopages 8: (2)17-30 (2013)*

160. **Tomás I**, Vértesy G, Gillemot F, Székely R: "Nondestructive Magnetic Adaptive Testing of Nuclear Reactor Pressure Vessel Steel Degradation", *J Nucl Mater 432: (1-3) 371-377 (2013), IF:1.211*

161. **Tomás I**, Vértesy G, Pirfo BS, Kobayashi S: "Comparison of four NDT methods for indication of reactor steel degradation by high fluences of neutron irradiation", *Nucl Eng Des 265: 201-209 (2013), IF:0.805*

162. **Tóth BG**, Péter L, Dégi J, Révész Á, Oszetzky D, Molnár Gy, Bakonyi I: "Influence of Cu deposition potential on the giant magnetoresistance and surface roughness of electrodeposited Ni-Co/Cu multilayers", *Electrochim Acta 91: 122-129 (2013), IF:3.777*

163. **Vancsó P**, Márk GI, Lambin P, Mayer A, Kim YS, Hwang C, Biró LP: "Electronic transport through ordered and disordered graphene grain boundaries", *Carbon 64: 101-110 (2013), IF:5.868*

164. **Vegetti A**, Radnóczi Gy, Ossi PM: "Role of embedded Carbon particles on the morphology, microstructure and transport properties of sintered ultra-high molecular weight polyethylene", *Carbon 65: 20-27 (2013), IF:5.868*

165. **Vehovszky B**, Kamasa P, Kovác J, Fogarassy Zs: "Complex study of h-induced structural rearrangements in FeZr glasses", *Mater Sci Forum 729: 509-514 (2013)*

166. **Veres T**, Cser L, Bodnarchuck V, Ignatovich V, Horváth ZE, Nagy B: "Investigation of periodic Ni-Ti multilayers", *Thin Solid Films 540: 69-72 (2013), IF:1.604*

167. **Vértesy G**, Mészáros I, Tomás I: "Nondestructive magnetic characterization of TRIP steels", *NDT&E INT 54: 107-114 (2013), IF:1.744*

168. **Vértesy G**, Tomás I: "Complex characterization of degradation of ferromagnetic materials by Magnetic Adaptive Testing", *IEEE T Magn 49: (6) 2881-2885 (2013), IF:1.422*

169. **Vértesy G**, Uchimoto T, Takagi T, Tomás I: "Nondestructive detection of local material thinning in ferromagnetic materials by Magnetic Adaptive Testing", *EJAM 5: (1) 7-14 (2013)*

170. **Vértesy G**: "Ferromágneses anyagok roncsolásmentes vizsgálata mágneses hiszterézis alhurkok mérése alapján", *Fizikai Szemle 5: 157-161 (2013)*

171. **Vukov J**, Szolnoki A, Szabó Gy: "Diverging fluctuations in a spatial five-species cyclic dominance game", *Phys Rev E Stat Nonlin 88 (2): 022123 (2013), IF:2.313*

172. **Vukov J**: "Csalni vagy nem csalni? - Matematikai komplexitás az emberi kapcsolatokban", *Természet Világa II. különszám: 103-106 (2013)*

173. **Wang Z**, Szolnoki A, Perc M: "Interdependent network reciprocity in evolutionary games", *Sci Rep 3: 1183 (2013), IF:2.927*

174. **Wang Z**, Szolnoki A, Perc M: "Optimal interdependence between networks for the evolution of cooperation", *Sci Rep 3: 2470 (2013), IF:2.927*

175. **Weltsch Z**, Fogarassy Zs, Lovas A, Takács J, Cziráki Á, Tichy G: "The contact angle between Ag-based melts and graphite substrate and the texture evolution during the subsequent solidification", *Acta Electrotech Inf 13: (1) 41-44 (2013), XXI International Materials Research Congress, Symposium 6B, Low-Dimensional Semiconductor Structures,: MRS Symposium Proceedings Volume 1534 Symposium 6B (Online Proceedings)., Pittsburgh: Materials Research Society, 2013. Paper imrc12-1534-s6b-p005. 1534*

176. **Zhuravlev K**, Malin T, Trubina S, Erenburg S, Dobos L, Pécz B, Davydov V, Smirnov A, Kyutt R: "EXAFS study of GaN/AlN multiple quantum wells grown by ammonia MBE", *Phys Status Solidi C Curr T Solid State Phys 10: (3) 311-314 (2013)*

177. **Zolnai Zs**: "Shape, size, and atomic composition analysis of nanostructures in 3D by Rutherford backscattering spectrometry", *Appl Surf Sci 281: 17-23 (2013), IF:2.112*